NASA CR-135408
HAC REPORT NO. P78-128
HAC REF. NO. D7597

FINAL REPORT

CLOSED CYCLE ELECTRIC DISCHARGE LASER DESIGN INVESTIGATION

PHILIP K. BAILY AND RICHARD C. SMITH

MARCH 1978

SPONSORED BY
NATIONAL AERONAUTICS AND SPACE ADMINISTRATION, LEWIS RESEARCH CENTER, CONTRACT NAS3-20100

AEROSPACE GROUPS
HUGHES
HUGHES AIRCRAFT COMPANY
CULVER CITY, CALIFORNIA

Accession Number: 3991

Publication Date: Mar 01, 1978

Title: Closed Cycle Electric Discharge Laser Design Investigation

Personal Author: Baily, P.K.; Smith, R.C.

Corporate Author Or Publisher: Hughes Aircraft Company, Culver City, CA 90230 Report Number: HAD P78-128

Report Prepared for: NASA, Lewis Research Center, Cleveland, OH Report Number Assigned by Contract Monitor: NASA CR-135408

Comments on Document: Archive, RRI, DEW

Descriptors, Keywords: Closed Cycle Electric Discharge Laser Design Investigation Carbon Dioxide Monoxide Space Airborne Heat Disposal Point Track Power Solar Generator Radiation

Pages: 00100

Cataloged Date: Nov 27, 1992

Contract Number: NAS 3-20100

Document Type: HC

Number of Copies In Library: 000001

Record ID: 25219

Source of Document: DEW

1. Report No.	2. Government Accession No.	3. Recipient's Catalog No.
CR-135408		

4. Title and Subtitle	5. Report Date
CLOSED CYCLE ELECTRIC DISCHARGE LASER DESIGN INVESTIGATION	March 1978
	6. Performing Organization Code

7. Author(s)	8. Performing Organization Report No.
Philip K. Baily, Richard C. Smith	P78-128
	10. Work Unit No. YOV 7305

9. Performing Organization Name and Address	11. Contract or Grant No.
Hughes Aircraft Company Centinela and Teale Streets Culver City, CA 90230	NAS 3-20100
	13. Type of Report and Period Covered: Final Report

12. Sponsoring Agency Name and Address	14. Sponsoring Agency Code
National Aeronautics and Space Administration Lewis Research Center Cleveland, Ohio	

15. Supplementary Notes

Project Manager, Jack G. Slaby
Laser and Energy Systems Branch
NASA, Lewis Research Center, Cleveland, Ohio

16. Abstract

The effort reported here deals with closed cycle CO_2 and CO electric discharge lasers. This effort was an analytical investigation to assess scale-up parameters and design features for CO_2, closed cycle, continuous wave, unstable resonator, electric discharge lasing systems operating in space and airborne environments. During the program, the scope was expanded to include the investigation of a space-based CO system. The study was conducted insofar as possible in the context of predicted 1990 technology.

The program objectives were the conceptual designs of six CO_2 systems and one CO system. Three airborne CO_2 designs, with one, five and ten megawatt outputs, were produced. These designs were based upon five minute run times. Three space-based CO_2 designs, with the same output levels, were also produced, but based upon one year run times. (This primarily meant that no consumables were allowed.) In addition, a conceptual design for a one megawatt space-based CO laser system was also produced. These designs include the flow loop, compressor, and heat exchanger, as well as the laser cavity itself. Design for the prime power, waste heat disposal system, and pointing and tracking were not pursued, although it became necessary to make certain scaling assumptions about these items. It is interesting to note that the designs resulted in a laser loop weight for the space-based five megawatt system that is within the space shuttle capacity. For the one megawatt systems, the estimated weight of the entire system including laser loop, solar power generator, and heat radiator is less than the shuttle capacity.

17. Key Words (Suggested by Author(s))	18. Distribution Statement
Electrical Discharge Laser CO_2 Laser CO Laser Closed Cycle Laser	Unlimited

19. Security Classif. (of this report)	20. Security Classif. (of this page)	21. No. of Pages	22. Price*
UNCLASSIFIED	UNCLASSIFIED	100	

* For sale by the National Technical Information Service, Springfield, Virginia 22161

SUMMARY

The NASA Lewis Research Center, as part of the NASA high power laser technology program, has been conducting investigations of different types of lasing systems. The purpose of these investigations has been the assessment of system effectiveness for delivery of high power laser beams for potential NASA missions such as long range power transmission. Nominal requirements to satisfy potential NASA missions include continuous multi-megawatt power output, high beam quality, closed cycle operation, light weight, high over-all system efficiency, and reliable operation for periods approaching a year. The effort reported here deals with closed cycle CO_2 and CO electric discharge lasers. This effort was an analytical investigation to assess scale-up parameters and design features for CO_2, closed cycle, continuous wave, unstable resonator, electric discharge lasing systems operating in space and airborne environments. During the program, the scope was expanded to include the investigation of a space-based CO system. The study was conducted insofar as possible in the context of predicted 1990 technology.

The program objectives were the conceptual designs of six CO_2 systems and one CO system. Three airborne CO_2 designs, with one, five and ten megawatt outputs, were produced. These designs were based upon five minute run times, Three space-based CO_2 designs, with the same output levels, were also produced, but based upon one year run times. (This primarily meant that no consumables were allowed.) In addition, a conceptual design for a one megawatt space-based CO laser system was also produced. These designs include the flow loop, compressor, and heat exchanger, as well as the laser cavity itself. Design for the prime power, waste heat disposal

system, and pointing and tracking were not pursued, although it became necessary to make certain scaling assumptions about these items.

The airborne systems were designed for maximum efficiency, but as a consequence of the extended run time for the space-based missions, real time waste heat disposal is required and the minimum system weight is not achieved at the optimum laser efficiency. Therefore, the airborne and space-based laser loop designs are different. It is interesting to note that the designs resulted in a laser loop weight for the space-based five megawatt system that is within the space shuttle capacity. For the one megawatt systmes, the estimated weight of the entire system including laser loop, solar power generator, and heat radiator is less than the shuttle capacity. While the CO system resulted in the lightest weight and highest efficiency, the significance of the weight difference is questionable in view of the state of the technology development in this area.

PREFACE

The work discussed in this report was performed for NASA Lewis Research Center under Contract NAS3-20100 with Mr. Jack Slaby as Contract Monitor. The study was performed within the High Energy Laser Systems Laboratory at Hughes Aircraft Company. Dr. Philip K. Baily served as Program Manager and Technical Director and Dr. Richard C. Smith performed the system scaling analyses. The system layout concepts and mechanical designs were under the direction of Mr. Frank Shannon. Mr. Frank Gump was responsible for the heat exchanger designs and analyses. Drs. Dennis Regan and Peter Shen were responsible for gas dynamic technology. In addition, this study drew heavily on prior and concurrent technology development in the High Energy Laser Device Department. Principle contributors to this work included R.A. Hill, G. Wakalopulos, L. Sutter, R. Korechoff, R. Washburn, F. Dolezal, E. Frysinger, and H. Bickert.

CONTENTS

CONTENTS (Continued)

LIST OF ILLUSTRATIONS

LIST OF ILLUSTRATIONS (Continued)

LIST OF ILLUSTRATIONS (Continued)

LIST OF TABLES

LIST OF TABLES (Continued)

1.0 INTRODUCTION

1.1 PROGRAM SCOPE

The NASA Lewis Research Center, as part of the NASA high power laser technology program, has been conducting investigations of different types of lasing systems. The purpose of these investigations has been the assessment of system effectiveness for delivery of high power laser beams for potential NASA missions such as long range power transmission. Nominal requirements to satisfy potential NASA missions include continuous multi-megawatt power output, high beam quality, closed cycle operation, light weight, high over-all system efficiency, and reliable operation for periods approaching a year. A previous study[1] dealt with a closed cycle gas dynamic laser. The effort reported here deals with closed cycle CO_2 and CO electric discharge lasers. This effort was an analytical investigation to assess scale-up parameters and design features for CO_2, closed cycle, continuous wave, unstable resonator, electric discharge lasing systems operating in space and airborne environments. During the program, the scope was expanded to include the investigation of a space-based CO system. The study was conducted in so far as possible in the context of predicted 1990 technology.

The program objectives were the conceptual designs of six CO_2 systems and one CO system. Three airborne CO_2 designs, with one, five, and ten megawatt outputs, were produced. These designs were based upon five minute run times. Three space-based CO_2 designs, with the same output levels, were also produced, but based upon one year run times. (This primarily meant that no consumables were allowed.) In addition, a conceptual design for a one megawatt space-based CO laser system was also

produced. These designs include the flow loop, compressor, and heat exchanger, as well as the laser cavity itself. Design for the prime power, waste heat disposal system, and pointing and tracking were not pursued, although it became necessary to make certain scaling assumptions about these items.

1.2 PROGRAM ORGANIZATION

The CO_2 EDL study was initially organized into two tasks. The first was a parametric component and system scaling analysis. This task provided guidance for the major system trade-offs and resulted in the choice of a nominal baseline design concept. The effort under this task is discussed in Section 3 of this report. Then the second task, component and system conceptual design, was pursued, resulting in the conceptual designs presented in Section 4. Because of the high potentially achievable efficiencies in CO systems, a third task was added to the program while the CO_2 study was in progress. This task was the scaling and conceptual design of a closed cycle cw CO electric discharge laser. The activity under this task is discussed in Section 5.

2.0 OVERVIEW OF THE STUDY

2.1 PERIPHERAL COMPONENT SCALING

While prime power and waste heat disposal system designs were not included in the scope of this study, it became apparent very quickly that these components play an important role in overall system design. For example, in the space-based system overall system weight is drastically affected by the heat radiation temperature since the radiator size is proportional to the fourth power of the temperature. The radiator weight loss to be obtained by increased temperature, however, is somewhat offset by the fact that increased temperature results in reduced laser efficiency requiring a larger and heavier prime power source. Consequently, the specification of the laser system design parameters should be a result of the influence of not only the laser system components, but also the prime power and waste heat disposal systems. In fact, the laser itself is by far the lightest part of the system. In order to perform a meaningful study, it became apparent that the overall system should be optimized and tradeoffs between the influences of the major subsystems should be made. This necessitated the choice of types of prime power and waste heat disposal systems so that scaling laws could be developed. For the airborne systems, a gas turbine driven super-conducting alternator was chosen as the prime power source and prechilled aircraft fuel was chosen as the heat exchanger fluid. After passage through the laser heat exchangers, this fluid is available for use as aircraft fuel. For the space-based systems, an erectable focussing solar collector heating a Brayton cycle generator was selected as the prime power source and an erectable teflon radiator was chosen for laser

system waste heat disposal. The collector and radiator are required to be maintained in positions facing toward and away from the sun, respectively.

2.2 DESIGN CONSTRAINTS

Near the beginning of the study, the issue of study scope was addressed and a set of guidelines was decided upon. The major concern was with the one year run time space-based systems. The first limitation was that the details of space station design, including such things as angular momentum conservation, would not be addressed. Also, detailed solution of gas leakage and material lifetime problems would not be attempted in a conceptual design study. The primary manifestations of the one year run time then are the requirement for virtually no consumables and steady state operation. Power must be provided and waste heat must be radiated in real time. In the airborne systems however, one way temperature changes in the coolant fluids are acceptable, since they need not be recirculated for five minute run times.

The method of excitation of the laser medium was chosen to be an electron ionized sustainer discharge. Vibrational excitation of the gas molecules is produced by the dc sustainer current. Optimization of the excitation efficiency is accomplished by proper choice of voltage. The input power is then determined by the current density which is independently controlled by the electron gun, which injects high energy ionizing electrons into the excitation region.

The energy and current density of the injected electrons determine the degree of ionization and consequently the sustainer current density in the laser medium. Alternative excitation schemes including rf discharges and ultra-violet pre-ionized sustainer discharges were briefly considered. However, the current state-of-the-art is further advanced for electron beam ionized sustainer discharges and this situation is unlikely to change in the near future. The principal difficulty with the use of electron beams has been the relative fragility of electron guns. Recently, Hughes has developed a rugged plasma discharge electron gun which does not use hot filaments and which should be suitable for reliable long run time operation. This device will be described in Section 3.3.4.

It was also considered desirable to treat the issue of sustainer discharge or electron beam induced molecular changes in the laser medium in this study. However, the current understanding of this problem is inadequate, and any treatment of the possible impact of this issue on long run time designs would be highly speculative. Consequently, it was regretfully decided not to treat this problem in the current study. Recent experiments at Lincoln Laboratories do indicate that the problem may be minor. If the problem turns out to be significant, it may necessitate the addition of an additional component to the laser loop. This component would be a compensator to artifically induce a compensating reaction for the specific process being stimulated in the laser excitation region. Alternatively, the precise gas mix in the laser loop may be chosen to minimize this problem. In any case, it is hoped that this issue will be experimentally addressed in the near future.

A major issue in the design of high efficiency high pressure cw electric discharge lasers is the proper treatment of mode-medium interaction. In these devices, the heat deposition in the laser medium within the optical extraction region is a function of and interacts with the optical intensity as influenced by the optical resonator mode distribution. This interaction has many forms and can be weak, strong, or even unstable. Proper excitation region and optical resonator design has been pursued recently with great vigor at Hughes and elsewhere, and great progress in the understanding of this problem has been made. It is clear that the medium will strongly affect the phase distribution of the laser beam and phase correction will be required on the resonator mirrors. It is reasonable to assume that by 1990 the prescription for detailed resonator design, including mode-medium interaction effects, will be well understood. For the present study, the precise details of the excitation region and optical resonator designs are not specifically defined; the method of excitation and size of the excitation region and resonator beam can however be determined.

For the CO_2 systems, only subsonic systems were considered. The designs were based upon single line operation on the $(00^\circ 1) \rightarrow (02^\circ 0)$ R-branch transition at approximately 9.3 microns. This choice enables one to take advantage of the higher quantum efficiency compared to the 10.6 micron $(00^\circ 1) \rightarrow (10^\circ 0)$ P-branch transition. For the CO system, the study included a

tradeoff between subsonic and supersonic operation. Multi-line operation over the four to six micron region was allowed, resulting in extremely high energy conversion efficiencies.

2.3 SYSTEM OPTIMIZATION CRITERIA

The optimization criteria for the airborne and space-based systems were different. The primary objective, for the airborne systems, was the attainment of high system efficiency, where efficiency is defined as the ratio of optical output power to input power. The input power includes sustainer discharge power, compressor drive power, electron gun electrical power, and miscellaneous power for pumps, controls, etc. The secondary objectives in the system scaling design were minimization of system weight, volume, and technical risk with their importance in that order.

For the space-based systems, weight was the most important factor because the system must be raised into orbit. Accordingly, the primary objective in scaling and designing the space-based systems was taken to be the minimization of system weight. The secondary factors were minimization of volume, maximization of efficiency, and minimization of technical risk in that order.

2.4 SUMMARY OF RESULTS

The airborne CO_2 designs consist of single flow loop one and five Megawatt systems. The ten Megawatt system consists of two five Megawatt system coupled optically. The overall electrical efficiencies, i.e., laser output power compared to total input power (discharge, compressor, and controls), range from 22.9 percent to 26.5 percent. The physical envelope for the largest system is approximately 41 ft by 15 ft by 13.5 ft. The total system weights are approximately 4,000, 20,000, and 40,000 kilograms for the one, five, and ten Megawatt systems respectively.

The space-based systems are somewhat different because of the one-year run time requirement, and the fact that weight rather than electrical efficiency was optimized. The overall efficiencies for these systems range from 15.1 percent to 20.4 percent. The laser loops for the one, five, and

ten Megawatt systems are approximately 2800, 18,000, and 36,000 kilograms respectively. When the weights of the solar collectors, prime power generators, and waste heat radiators used in our system scaling and overall weight minimization trade-off are added to these numbers, then the total system masses become approximately 20,400, 83,700, and 166,300 kilograms for the one, five, and ten Megawatt systems respectively. The weight of the total one Megawatt system is less than the space shuttle payload capacity. For the one Megawatt system approximately 2.5 percent of the collected solar radiation is converted to 9.3μ laser radiation.

The one Megawatt CO system study produced a supersonic flow system design with an overall electrical efficiency of 22.7 percent, a laser loop weight of approximately 2800 kilograms (but slightly less than that of the CO_2 system), and an overall system weight of approximately 17,000 kilograms. The solar-to-laser power conversion efficiency is 3.8 percent. The approximate weight saving of 3400 kilograms must however be viewed in light of the fact that CO laser development is not as far along as is CO_2 development, and the weight estimate for the CO system is therefore somewhat less certain.

3.0 COMPONENT AND SYSTEM SCALING ANALYSIS (CO_2 SYSTEMS)

3.1 AIRBORNE PERIPHERALS

This study is nominally concerned with characterization of the power conditioning and laser loop for airborne and space laser systems. Since the components with which we are to be mainly concerned constitute a small fraction of the total system mass and volume, some assumptions about prime power and waste heat disposal systems must be made. In scaling power generation equipment for an airborne system, one is presented with alternatives of various degrees of feasibility for a 1990 system. A conventional system might consist of either a gas turbine or a stored-oxidizer combustion turbine turning an alternator. The relative merits of these depend upon altitude and mission time because the former determines the oxygen available to an air-breathing turbine while the latter determines the mass of stored oxidizer required.

For an operating time of 300 seconds, the stored oxidizer turbine provides the least massive system for missions above 6000 meters[2], so this type of prime mover was assumed in the system scaling. Superconducting windings will be included in the proposed airborne system, because replacement of conventional generator windings with them provides a mass saving of about 100 kg per megawatt of electrical power generated.

For prime mover and alternator, a magnetohydrodynamic (MHD) generator system could have been chosen. The MHD generator appears to be more advantageous for high power systems. This less developed approach appears to offer no mass advantage for a 1 MW laser, but perhaps a 30 percent or 500 kg advantage for a 5 MW system[3]. This somewhat more speculative power system was not chosen for our study but should be considered for the larger systems if development proceeds rapidly in the

next 5-8 years. The alternative of stored chemical energy was also considered. However for a 5 minute mission, stored energy devices, e.g., rechargeable AgO-Zn batteries, do not appear to be competitive.

Of the four turbine fuels considered, one, hydrazine, is a monopropellant and the other three are bipropellants, namely, liquid oxygen (LOX)/liquid hydrogen, LOX/ammonia, and LOX/JP4. For a 300 second run time and a 1 MW laser system with an efficiency of 25 percent, scaling projections for 1990 [3] provide the comparison shown in Table 3-1.

The favorable mass and volume of hydrazine is deemed insufficient compensation for its toxicity and corrosiveness. The $0.4m^3$ volume advantage over $JP4/O_2$ is more apparent than real since, with minor modification, the JP4 can be withdrawn from the aircraft fuel tanks directly. Either a substantial redesign of a portion of the fuel tank must be done or the N_2H_4 tank would have to be placed in the cargo space being utilized by the laser system. The large tankage volume requirement for H_2/O_2 arising from its low density and low storage temperature argues against it for airborne application. The 600 kg mass penalty attendant upon selecting $JP4/O_2$ instead of H_2/O_2 seems palatable, especially since no special provisions for handling or storing the JP4 are required. Ammonia offers no advantage over JP4 and is not available as aircraft fuel. Thus $JP4/O_2$ is used in our system study.

TABLE 3-1. TURBINE FUEL PARAMETERS

Fuel (Mass Ratio)	Fuel Mass (kg)	Tankage Mass (kg)*	Tankage Volume (m^3)*	Total Mass
N_2H_4	910	30	1.15	940
H_2/O_2 (1:1)	270	300	2.60	570
NH_3/O_2 (4:1)	1090	80	1.45	1170
$JP4/O_2$ (2:1)	1090	80	1.55	1170

*For cryogens, 1-2 week storage assumed

Laser waste heat will be disposed of by transfer in a heat exchanger from the laser gas to another fluid which can be jettisoned. Several fluids were evaluated as potential coolants for a 1 MW laser system whose operating parameters were similar to those finally selected. Table 3-2 presents the masses and volumes associated with the various choices, including the trade-off between coolant flow and heat exchanger mass for one candidate, H_2 gas, as an example. Since JP4 could be stored chilled, heated in the heat exchanger, and then made available to the aircraft fuel supply it was so far ahead of the other contenders that it was selected as the coolant without further consideration. For this small a fraction of the total system mass and volume, packaging considerations discussed in Section 4 can dictate exact dimensions and flow rate. The tankage volume for JP4 is that associated with a vessel to maintain the chilled JP4 thermally isolated from the rest of the fuel. It is assumed that this volume will come in part from the aircraft's fuel storage.

3.2 SPACE PERIPHERALS

For a space laser system, it is not possible to treat heat disposal and prime power as ignorable elements during laser cavity optimization and then simply estimate mass and volume for them to obtain system size. In the short run time airborne case, this is nearly possible because high cavity efficiency results in low waste heat and low input power requirement. For a one-year run time in space, heat must be radiated as it is produced. The amount of heat radiated by a surface increases as the fourth power of the temperature of the radiator. Increased radiation capability decreases radiator size and weight. This provides a reason to desire high temperatures in the system, while low temperature produces the more efficient laser cavity. Briefly stated, as temperature increases:

1. Cavity efficiency decreases (for example, see Figure 3-1).
2. Power production equipment size increases approximately linearly with increasing electrical power requirement.
3. Radiator size decreases as T^4.

If system mass is the major optimization criterion, then high cavity efficiency must be sacrificed.

TABLE 3-2. CANDIDATES FOR HEAT EXCHANGER COOLANTS (AIRBORNE SYSTEMS)

Coolant	Coolant Mass (Kg)	Heat Exchanger Mass (Kg)	Heat Exchanger Volume (M^3)	Tankage Mass (Kg)	Tankage Volume (M^3)	Total Mass (Kg)	Total Volume (M^3)
Trichloroethylene	15,900	110	0.20	590	20.0	16,600	20.2
JP4	4,500	220	0.40	215+	0.4++	435*	0.8*
H_2 Gas	500	220	0.40	1,000	7.8	1,720	8.2
H_2 Gas	460	320	0.59	920	7.1	1,700	8.7
H_2 Gas	360	390	0.73	720	5.6	1,470	6.3
H_2 Gas	280	480	0.89	560	4.3	1,320	5.2
H_2 Gas	260	610	1.13	520	3.9	1,390	5.0
O_2 Gas	9,600	220	0.40	790	16.5	10,600	16.9
N_2 Gas	8,300	220	0.40	700	14.2	9,200	14.6
H_e Gas	1,700	220	0.40	2,040	23.3	3,960	23.7

\+ - excess tankage weight to store JP4 at 180°K

++ - excess volume of tankage walls due to 180°K storage

* - does not include mass and volume of JP4 which will return to the aircraft fuel supply

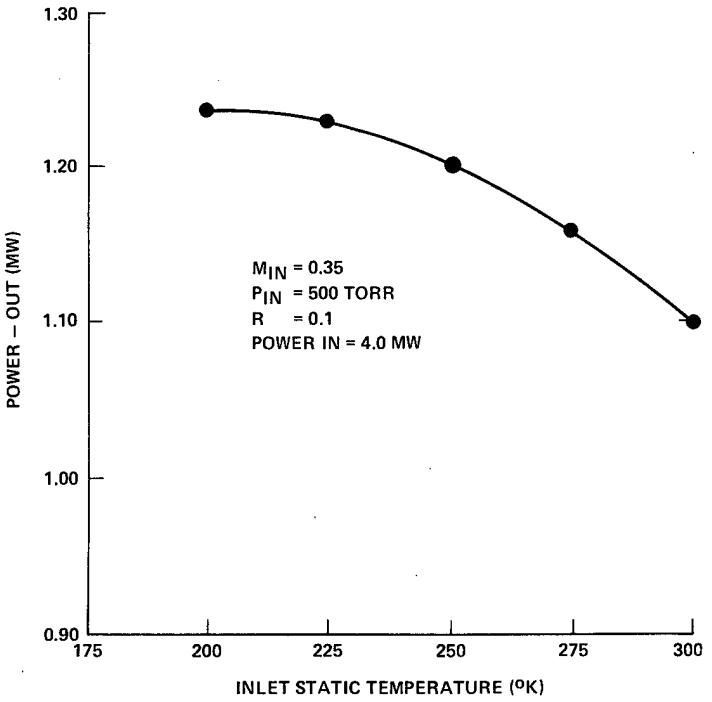

Figure 3-1. Extraction versus temperature (constant inlet pressure).

The power source options considered are closed thermodynamic and magnetohydrodynamic cycles driven by either a solar concentrator or a nuclear reactor, and a photocell array. For a power cycle efficiency of 30 percent, the specific mass of a 1990 reactor with a shield sufficient to produce a 10 degree shadow zone with a dose rate of 10^{-2} rem/hr at the shield is likely to be near 0.75 kg/kwe[4]*, while if in addition, a full peripheral shield capable of reducing the maximum dose rate to a 1 rem/hr is required, this estimate is increased to 2.15 kg/kwe[4]. An array of individually steerable reflecting facets which would concentrate 80 percent of the incident solar flux upon the heat addition stage of the same cycle would weigh about 0.29 kg/M^2[5], resulting in a specific mass of 0.83 kg/kwe for the collector. The choice between the concentrator and the reactor hinges upon the quantity of shielding specified. It is assumed that, if a large reactor is permitted to be launched into orbit at all, concern for the result of a possible unscheduled return to earth will cause the heavier shielding to be required.

*kg/kwe = kilogram/electric kilowatt

Thus the solar concentrator will have a large mass advantage over the nuclear reactor.

A photocell array, which does not require a power cycle at all, might well weigh as little as 1.36 kg/kwe by 1990 [6]. Any reasonable estimate of the mass of the electricity generating cycle results in photocells providing the least massive system but proposed solutions to the problem of placing them into orbit intact have raised the volume requirement to very high levels. For example, one might separate layers with empty space by attaching them to the walls of the shuttle and putting them in tension. Interlayer separation would need to be enough to avoid them striking one another during periods of high induced vibration. This method, while avoiding mass increase from buffer material, still fills up shuttle volume rapidly. The relative fragility of photocells led us to choose a thermodynamic power cycle in our scaling estimates.

The system conceptual design will include a reflector, composed on individually steerable facets, which concentrates incident solar radiation onto the heat addition stage of either a thermodynamic or magnetohydrodynamic cycle. Recently, a space-based solar Brayton cycle composed of modules designed to generate a minimum of 1000 megawatts of electricity over 30 years of service has been described[7]. System specific mass, exclusive of transmission equipment, is 4 kg/kwe, of which the radiator system accounts for about one-half. Radiator mass can be expected to scale from this larger module to systems discussed in this study and it is assumed that the rest of the equipment does also. For the purposes of this study, the implication of each of two specific mass figures will be examined. In the conceptual designs for this study, two improvements on the above figure will be assumed. Specifically, it will be assumed that the radiator mass can be reduced by one-half through the use of a high temperature version of an aluminum tube and teflon composite panel described by Cox, et. al.[8] as a replacement for stainless steel, and that the rest of the system mass can be halved through use of high technology materials and through designing for one year of activity rather than thirty. In addition to this, the consequences of failure to reduce the 4 kg/kwe figure will be discussed. In summary, a specific mass of 2 kg/kwe for production

of electricity will be assumed and the changes from the baseline case that occur if only 4 kg/kwe is realizable by 1990 will be discussed.

For the rather modest temperature of the laser waste heat (≤575 K), there is little question that lightweight radiator panels of the type mentioned above will be available within 10-15 years. In fact, two designs which are nearly suitable have already been reported in the literature[8]. In both of these, the panels are made of a sandwich-like composite material. The outer layer is Teflon which provides strength and resistance to radiation damage. A highly conducting wire mesh, which provides the lateral heat conductance is bonded to the teflon. The third layer is a film of silver deposited on the teflon-wire mesh combination which reflects the incident solar radiation which passes through the teflon. In the reference cited, a two-sided radiator is described in which the tubes through which the heat exchanging fluid flows are exclosed between two such three-layer compositions. The spacing of the tubes and the thickness of the materials in the composite are described as being selected to obtain minimum weight per unit of heat radiated. Precise dimensions are not now available in the literature. The composite material is stored rolled up like a window shade and deployed by fluid pressure. In the second design a hard flexible tube composed of spring-deployed aluminum which is stored in a helical pattern provides the support for the composite material. The latter, which has a wet specific mass of 1.67 Kg per square meter of panel area and an effective temperature range of 180-420°K, has already been tested in concept by a small "test article"[8]. For the scaling analysis, a slight mass reduction to 1.6 kg/m^2 and an increase in temperature range to include 550 K are projected for 1990. Only one-sided radiation is assessed so that, panel area and radiator area are the same. The excess mass estimate inherent in this scaling figure covers the stiffening required for a single side of the sandwich.

3.3 LASER COMPONENTS

3.3.1 Power Conditioning

The power conditioning equipment is required to convert the primary high voltage ac electrical power to dc sustainer power, dc electron gun power, and low voltage ac control power. This will necessitate the use of

transformers, rectifiers, and filters. The discussion of the design concepts chosen for these components will be deferred to Section 4. It is clear, however, that the use of advanced concepts can result in small weights and volumes for these components. For the scaling analysis, it was anticipated that the weight of the power conditioning would be less than ten percent of the total laser weight. Therefore this was ignored in the baseline system scaling. This was indeed justified during the system conceptual design, as discussed in Section 4.

3.3.2 Compressors

The compressor, which restores the stagnation pressure lost by the laser gas in the loop, is also a small part of the system. Scaling techniques described by Young & Kelch[1] will be used to obtain approximate masses and volumes for the units required for our loops. In that work, axial compressors were found to be superior to centrifugal in adiabatic efficiency and smaller in diameter for corrected mass flows of 16-68 kg/sec and pressure ratios of 2.0-3.5. The systems considered here are within or near enough to those ranges to indicate that the axial compressor is better for our purpose. Linear extrapolation of Figure 24 from Young & Kelch, (A nearly linear curve of adiabatic efficiency versus compressor work per unit mass of gas) yields values of compressor efficiency for systems considered here between 0.850 (1 MW space laser) and 0.863 (1 MW airborne laser). For convenience, a constant value of 0.86 was adopted for all compressors in this study.

Well-designed axial compressors provide 1.2-1.3 pressure ratio (PR) per stage. Thus, if a PR of 1.95 is required, 3 stages are assumed since $(1.95)^{1/3} \simeq 1.25$. Mass and length per stage are scaled by Young & Kelch as follows:

$$\text{Mass} \sim (M_s)^{1.3}$$

$$\text{Length} \sim (M_s)^{0.5}$$

in which M_s is the corrected mass flow, defined by

$$M_s = \frac{\dot{M}\left[\frac{T}{T_s}\,\frac{W_s}{W}\right]^{1/2}}{P/P_s};$$

where

$\dot{M}$ = actual mass flow

T, P, W = temperature, pressure, mean molecular mass of laser gas

T_s, P_s, W_s = temperature, pressure, mean molecular mass standards

The usual standard conditions are $T_s = 288°K$, $P_s = 1$ atm., $W_s = 28.8$.

The compressor scaling for the 1 MW airborne system is a typical example of the procedure outlined above.

Reference Case (after Ref. 1)		1 MW Airborne EDL
$\dot{M}_s$ (kg/sec)	17.9	20.5
PR	3.42	1.64
No. of Stages	6	2 ($1.64^{1/2} = 1.28$)
Rotor Diameter (cm)	40	43 $\left(= 40 \times \sqrt{\frac{20.5}{17.9}}\right)$
Length of 2 stages (rotors + stators) (cm)	27	29 $\left(= 27 \times \sqrt{\frac{20.5}{17.9}}\right)$
Mass (kg)	290	115 $\left(= 290 \times \frac{2}{6} \times \left(\frac{20.5}{17.9}\right)^{1.3}\right)$

3.3.3 Heat Exchangers

Preliminary evaluation indicated that plate-fin, gas-to-liquid, counter-flow heat exchangers made of aluminum are capable of providing the required temperature control with low mass and pressure drop. Table 3-3 shows the performance parameters of such a design for a trial case similar to the 1 MW airborne design. Heat exchanger mass will clearly be a minor part of any of the systems considered. Higher laser gas temperatures are required in the space-based cases by considerations

TABLE 3-3. HEAT EXCHANGER PERFORMANCE FOR A 1 MW SYSTEM

Coolant	JP4
Heat load (megawatts)	2.22
Coolant flow rate (m^3/sec)	0.020
Gas pressure drop (torr)	51
Heat exchanger mass (Kg)	210
Heat exchanger volume (m^3)	0.40

discussed in Section 3.4. Therminol 55, a heat exchanger liquid that does not vaporize at such temperatures has been chosen for those systems.

3.3.4 Electron Guns

An electron gun (E-gun) provides external control of the discharge in the laser cavity. The injected high energy electrons maintain the laser medium conductivity at the level needed to input the electrical power by partially ionizing the gas. This control of the conductivity permits separate selection of the sustainer electric field and the input electrical power (since there is now no fixed relation between current and field). As will be discussed in Section 3.4, the efficiency of coupling of the discharge power into the gas depends strongly upon the electric field.

A number of E-gun types have been described in the literature. In the thermionic emitter, the cathode is heated to high temperature (2000 K) and emits electrons which are then extracted and accelerated by electric fields. A directly heated device of this kind is a wire made of, e.g. tungsten, with a current flowing through it. The need to be its own heater dictates that the cathode not be overly large in cross section. More flexibility in choice of cathode shape and material is provided if the functions of electron emission and heating are separated, that is, if the cathode is indirectly heated. Whether the cathode is directly or indirectly heated, thermionic emitters are vulnerable to poisoning, i.e., deterioration in

emission performance due to chemical reaction, since the temperature is necessarily very high. Thus, a high vacuum (10^{-6} torr) is needed. In addition, the elevated temperature makes for irreversible damage should the cathode be accidently exposed to the atmosphere. A cold cathode would not be vulnerable to poisoning and vacuum failure damage. A simple field emission device is not useful for cw systems since the electrons are being extracted by a field high enough to simulate a short circuit between the electrodes. This type of electron generation is suitable only for an output of short bursts of electrons. The plasma cathode gun is a cold cathode device which does not suffer from this difficulty. In this type of E-gun, as Figure 3-2 suggests, a hollow cathode discharge is maintained and electrons are extracted therefrom. This device does not require a high vacuum (pressure $\sim 20\mu$) and is not susceptible to poisoning. Another difficulty common to all the above guns is illustrated in Figure 3-2. The emitter has to be at high negative voltage with respect to the laser cavity. Typically the cavity is at ground and the emitter is at high negative potential.

The Ion Plasma E-gun developed recently at Hughes reduces the ubiquity of high voltage. Ions, rather than electrons, are extracted from a plasma and accelerated into a cold cathode. The electrons emitted as a result of the collisions are then accelerated through an exit window into the laser cavity as shown in Figure 3-3. Although the cathode must still be maintained at high negative voltage, the plasma discharge need not be and so modulation is done with respect to ground. Devices of this type have been built and successfully operated at Hughes and are light and quite rugged. The Ion Plasma gun is included in all laser systems in this study.

The exit window, which separates the laser cavity from the electron gun, is vitally important since the high voltage electrons must pass through it and therefore interact with it. Because scattering depends upon the thickness of the foil material and upon the square of its atomic number, it is important to use a low Z material that is as thin as possible and still be able to withstand the pressure difference across it (1/2-1 atmosphere). One mil beryllium is chosen as the best answer to these requirements.

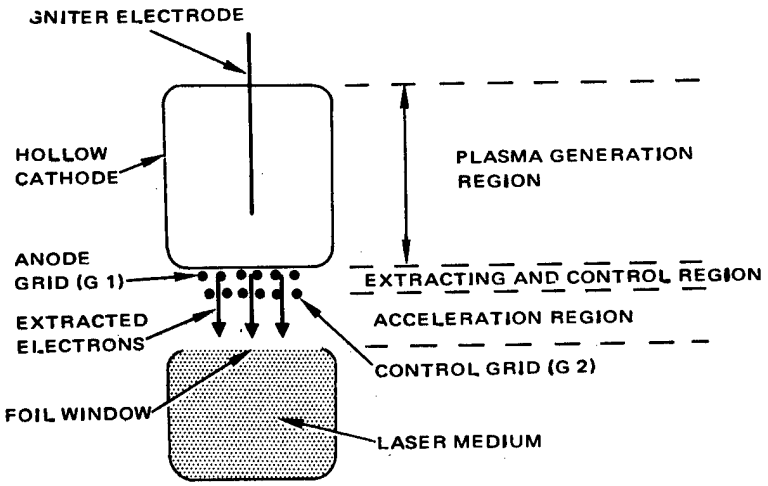

a. Cross section of structural design

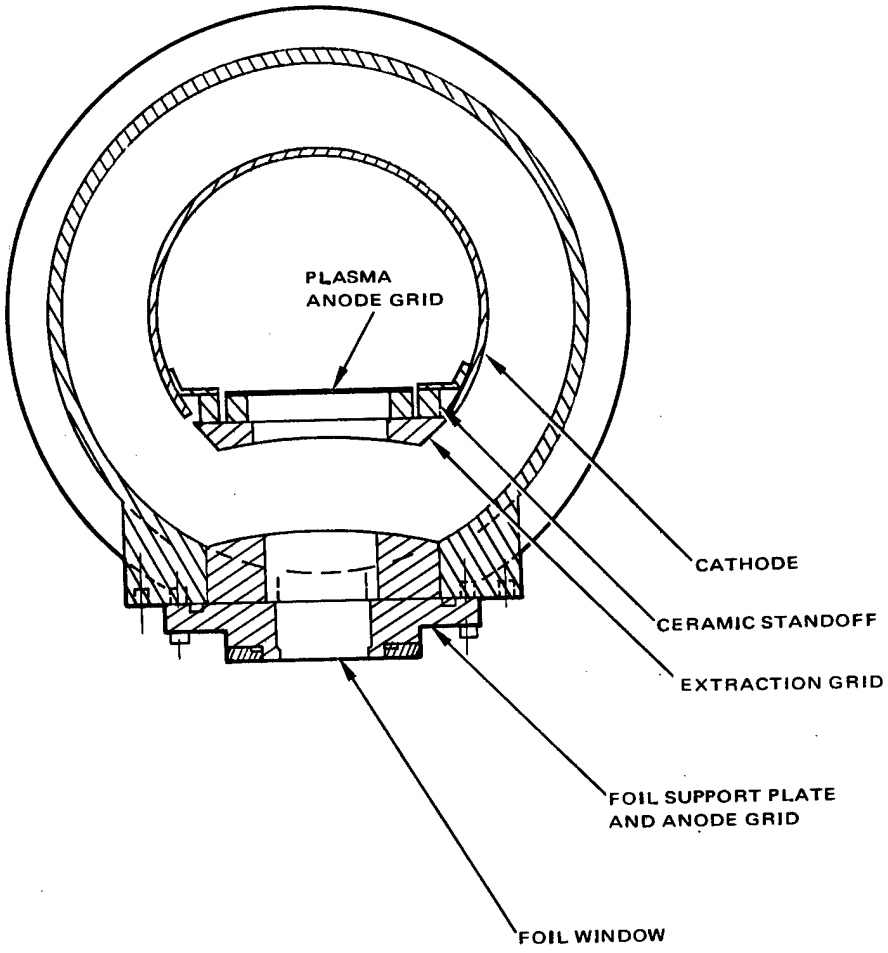

b. Operating schematic

Figure 3-2. Plasma cathode electron gun.

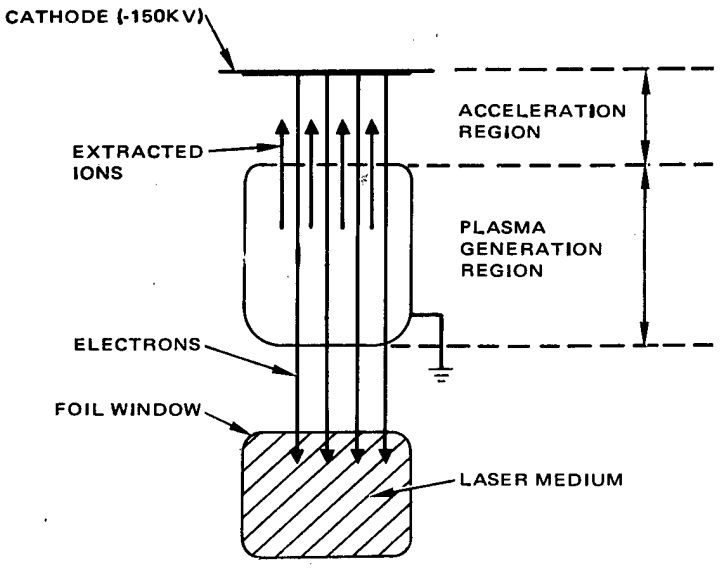

a. Operating schematic

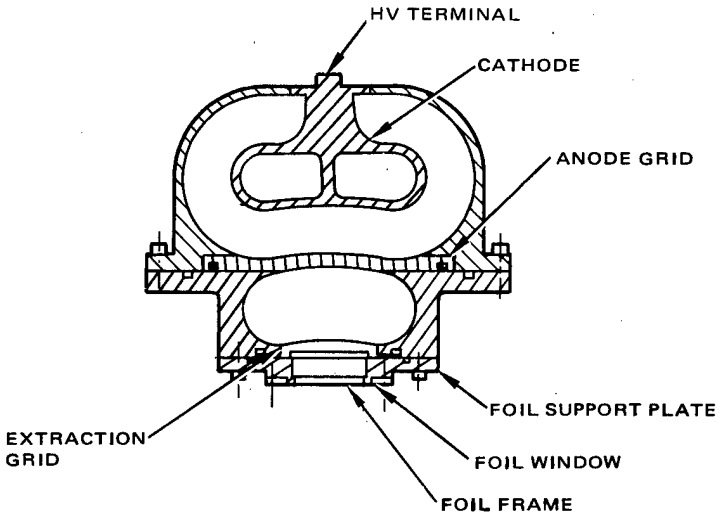

b. Cross-section of structural design

Figure 3-3. Ion plasma electron gun.

3.3.5 Nozzles

The usual method for designing two-dimensional nozzles at Hughes uses the hodograph transformation equations of Libby and Reiss [9]. Flow separation is prevented by requiring that the velocity increase monotonically through the nozzle. This design has had wide and successful application, but one may wish for a more compact contraction section than it dictates. For the contraction ratio of 4.86 in our 1 MW airborne system, a nozzle length of about 135 cm results from use of the hodograph method.

Morel[10] has described a new method of designing two-dimensional nozzles using two intersecting cubic arcs to determine the shape of the wall. Although it is not clear that cubic arcs are optimal for two-dimensional design (Morel found it so for axisymmetric nozzles), for the same 1 MW airborne case, Morel's method produces a nozzle about 74 cm long. It seems reasonable to assume that this or some similar design procedure will, by 1990, enable one to build reliable nozzles of about the length which the cubic design indicates. Therefore, such a nozzle design will be assumed for the system scaling.

3.3.6 Diffusers

In order to provide sufficient pressure recovery for efficient heat exchanger and compressor operation, a diffuser must be used to decelerate the flow emerging from the laser cavity. The use of vanes permits a much wider-angled and therefore shorter diffuser. Figure 3-4 shows a typical design of this sort. There is little doubt that efficient pressure recovery is possible with a $2\theta = 40°$, as Figure 3-5 indicates.[11] Although data on the 5-vaned diffusers is not available, it is anticipated that a value similar to the 4-vaned value shown can be realized, producing a pressure recovery coefficient of about 0.7. The scaling study will use this number and 5-vaned diffusers will be assumed.

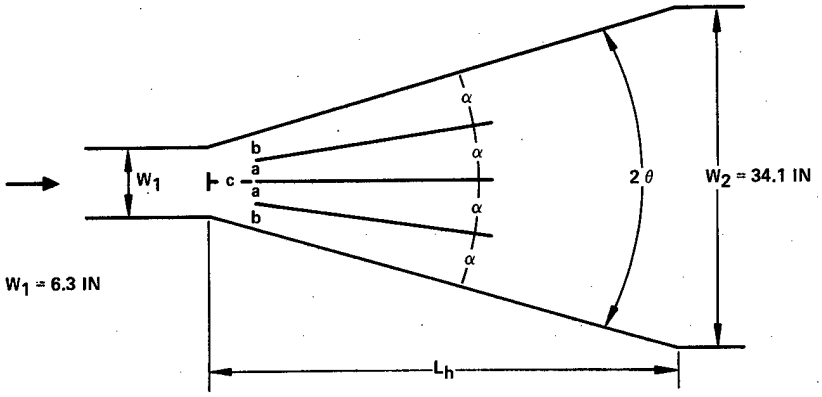

3 VANE DIFFUSER

M_1 = 0.6; M_2 = 0.11	2 θ = 32°	a = 1.51 IN
R_1 ≈ 10^6	α = 8°	b = 1.82 IN
δ^*/W_1 ≈ 0.05	A_r = 5.41 (AREA RATIO)	c ≈ 4.1 IN
C_p ≈ 0.71*	AS ≈ 5 (ASPECT RATIO)	f = 24.22 IN
η_D ≈ 0.73*	L_h = 4.04 FT	

*ESTIMATE

Figure 3-4. Typical diffuser design.

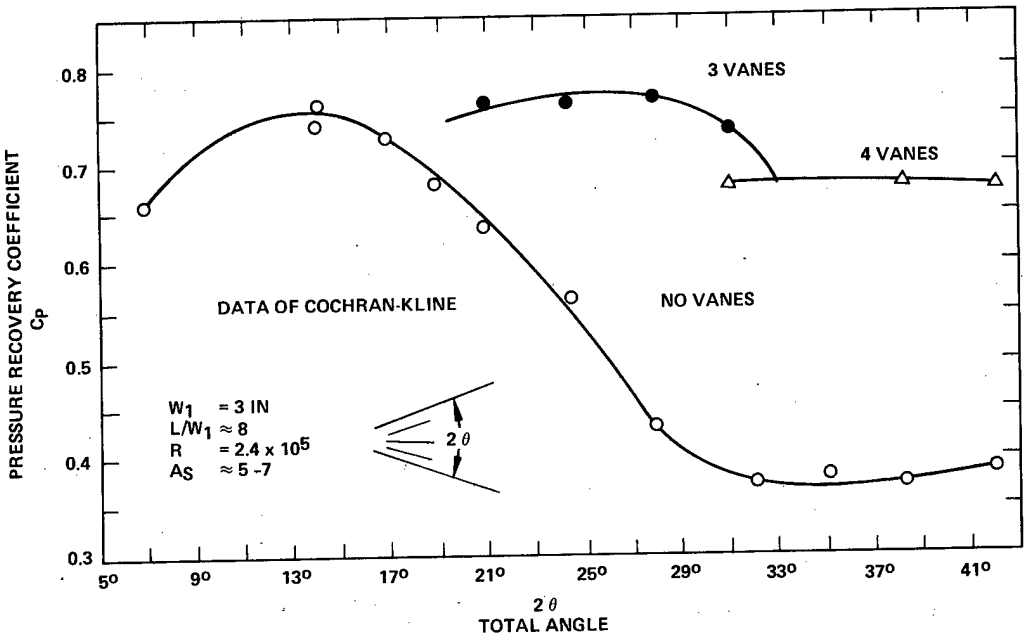

Figure 3-5. Diffuser pressure recovery.

3.3.7 Optical Extraction

A confocal unstable resonator is the most likely choice for these systems. However, in a large system, alignment sensitivity and beam quality can be adversely affected by use of a single large resonator, with many limiting aperatures and a long gain path inside the resonator. The use of a Master Oscillator-Power Amplifier (MOPA) configuration may offer the opportunity to have a well-defined higher quality resonator mode subject to lower distortion levels. In a MOPA configuration, a small master oscillator (most likely an unstable resonator) covering part of the excited laser medium provides a high quality laser beam which is then amplified in the remaining medium to achieve the desired power. In the amplifier portion, power is extracted from the laser medium with a simple optical pass. Threshold gain, per unit length in the oscillation, however, is larger and extraction efficiency here suffers slightly. In a very high power system where the oscillator output flux is very high, sufficient saturation may be present in the single pass amplifier to provide good extraction efficiency there. The effect was analyzed, in the 10 megawatt system, of dividing the optical train at various points into an oscillator and an amplifier. The results are shown in Figure 3-6. (It is assumed that the remainder of the active medium is in the amplifier pass.) For example, dividing the gain medium equally into a master oscillator and a power amplifier results in a 2.7 percent loss in cavity extraction efficiency. During the detailed design effort this loss will be weighed against the engineering advantages of such a configuration. This will involve the actual package geometry. For example, a large number of folds in the optical train will impact the beam quality degradation in the resonator and tend to favor a MOPA configuration. For the scaling analysis, a simple unstable resonator geometry was utilized.

The selection of geometric output coupling can be done without much reference to the inlet pressure, temperature, etc. so long as the system remains highly saturated. Figure 3-7 shows that low output coupling results in the highest efficiency, which is to be expected for constant input power since threshold gain is then lowest. (Effective reflectivity is defined as one minus the output coupling.) Low outcoupling does not produce a beam which iw well confined in the far field, as Figure 3-8 shows. In the unstable

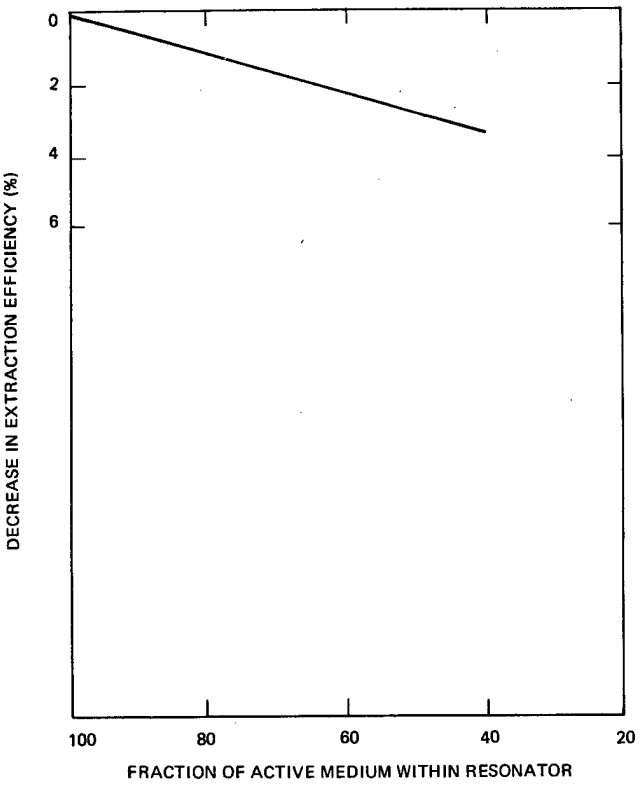

Figure 3-6. Effect of division of resonator into MOPA.

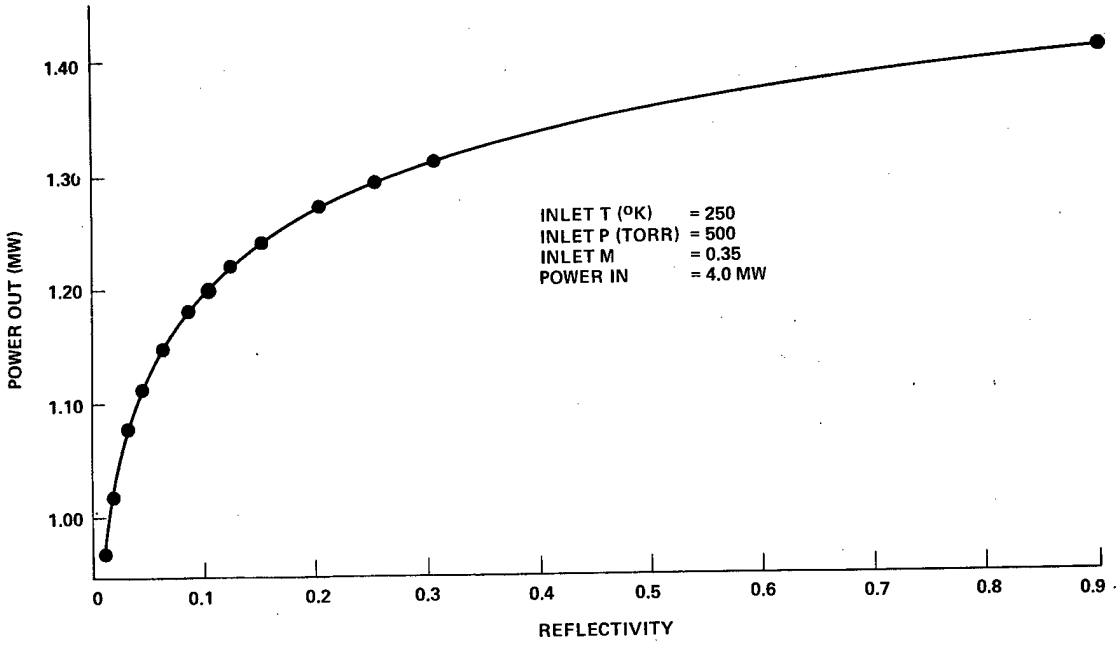

Figure 3-7. Extraction versus effective reflectivity.

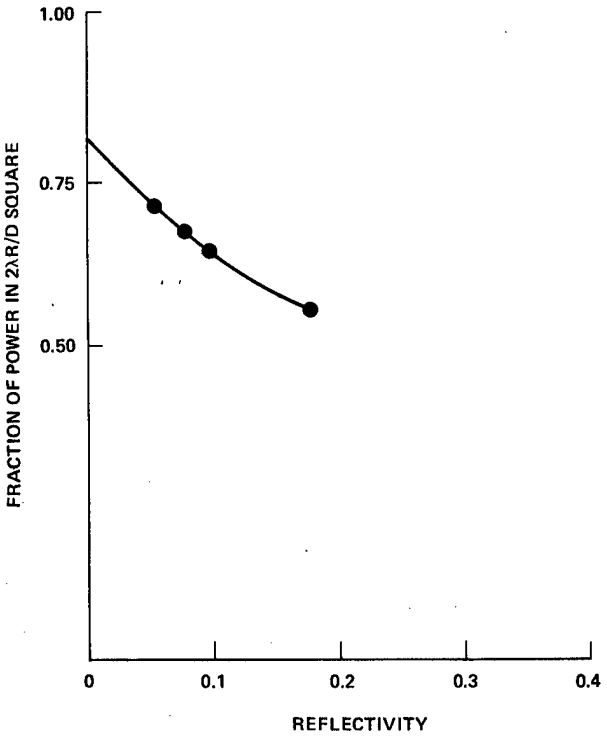

Figure 3-8. Relative far field power versus effective reflectivity. (Percent of near field power).

resonator, this result is easy to anticipate since low output coupling corresponds to a thin annular output beam. Figure 3-9, the product of the previous two figures, indicates that 96 percent output coupling produces the highest power on target. To profit from this high an outcoupling, one would require a beam control system with no more than 4 percent obscuration. The conceptual designs will utilize 90 percent output coupling, which permit them to match up well with more easily implemented 10 percent obscured beam control subsystems. This figure results in 4 percent less far field power than that obtained with a 96 percent outcoupled laser with a 4 percent obscured beam control package. Selection of other system parameters will be seen to be unaffected by the choice made for output coupling.

Another issue to be considered in any optical design is the mirror loading limit to prevent distortion and ultimately burn-out. This, of course, depends upon the mirror design and the reflectivity of the coating. At 10.6 microns, the currently achievable reflectivity on a reliable basis is 99.8 percent. A reasonable projection for 1990 is 99.95 percent. Using

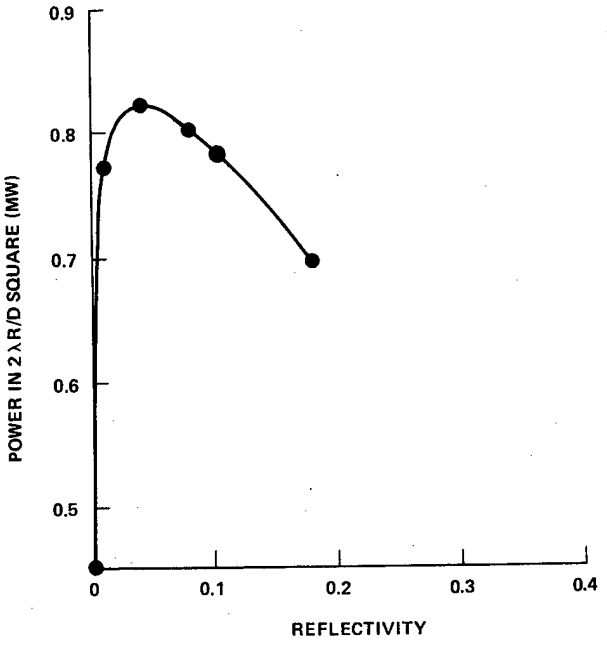

Figure 3-9. Absolute far field power versus effective reflectivity. (Actual power taking into account the variation in extracted power.)

this number, and current mirror designs, to keep the phase distortion under one optical wavelength, the incident flux should be kept below 500 kW/cm^2. (For 99.8 percent reflectivity, the flux limit would be 125 kw/cm^2.) If P_o is the output power, and D is the side of a square mirror (a square output beam is assumed), then the flux density for a ten percent obscured beam is equal to $P_o/0.9\ D^2$. To keep this number below 500 kW/cm^2, the beam sizes for the one, five, and ten megawatt devices must be bigger than 1.5, 3.3, 4.7 cm respectively.

3.3.8 Discharge Cavity

The Hughes computer program, LASER 7, which models the kinetics and gas dynamics of a longitudinal discharge laser cavity, was used to select operating parameters. Small signal gain values calculated by this code agree well with experimental measurements. Power loss mechanisms which are not modelled include diffraction, mirror absorption, aerowindow effects, and boundary layer growth, all of which affect the efficiency of all cases considered to approximately the same extent. These losses therefore do not

affect basic parameter selection. In the final conceptual design, corrections are made for these effects.

The efficiency with which power from the electrical discharge can be pumped into the upper laser level depends upon the gas mixture and the value of the sustainer electric field divided by the number density of gas molecules (E/N) in the discharge region. If E/N is too low, the secondary electrons do not acquire enough kinetic energy between collisions to excite vibrational levels which will feed the upper laser level, while if it is too high, collisional excitation of electronic states and even ionization will occur. Figure 3-10 shows pumping efficiency versus E/N for 6 candidate gas mixtures as computed by numerical solution of the Boltzmann equation using the Hughes Boltzmann code. The longitudinal discharge geometry demonstrated at Hughes[12] provides a nearly constant E/N (variation ≤5 percent). A conditional selection is made here of the mixture in which helium, nitrogen and carbon dioxide are in the molar ratio 8:7:1 because it has the highest peak pumping efficiency. The maintaining of nearly constant E/N is a powerful advantage because electrical arcs tend to appear in the cavity at about 2.4×10^{-16} volt-cm^2, and because the onset of attachment as a significant electron loss mechanism at about 2.1×10^{-16} volts/cm^2 can produce a local

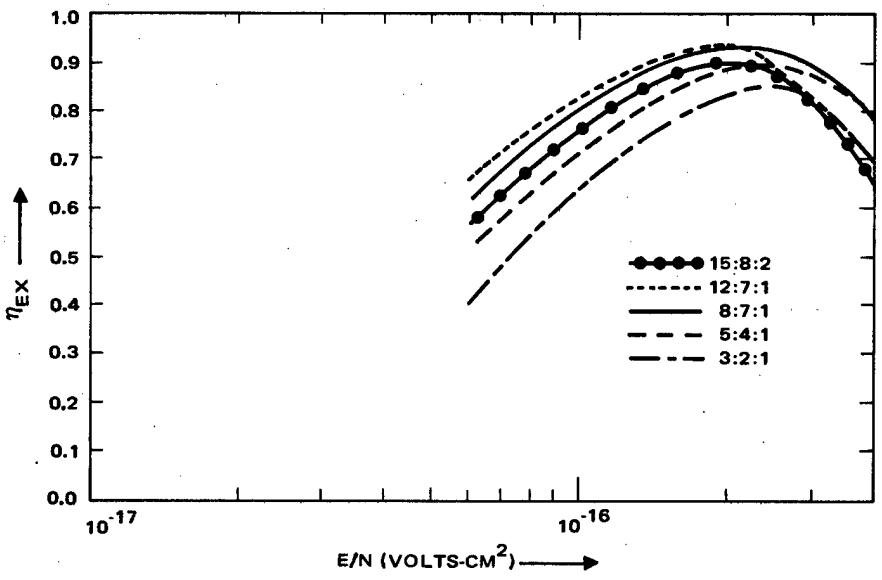

Figure 3-10. Calculated pumping efficiencies as a function of E/N.

E/N instability which drives the system quickly to the arcing regime. For a discharge arrangement in which E/N varied significantly through the laser cavity, unfavorably low E/N (and consequently lowered excitation efficiency) would have to be tolerated in parts of the cavity to avoid arcing.

While selection of an operating point requires variation of the inlet temperature, pressure, and Mach number in combination, single parameter variation about a system which meets the output power goal is a valuable guide to the influences of each. Figure 3-11 initiates the impression that low pressure and temperature are promoters of cavity efficiency. Qualitatively this could be anticipated since the collisional deactivation time of the upper laser level increases with both decreasing temperature and decreasing pressure. Decreasing temperature also decreases thermal population of the lower level. Inlet Mach number influences output power somewhat less over the range of

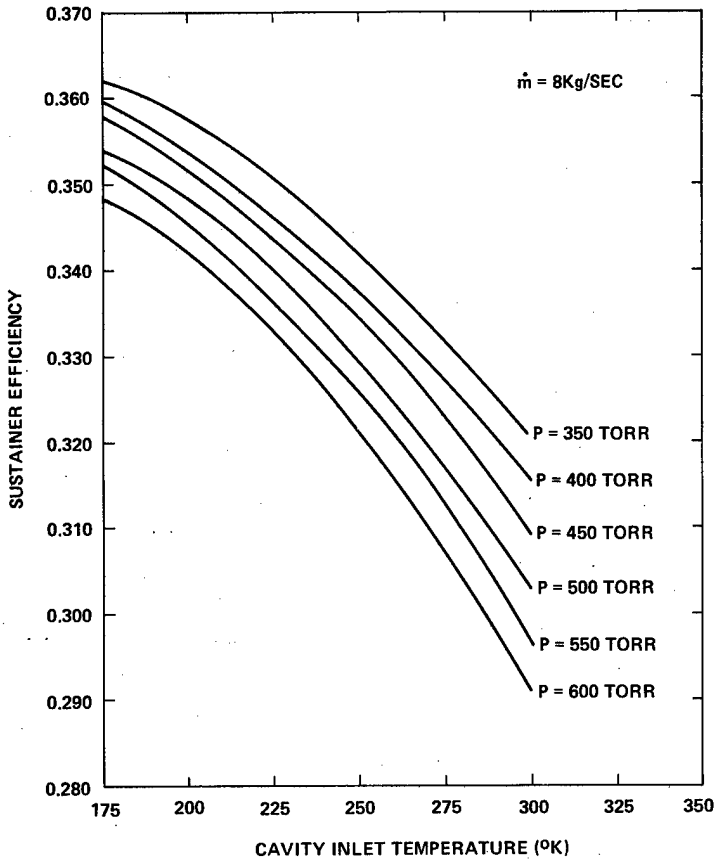

Figure 3-11. Sustainer efficiency versus temperature.

interest then do temperature and pressure, as Figure 3-12 indicates. For a given temperature and pressure, Mach number determines mass flow and a major effect in this figure is the reduced temperature in the latter part of the cavity at higher mass flow.

Figure 3-13 shows the vibrational levels of the CO_2 molecule which are involved in laser transitions. The (00°1) → (10°0) P-branch transition produces the usual 10.6μ radiation, and the (00°1) → (02°0) R-branch transition yields 9.3μ radiation. The choice between them involves a weighting of the advantage of the former, lower threshold gain, against that of the latter, higher quantum efficiency. For a large high gain system, threshold is easily achieved so the lower threshold gain of the 10.6μ line is relatively unimportant. In such systems the higher quantum efficiency at an output wavelength of 9.3μ results in higher extraction efficiency so it will be used in this study. Figure 3-14, when compared to Figure 3-15, provides an idea of the advantage available from this selection.

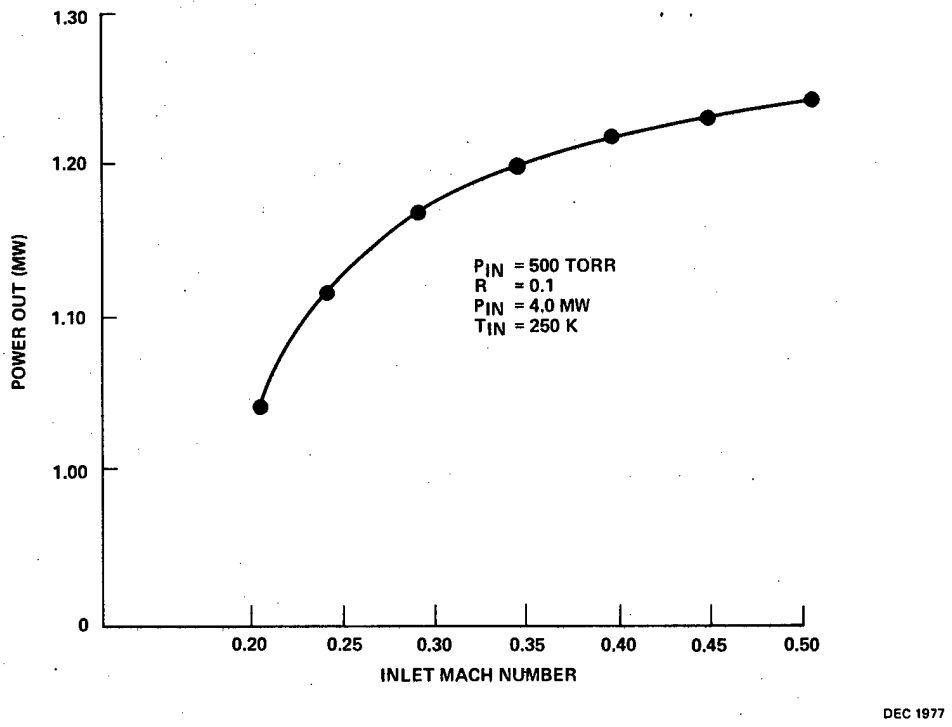

Figure 3-12. Extraction versus Mach number.

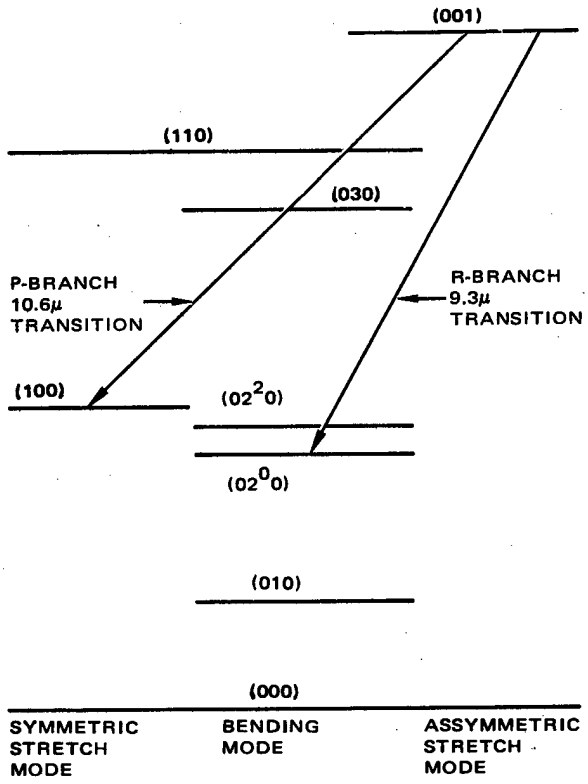

Figure 3-13. CO_2 vibrational energy levels.

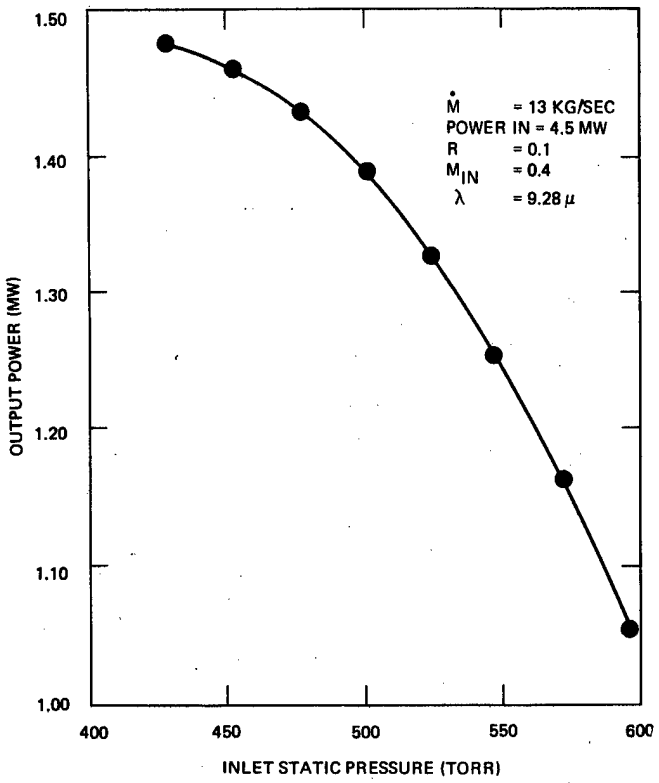

Figure 3-14. Extraction versus pressure (9.28μ).

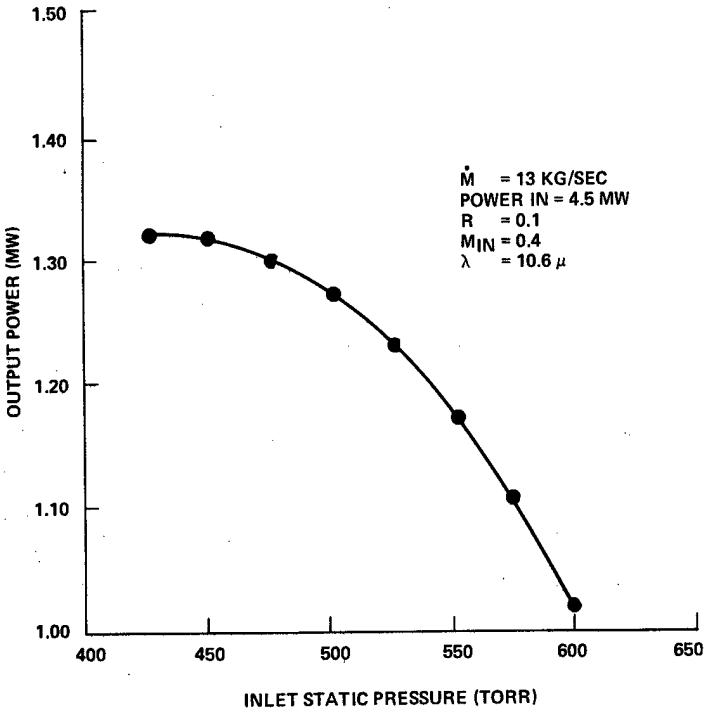

Figure 3-15. Extraction versus pressure (10.6μ).

Sufficient gain length must be used without putting absurd requirements upon packaging or requiring so many folds in the resonator that the optics losses become excessive. For a system with parameters similar to the 1 MW airborne system, Figure 3-16 indicates the effect of gain length upon extraction efficiency maintaining a constant input power. The effect is not great since the system is far from being marginal. Gain length above 300 cm does not enhance cavity efficiency greatly, and so this figure is selected for the 1 MW systems. Beyond this value, both cavity flow-width (i.e., optical length) and mass flow increase with reduced compensation in cavity efficiency. The 4 x 4 cm cavity cross-section chosen allows: high specific power loading without unduly high sustainer current densities which could place severe stresses on electrode designs and/or electron beam current density requirements.

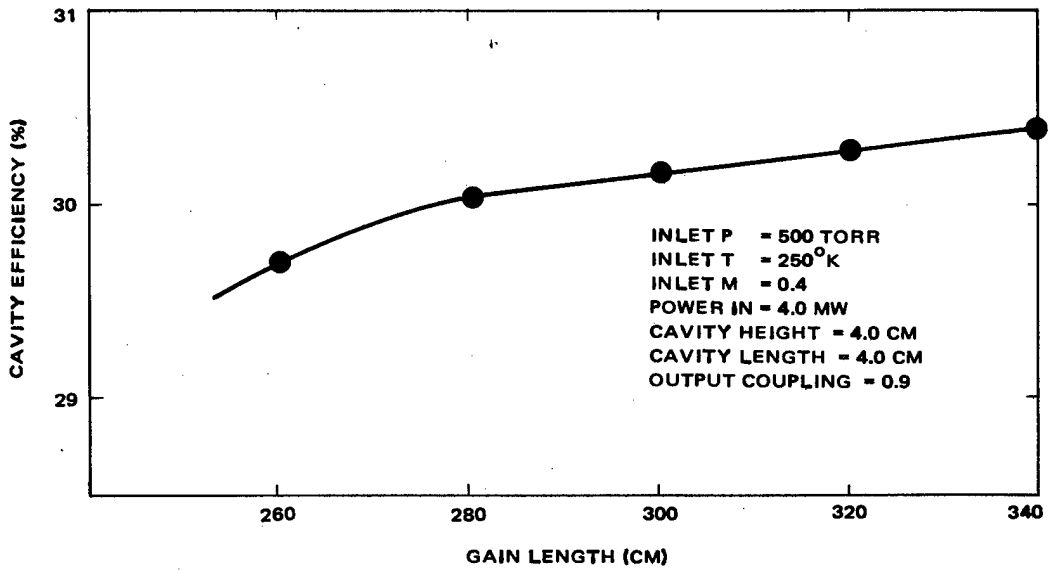

Figure 3-16. Cavity efficiency versus gain length.

3.4 PARAMETER SELECTION

3.4.1 Airborne Systems

As already stated, the task here is almost equivalent to finding which parameters result in the lowest input sustainer power. "Almost" because the use of chilled JP4 as the coolant places a lower bound upon the cavity inlet temperature. This multiconstituent fuel becomes somewhat slushy before actually freezing so it was assumed that 220 K, the lowest temperature at which military jet aircraft must be certified, is the JP4 minimum. This turned out to limit cavity inlet temperature to ≥ 250 K.

The 8:7:1 gas mix provides the most efficient system because of its higher pumping efficiency. With low pressure already seen to be very advantageous, the idea is to select a Mach number and pressure combination that provides enough mass flow so that the flow does not choke in the diffuser. The combination of M = 0.4 and pressure equal to 350 torr gives the best cavity performance for the 1 MW system among those sets of parameters which avoid flow-choking downstream. For example, Figure 3-17 shows the manner in which cavity efficiency varies with pressure in the vicinity of the selected parameters. As expected, it decreases monotonically with increasing pressure. The pressure below which choking occurs at the efficiencies calculated is indicated.

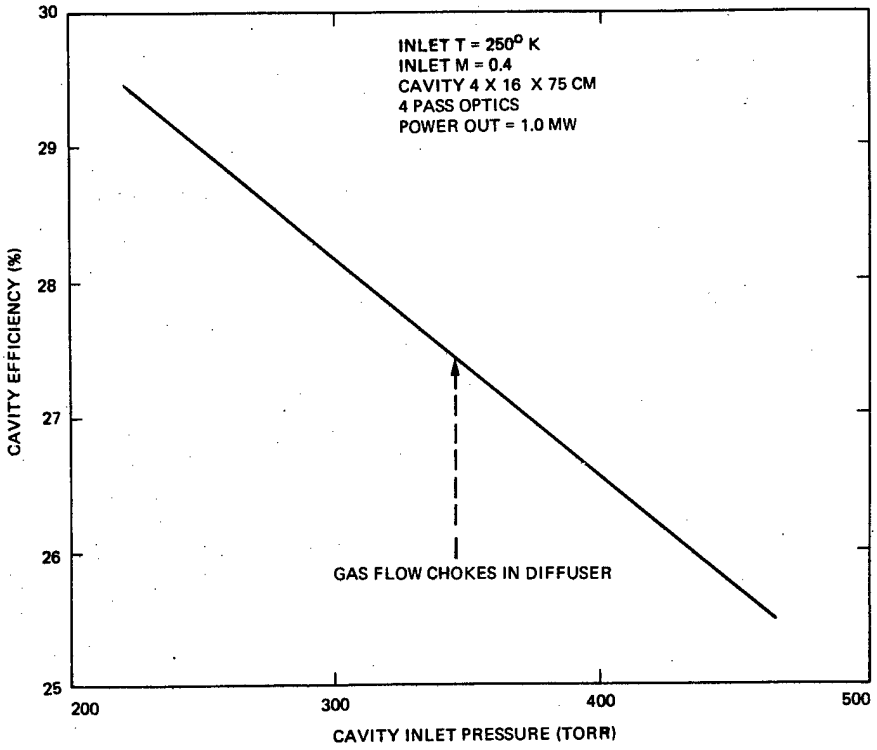

Figure 3-17. Cavity efficiency versus pressure.

Because the design considerations are the same for the larger systems as for the 1 MW system the same set of parameters is optimal for them. Cavity optimization is equivalent to system optimization for the airborne cases, so these parameter sets form the bases for the more detailed conceptual designs. Table 3-4 summarizes the airborne laser system parameters.

3.4.2 Space Systems

The goal of mass minimization requires the consideration of means to raise the temperature at which waste heat is radiated above the levels which are compatible with an efficient cavity in an ordinary closed cycle system. Two means to this end are available - namely 1) raising cavity inlet temperature and 2) use of refrigeration. The former is self-explanatory and the latter involves compressing the laser gas to a higher pressure than that required to produce correct cavity inlet pressure. It exchanges waste

TABLE 3-4. AIRBORNE SYSTEM PARAMETERS

Output power (MW)	1	5	10 - 2 cavities of 5 MW output dimensions chosen for packaging reasons
Output wavelength (μ)	9.3	9.3	
Inlet Mach no.	0.4	0.4	
Inlet temperature (K)	250	250	
Inlet pressure (Torr)	350	350	
Gas Mix $He:N_2:CO_2$	8:7:1	8:7:1	
Mass flow (kg sec^{-1})	7.79	38.97	
Cavity width (cm)	75	200	
Output coupling	0.90	0.90	
No. optical passes (cm)	4	6	
Cavity length (cm)	4	5	
Cavity height (cm)	16	30	
Sustainer power (MW)	3.644	15.859	
Compressor power (MW)	0.619	2.204	
Electron beam power (MW)	0.085	0.381	
Allowance for pumps (MW)	0.025	0.125	
Total electrical power (MW)	4.373	18.569	
Efficiency	22.9%	26.5%	

heat at the resulting higher temperature with the heat exchanger fluid and is then expanded through a turbine to reduce pressure and recover some of the excess compressor work done upon the gas. Figure 3-18 shows in simplified form the difference between a laser loop that uses refrigeration and one that does not. Both temperature raising schemes involve considerably more input energy.

In the figures and tables which follow in this section, a scaling of the comparatively small system elements - compressors, turbines, laser loop ducting, electron beamguns, and power conditioning equipment according to Davis and Wilcox[3] is assumed. Since these elements are subject to more thorough design in this study, the more detailed engineering analysis elsewhere in this report results in different final numbers for these than used in

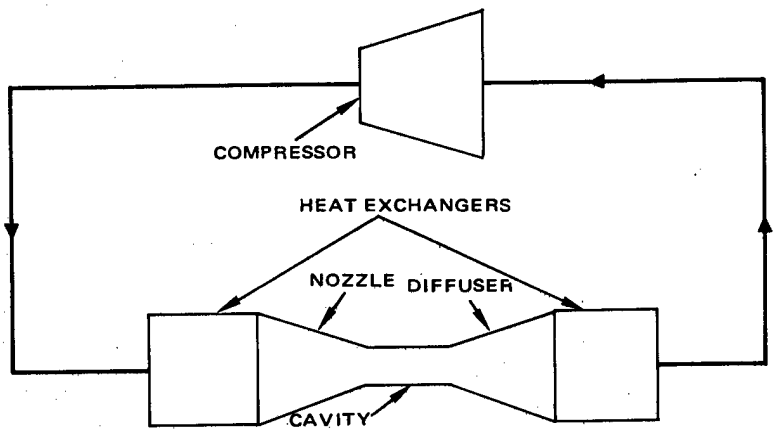

Figure 3-18. (a) Laser loop of the type used in airborne systems.

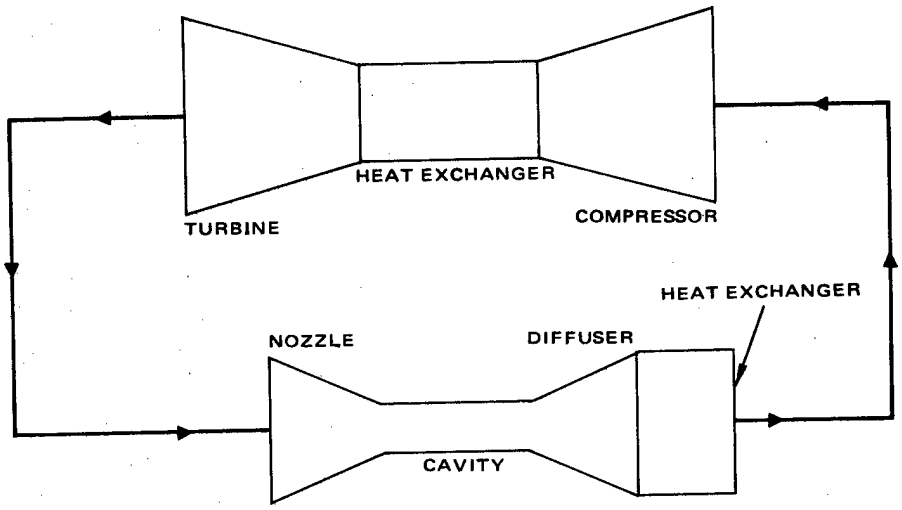

Figure 3-18. (b) Refrigerator laser loop for space systems.

the scaling. They are not major fractions of the mass and are not terribly sensitive to electrical power requirement so the system parameters selected in this section are not altered by a more detailing sizing of the minor constituents of the laser loop.

The combination of inlet conditions and effective radiation temperature providing the least massive system must be selected, where it is understood that raising the radiating temperature is done at an appreciable energy cost. Figure 3-19 presents the curve containing the operating conditions providing

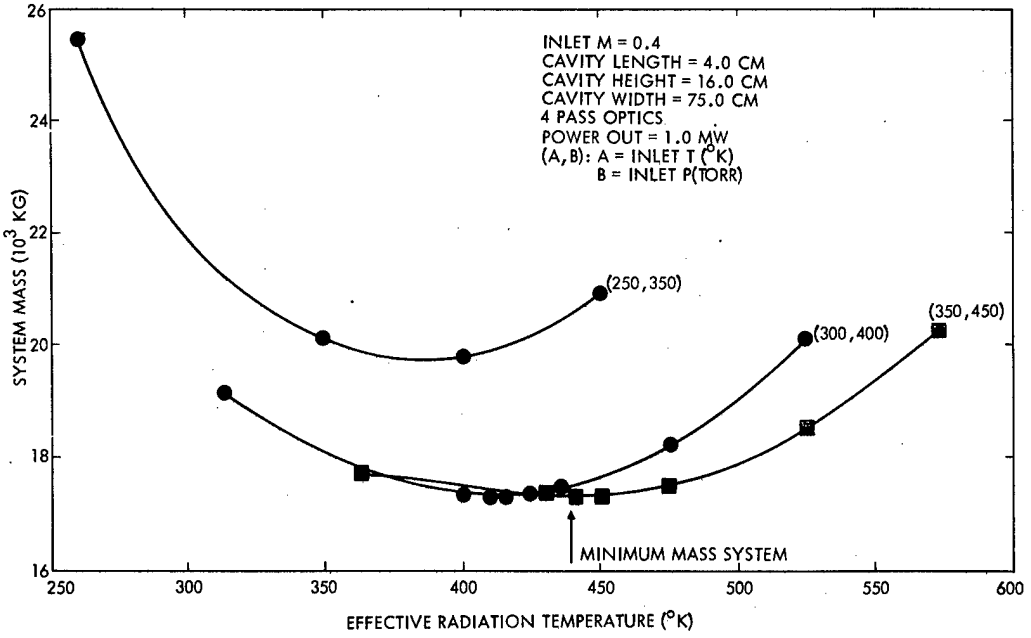

Figure 3-19. System mass versus effective radiation temperature for 2 kg/kwe electric power production system (1 MW laser output power).

the lightest system as well as some representative curves whose minima are higher than that for the curve on which inlet pressure is 450 torr and inlet temperature is 350°K. The figure illustrates the method of selection and covering it with all of the pressure-temperature combinations considered would render it unreadable. In the same spirit, Figure 3-20 points out that different inlet conditions are desirable if one adopts 4 kg/kwe as the mass of the electrical power supply system. In that case, the growth of the power production system overcomes the decrease in radiator size with increasing radiation temperature at a lower cavity temperature because it is a much larger part of the total mass. Figure 3-21 presents the 2 kg/kwe results for the 5 MW system while Figure 3-22 shows the cavity parameters providing the least total mass if the 4 kg/kwe power supply figure is assumed. Packaging considerations (as discussed later) lead to the design for a 10 MW system consisting of two parallel 5 MW systems. Therefore the same parameters apply for both the 5 MW and the 10 MW power levels.

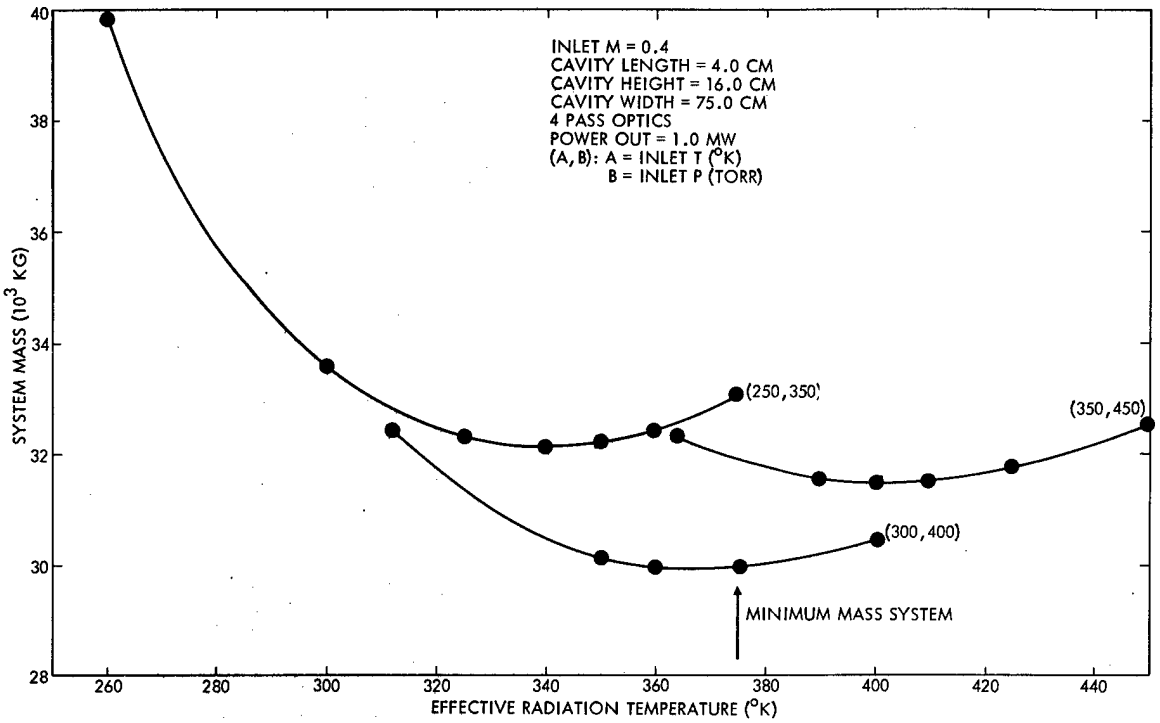

Figure 3-20. System mass versus effective radiation temperature for 4 kg/kwe electric power production system (1 MW laser output power).

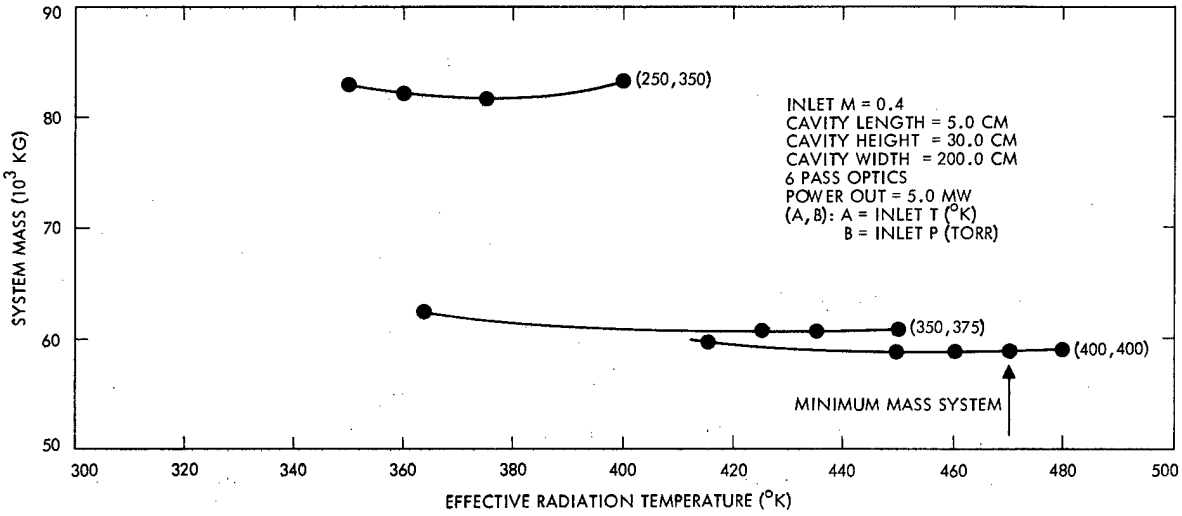

Figure 3-21. System mass versus effective radiation temperature for 2 kg/kwe electric power production system (5 MW laser output power).

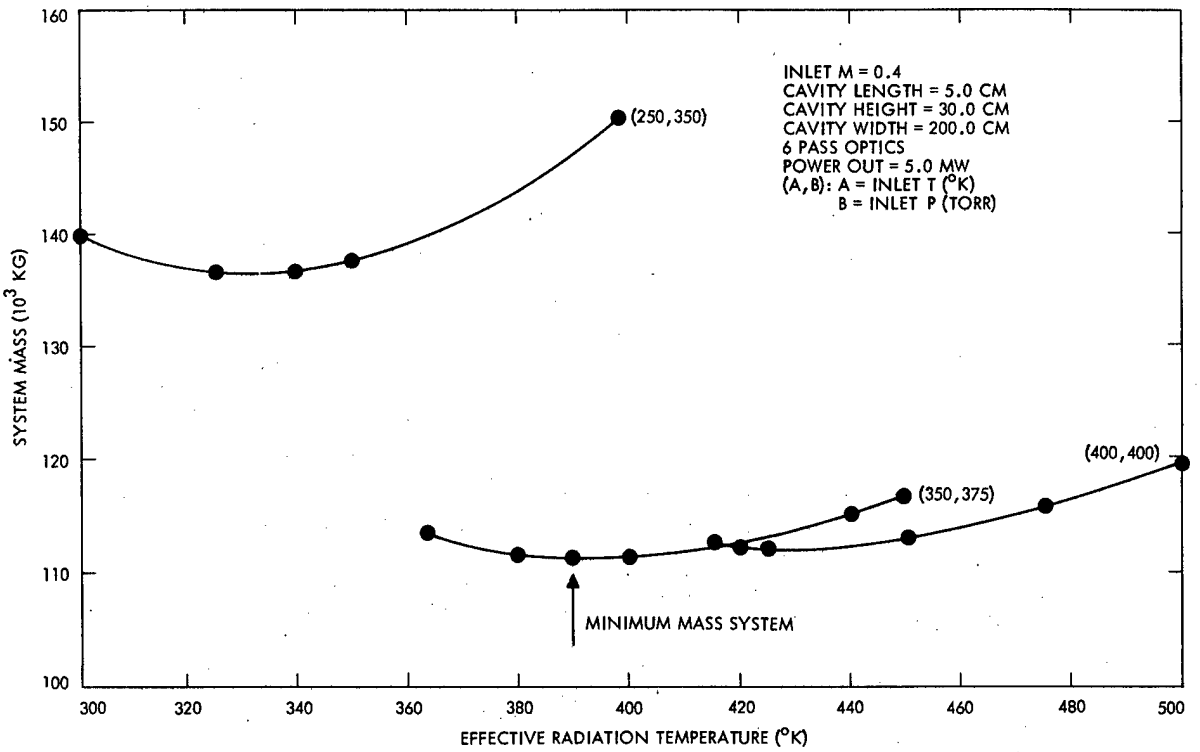

Figure 3-22. System mass versus effective radiation temperature for 4 kg/kwe electric power production system (5 MW laser output power).

It is of interest to note that, for space based operation, minimization of the mass of the various laser systems has driven the operating points away from the low temperature and pressure regime most conducive to high cavity efficiency. The advantage of 9.3μ over 10.6μ output wavelength is now not so obvious. A comparison between the two wavelengths at the cavity operating conditions selected for the space based system is presented in Figure 3-23. Cavity efficiency provides an accurate comparison because, for fixed inlet conditions, higher efficiency means that both input electrical power and waste heat are lower. It is seen that the intersection point of the two curves is near 1 MW output power. Table 3-5 is a summary of parameters for the space-based cases, including a 1 MW, 10.6μ system. Table 3-6 summarizes the parameters if one uses the assumption that the solar-to-electric power conversion system will weigh 4 kg/kwe rather than 2 kg/kwe, the baseline assumption.

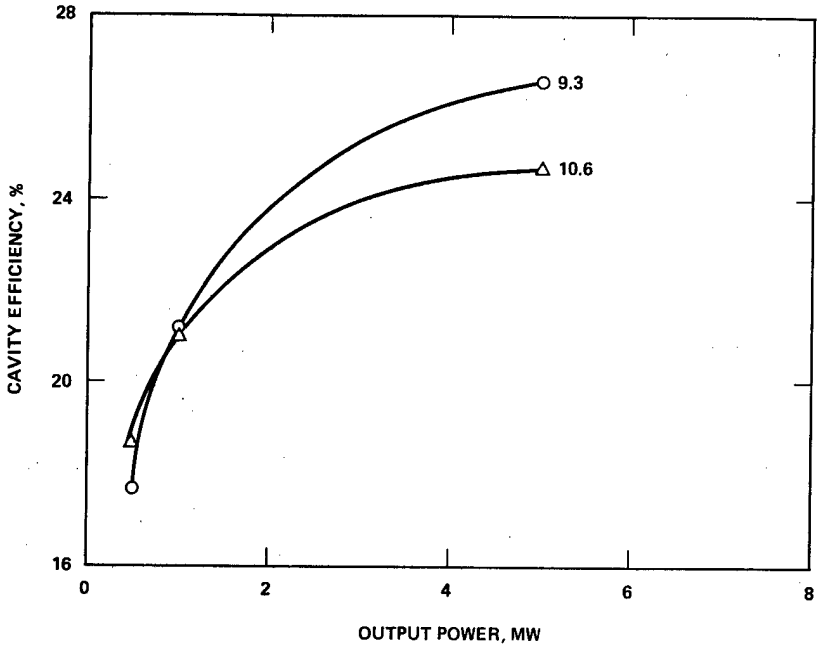

Figure 3-23. Comparison of 9.3μ to 10.6μ.

TABLE 3-5. SPACE SYSTEM CONCEPTUAL DESIGN PARAMETERS (2 kg/kwe)

System	1 MW, 9.3μ	1 MW, 10.6μ	5 MW, 9.3μ	10 MW, 9.3μ - a double 5 MW system
Gas Mix He:N_2:CO_2	8:7:1	8:7:1	8:7:1	
Inlet Pressure (Torr)	450	450	400	
Inlet Temperature (°K)	350	350	400	
Inlet Mach Number	0.4	0.4	0.4	
Mass Flow (kg/sec)	8.47	8.47	35.21	
Cavity Width (cm)	75	75	200	
No. Optical Passes	4	4	6	
Output Coupling	90%	90%	90%	
Cavity Length (cm)	4	4	5	
Cavity Height (cm)	16	16	30	
Sustainer Power (MW)	4.720	4.783	18.750	
Net Turbo Power (MW)	1.675	1.699	4.761	
Electron Beam Power (MW)	0.203	0.204	0.874	

(Continued next page)

(Table 3-5, concluded)

Allowance for Pumps (MW)	0.025	0.025	0.125
Total Power (MW)	6.623	6.711	24.510
Efficiency	15.1%	14.9%	20.4%
Preliminary Mass Estimate (10^3 Kg)	17.32	17.55	58.74

TABLE 3-6. SPACE SYSTEM PARAMETERS FOR 4 KG/KWE

System	1 MW, 9.3μ	5 MW, 9.3μ	10 MW, 9.3μ
Gas Mix He:N_2:CO_2	8:7:1	8:7:1	A double 5 MW system
Inlet Pressure (Torr)	400	375	
Inlet temperature (°K)	300	350	
Inlet Mach number	0.4	0.4	
Cavity width (cm)	75	200	
Cavity height (cm)	16	30	
Cavity length (cm)	4	4	
No. of optical passes	4	6	
Output coupling	90%	90%	
Sustainer power (MW)	4.037	17.310	
Net turbo power (MW)	1.294	3.513	
Electron beam power (MW)	0.140	0.700	
Allowance for pumps (MW)	0.025	0.125	
Total electrical power (MW)	5.496	21.648	
Efficiency	18.2%	23.1%	
Preliminary mass estimate (10^3 Kg)	29.9	111.4	

4.0 CONCEPTUAL DESIGNS (CO_2 SYSTEMS)

The objective of the conceptual design effort was the translation of component material and performance specifications into realistic weight and volume allocations and overall synthesis into a packaged system configuration. The system packages for the five and ten megawatt airborne CO_2 EDL systems were configured to fit within the cargo envelope of the C5A aircraft. The 1 MW airborne package is sufficiently small that other aircraft can be used as the host. The space-based systems have been configured for transportation in the space shuttle. The weights and volumes of the one and five megawatt laser systems allow transportation within the space shuttle of the laser systems; the ten megawatt system is approximately 30 percent heavier than the shuttle capacity. In the case of the one megawatt system, the laser system, solar collecting power generator, and waste heat disposal system together, are within the weight capability of the space shuttle. The following sections will discuss the various laser system components. The overall system packages will be discussed at the conclusion of this section.

4.1 POWER SUPPLY SYSTEMS

The laser power supply system consists of two basic parts — the prime power generation and the power conditioning. The distinction is indicated in Figure 4-1. Prime electrical power is generated at a voltage slightly higher than the sustainer voltage. This is then conditioned to meet the system requirements.

In the airborne systems, gas generators and superconducting alternators have been selected for prime power. The system electrical requirements and the resultant weights and volumes are shown in Table 4-1. A

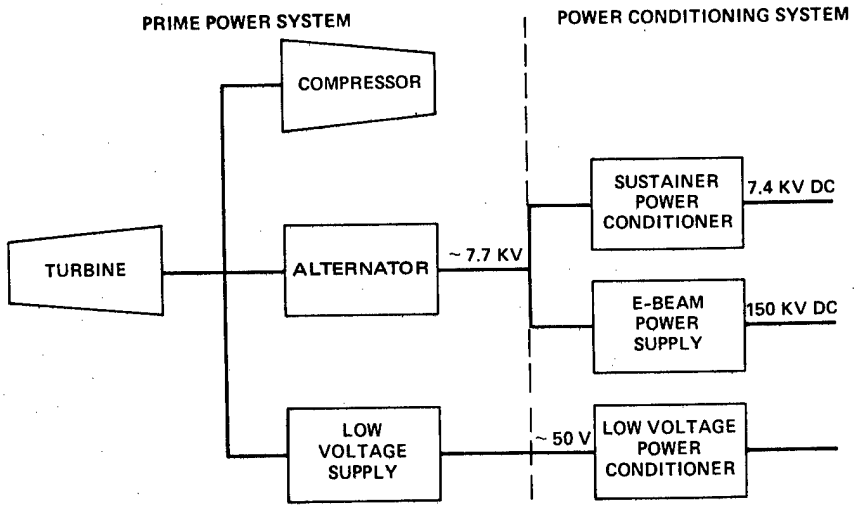

Figure 4-1. Power supply system.

TABLE 4-1. PRIME ELECTRICAL POWER SOURCE — AIRBORNE SYSTEMS

Gas generator with superconducting alternator Fuel: JP4/liquid O_2, 2/1				
	Prime Power (MW)	APU Mass (kG)	Specific Mass (kG/MW)	Volume (M^3)
1 MW	4.35	500	115	0.34
5 MW	19.1	1850	97	1.14
10 MW	38.0	3460	91	2.01

A separate turbo-compressor is used to circulate the gas. (The "turbine" shown schematically in Figure 4-1 is really two turbines, each integrated into either a compressor or alternator.) For the space-based systems, solar energy operates a Brayton cycle generator to provide prime power. The turbine shaft power is used to circulate the gas and to drive an electric generator. The system requirements are summarized in Table 4-2. In

TABLE 4-2. POWER REQUIREMENTS – SPACE SYSTEMS

Power Conditioning
- Sustainer (5 - 20 - 40 Mwatts, 7.4 kV)
  - Rectifier
  - Filter
  - Interrupter switch
- Electron gun (200 - 875 - 1750 kwatts, 150 kV)
  - Transformer
  - Rectifier
  - Filter
  - Interrupter switch

Prime Power
- Mechanical (Compressor Drive)
  - 2.6 MW, 7.6 MW, 15.2 MW
- Electrical (7.7 kV)
  - 4.1 MW, 15.9 MW, 31.8 MW

Total
- 6.7 MW, 23.5 MW, 47.0 MW

these systems, part of the mechanical power, as explained in Section 3, is recovered and converted to electricity. For example, the electric power requirement for the one Megawatt system from table 3-5 is approximately 5.0 Megawatts. Of the 2.6 Megawatts of prime mechanical power, 900 kilowatts is recovered. Thus, the prime electrical power requirement is only 4.1 Megawatts. The estimated prime power system weights for the space-based system are shown in Table 4-3.

The power conditioning for all systems is basically the same. A typical sustainer power conditioning circuit (rectifier and filter) is shown in Figure 4-2. The rectifiers and filters convert the ac voltage to the dc voltage and the ripple level required for the excitation region. The switch S_1 inserts resistance at turn-on to prevent LC ringing and overshoot. The components

TABLE 4-3. PRIME POWER SOURCE – SPACE SYSTEMS

Collector composed of individually steerable facets concentrates solar flux into heat addition stage of Brayton cycle			
	Collector Mass (10^3 kG)	Brayton Cycle Mass (10^3 kG)	Alternator Mass (10^3 kG)
1 MW	8.6	4.2	0.268
5 MW	31.6	21	0.762
10 MW	63.3	42	1.327

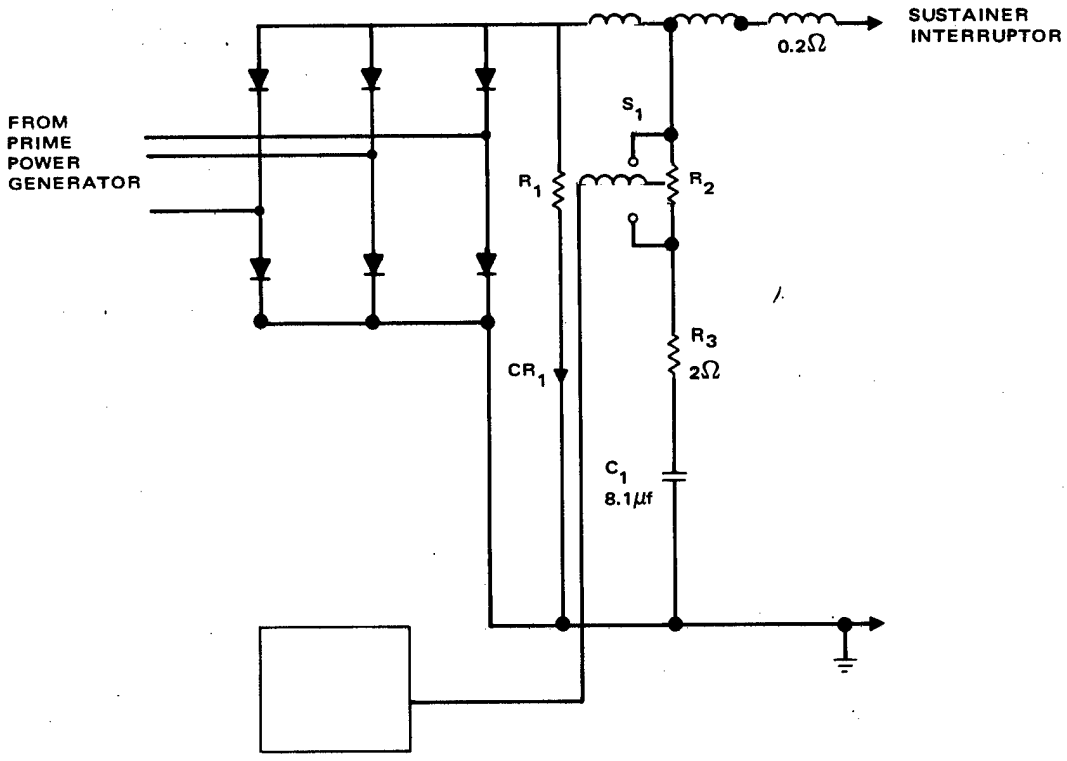

Figure 4-2. Sustainer rectifier/filter design.

R_2 and CR_1 damp out the stored LC energy during an arc to prevent high voltage damage and allow rapid turn-on.

In addition, there is a sustainer interrupter circuit to prevent damage during an arc. The sustainer/interrupter delays sustainer current at turn-on and also interrupts the flow of sustainer current during an arc. The sustainer/interrupter is a Hughes-developed dc current interrupter which during an arc causes a pulsed interruption in the sustainer current for enough time to allow an SCR stack to recover the forward blocking capability — the interruption being generated by releasing the energy stored in the interrupter choke. A simplified schematic is shown in Figure 4-3.

The electron gun power conditioning will not be completely independent but will take the rectified voltage from the sustainer rectifier and convert this to the required 150 kilovolts for the electron guns. The output of the sustainer rectifier goes to an inductor input filter. The inductor will limit surge currents and will reduce conducted electromagnetic interference. The output of the filter then goes to the 150 kV resonant charging power supply which consists of multiple resonant charging SCR switching circuits and a flyback transformer. A simplified schematic of the proposed design is shown in

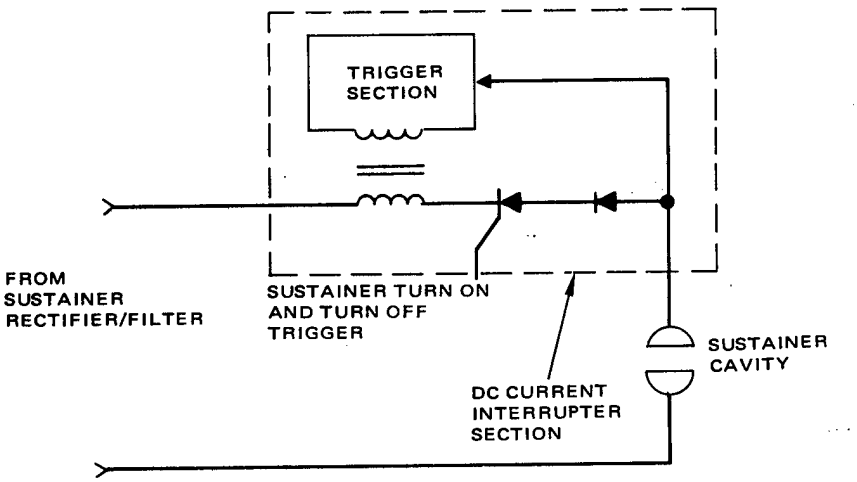

Figure 4-3. Sustainer interrupter design.

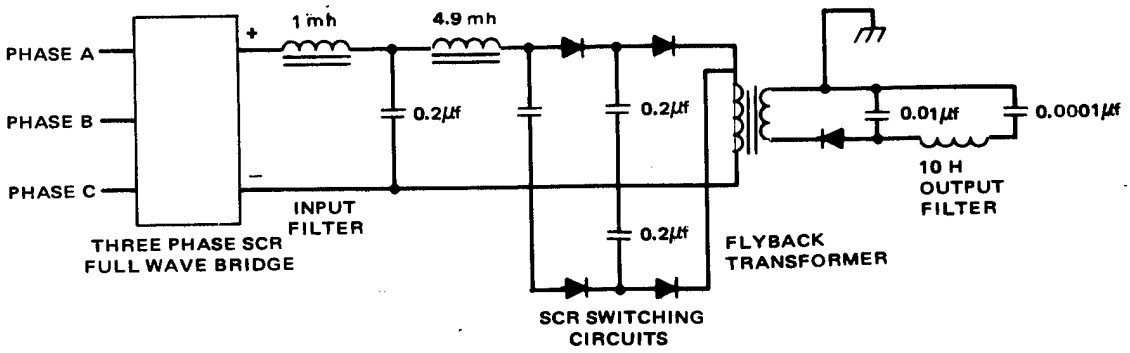

Figure 4-4. Electron gun power conditioning design.

Figure 4-4. The actual final filter component values and switching repetition rate will be determined by the value of the leakage inductance in the flyback transformer. Since the proposed resonant charging scheme transfers energy through a flyback transformer, the output voltage is regulated by sensing the output voltage and feeding that signal back to the drive circuits, controlling their switching rate (number of resonant charging cycles performed per second). The advantage of this design is that it may have its output shorted indefinitely without damage to any of its components.

Power conditioning volume and weight estimates including packaging and cooling (but no pumps or external heat exchangers) are shown in Table 4-4.

4.2 EXCITATION REGIONS

The excitation region consists of the inlet nozzle, laser cavity, and diffuser, as illustrated schematically in Figure 4-5. The estimated dimensions are also shown. Typical laser nozzle designs in current use at Hughes are based on a hodographic design technique. The cubic nozzle design discussed in Section 3 has been chosen for this future application and results in a shorter nozzle design. Nozzle inlet-to-outlet area ratios are shown on Table 4-5, along with estimated lengths.

TABLE 4-4. POWER CONDITIONING VOLUME AND WEIGHT ESTIMATES

	1 MW		5 MW		10 MW	
	Vol (ft^3)	Wt (lbs)	Vol (ft^3)	Wt (lbs)	Vol (ft^3)	Wt (lbs)
Sustainer Rectifier/ Filter	4	250	6	350	10	500
Sustainer Interrupter	1	39	2	46	3	70
Electron Gun Power Conditioning	4.5	107	4.5	119	4.5	130

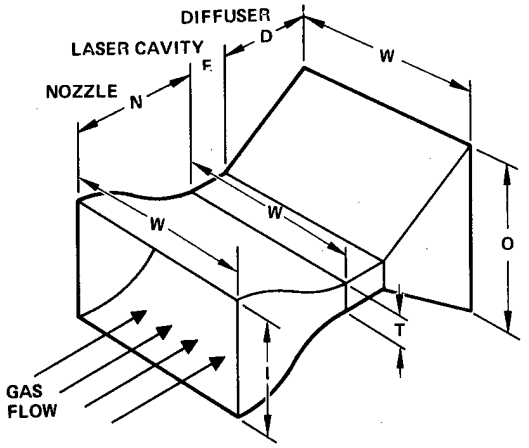

	POWER	I (CM)	T (CM)	O (CM)	W (CM)	N (CM)	E (CM)	D (CM)
AIRBORNE	1	77.7	16	104	77.7	73.7	20	104
	5	203	30	171	203	128.2	37.5	193.7
	10*	203	30	171	203	128.2	37.5	193.7
SPACE	1	79.5	16	99.3	77.7	73.7	20	114.3
	5	161.5	30	167.6	203	128.3	37.6	189.5
	10*	161.5	30	167.6	203	128.3	37.6	189.5

*TWO CAVITIES OF THESE DIMENSIONS ARE EMPLOYED

DEC 1977

Figure 4-5. Excitation region.

TABLE 4-5. NOZZLES

	Area Ratio	Length (cm)
1 MW-airborne	4.86	73.7
5 MW-airborne	4.40	128.3
10 MW-airborne	4.40	128.3
1 MW-space	5.10	77.3
5 MW-space	4.73	137.9
10 MW-space	4.73	137.9

The diffuser design is based upon one-dimensional expansion using multi-vane diffusers, as illustrated in Figure 4-6. The diffuser parameters are shown in Table 4-6; the number of vanes has been chosen so that the expansion per "wall" is in the optimal 7^{o}-10^{o} range.

The laser cavity is scaled on the basis of a longitudinal (parallel to the gas flow) sustainer discharge enabling the maintenance of high E/N and consequently high excitation efficiency. In addition, nearly perfect discharge confinement is achieved. Porous screen electrodes are used with the anode upstream of the cathode. Since recent experimental work at Hughes[12] indicates that high power loadings can be achieved and the discharge model

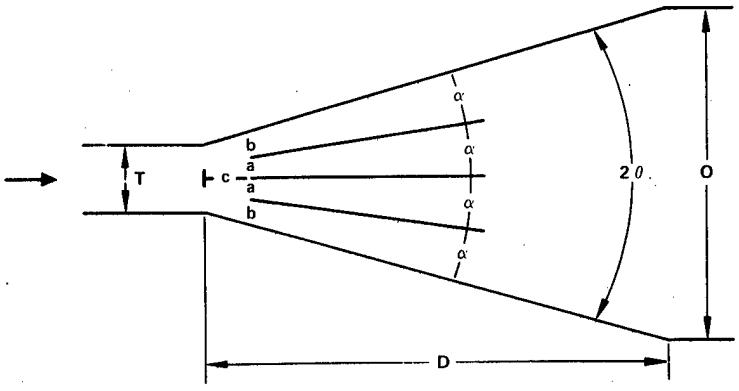

Figure 4-6. Typical diffuser design.

TABLE 4-6. DIFFUSERS

Vaned, diffusion in one dimension. Expansion per "wall" in optimal 7^{o}-10^{o} range					
	2θ (^{o})	No. Vanes	Length (cm)	Area Ratio	Pres. Recovery (CP)
1 MW-air	40	5	46.8	6.5	0.7
5 MW-air	40	5	75.0	5.7	0.7
10 MW-air	40	5	75.0	5.7	0.7
1 MW-space	40	5	44.3	6.2	0.7
5 MW-space	40	5	71.8	5.5	0.7
10 MW-space	40	5	71.8	5.5	0.7

used accurately predicts small signal gain and gas density, the cavity scaling can be made with confidence. Referring to Figure 4-5, the dimension labelled T is sufficiently large that at the gas pressures of interest it is desirable to have two electron guns, one on either side of the flow channel, to insure good medium coverage. Accordingly the designs have allowed for two guns in the weight, volume, and electrical power budgets.

4.3 ELECTRON GUNS

Each laser excitation section will have two ion plasma electron guns mounted to it. The principals of operation of this gun have been previously discussed in Section 3.3.4. In addition the electrical and mechanical design concepts have been indicated. The required electron beam current density into the medium has been computed as part of the sustainer cavity scaling. The electron beam requirements are tabulated in Table 4-7. Using these requirements and the cavity sizes specified in Section 4.2, the electron gun power requirements shown in the last column have been estimated. (The powers in the one and five megawatt systems are for two guns per system;

for the ten megawatt system, four guns are required.) The estimated gun sizes and weights are shown in Table 4-8. The weights are for a single gun of the size indicated. The diameter refers to the cylindrical outer shell diameter.

TABLE 4-7. ELECTRON GUN ELECTRICAL PARAMETERS

	Voltage (kV)	Current Density (ma cm^{-2})	Power (MW)
Low power-air	150	0.47	0.085
Medium power-air	150	0.42	0.381
High power-air	150	0.42	0.762
Low power-space	150	1.13	0.203
Medium power-space	150	0.97	0.874
High power-space	150	0.97	1.750

TABLE 4-8. ELECTRON GUN MECHANICAL PARAMETERS

	Airborne			Space		
System Power	1 MW	5 MW	10 MW	1 MW	5 MW	10 MW
Number	2	2	4	2	2	4
Diameter (cm)	25.4	25.4	25.4	25.4	25.4	25.4
Length (window) (cm)	77.7	203	203	77.7	203	203
Length (cm)	103	228	228	103	228	228
Weight (kg.)	59	104	104	59	104	104

4.4 RESONATORS

Because the details of the excitation section are not defined, the precise resonator optics cannot be defined either. It is known that because of the strong coupling between the electrical power loading, the optical power extraction, and the gas density, an inhomogeneous refractive index variation will be present. This will most assuredly require compensation on each pass through the medium by a figured folding mirror. The precise nature of this optical figure depends upon the resonator output coupling and Fresnel number as well as the parameters mentioned above. The specification of the optical figure will probably contain terms through fourth order, and fabrication by a computer controlled polishing machine will be required. In any case, all the one and five megawatt systems will be folded unstable resonators. The ten megawatt systems will be master oscillator/power amplifier (MOPA) configurations with half of each system serving as an unstable resonator master oscillator. In all cases, square beams will be used for maximum medium coverage. This will also provide more uniform extraction transvers to the flow direction than would circular beams.

Line selection to obtain the 9.3 micron (001) → (020) R-branch transition can be achieved by either of two methods. The first method is the use of a diffraction grating in the resonator. This grating would be mounted in Littrow for the appropriate wavelength and would be designed to have sufficient dispersion to prevent other lines from oscillating simultaneously. Current technology is adequate for fabricating such gratings on cooled substrates for use at low powers. However, the substrate absorption is five to ten times greater than with ordinary mirrors; this presents serious problems at high power. Grating fabrication is being improved and it is possible that this absorption will be reduced substantially in the near future. The alternative wavelength selection method involves the use of selective reflectivity coatings in the resonator mirrors. Special coatings would be required on several of the resonator folding mirrors in order to prevent oscillation on the higher gain (001) → (100) P-and R-branch and (001) → (020) P-branch transitions. This method is feasible with current technology, although

coating durability is a question. Development over the next several years should solve this problem. Thus, in the 1990 time frame it is likely that two line selection methods will be available. If coating technology is appropriately developed, it is the more convenient choice.

4.5 EXIT WINDOWS

Either an aerodynamic or a material window can be considered. The material window has the advantages of lesser system weight, volume and complexity. It has the capability of supporting high pressure ratio and accommodating rapid variation in ambient environment. On the other hand, the window absorbs a small portion of the incident beam flux, mostly through surface absorption. The absorbed energy sets up a temperature gradient in the solid and causes beam degradation. Excessive surface absorption may even cause the structural failure of the window material.

The rotating solid window provides a means to distribute the incident beam over a larger window area and hence to reduce the beam flux through

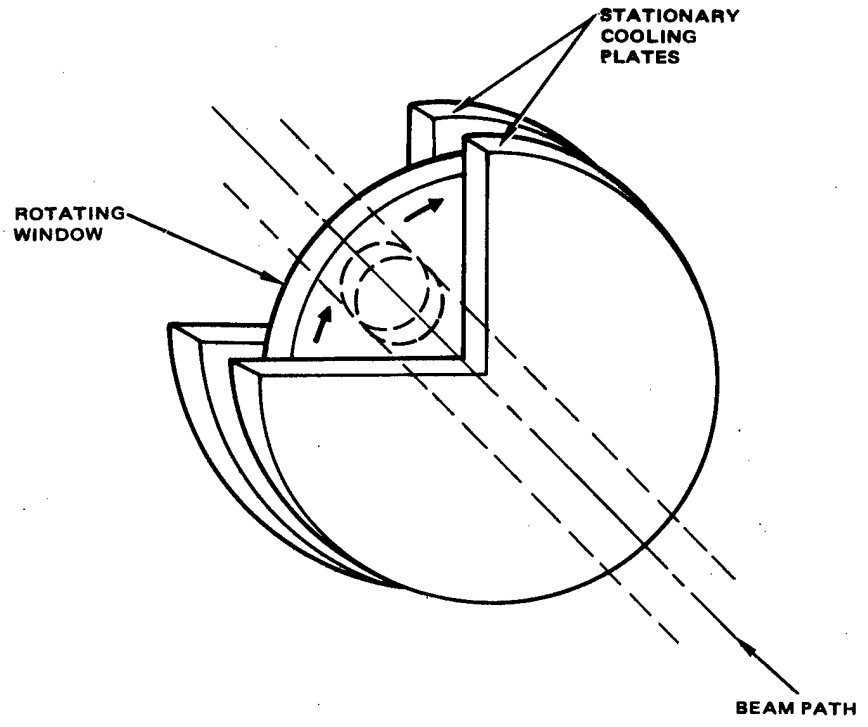

Figure 4-7. Rotating window concept.

the window. Recent analysis [13] indicated that a rotating ZnSe window as shown schematically in Figure 4-7 is capable of accommodating the incident beam flux of 50,000 watts/cm^2 without risk of structural damage. However, the beam degradation caused by the thermal gradient in the solid may be the limiting factor of the solid window in high energy laser applications. To reduce the surface heating, a cooling gas may be introduced between the cooling plate and window surface as shown in Figure 4-7 to remove heat from the window surface. Figure 4-8 shows the calculated Strehl ratio versus the incident beam flux for various gap widths, where helium is used for the cooling gas and the cooling plate is maintained at room temperature. (The Strehl ratio is the ratio of peak intensity in the far field to that for a perfect beam.)

For the space mission, the aerodynamic window is inherently not applicable. Hence, the rotating material window should be considered as the

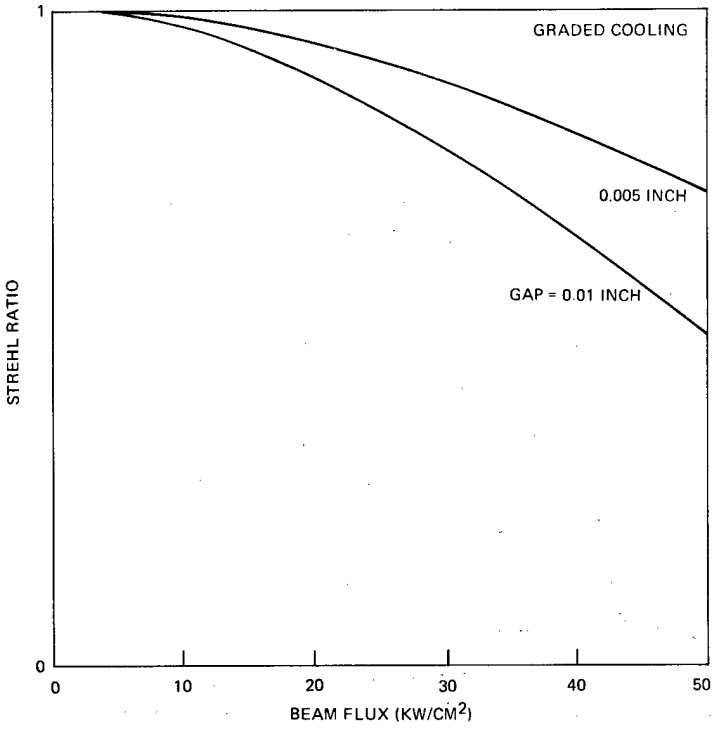

Figure 4-8. Beam degradation through the rotating ZnSe material window for various cooling methods.

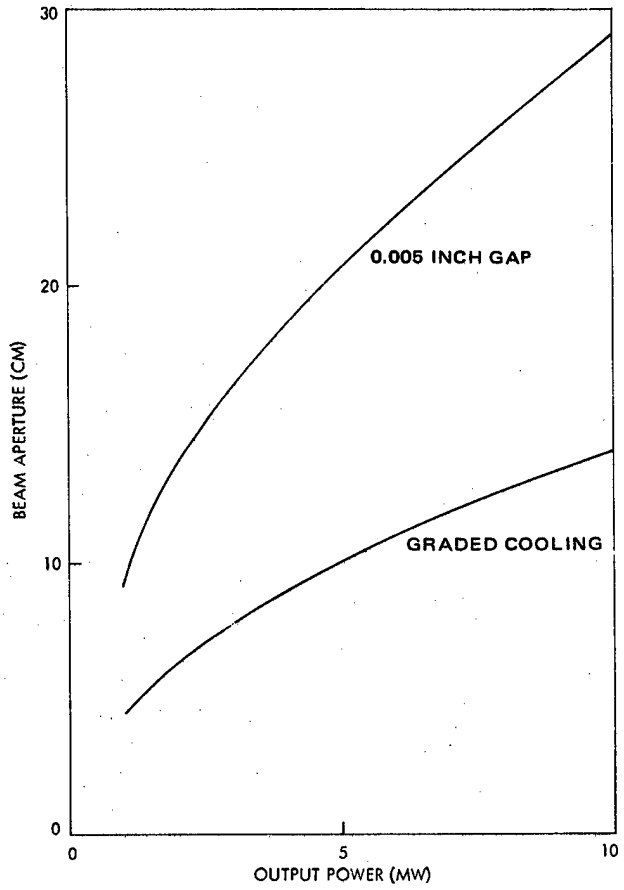

Figure 4-9. Required beam aperture for rotating ZnSe material window.

only candidate. To design the solid window for a given laser output power, one must expand the beam aperture to lower the beam flux through the window. Figure 4-9 shows the calculated beam diameter in cm versus the laser output power to give the Strehl ratio of 97 percent for gaps of 0.005 inch and 0.01 inch. It is believed that the curve for a 0.005 inch gap is representative of current technology and the curve for a graded cooling is certainly possible by 1990. Therefore, the graded cooling design has been chosen; this conceptual design results in the sizing shown in Table 4-9.

TABLE 4-9. ROTATING ZnSe WINDOW FOR SPACE SYSTEMS

Laser Power	Aperture Size	Window Weight	Window Volume
1 MW	4.5 cm square	42 kG	0.028 M^3
5 MW	10 cm square	140 kG	0.093 M^3
10 MW	14.5 cm square	236 kG	0.157 M^3

The aerodynamic window is an alternative to the material window for the shorter run time high energy laser applications. Although it has no material limitation, it is limited by the pressure ratio across the window and it is vulnerable to ambient pressure fluctuations. Furthermore, a separate flow system is required to run the aerodynamic window. Subsonic aerodynamic windows, such as the transverse window, axial window, and impacting jet window, have the advantage of low optical degradation, but they only support low pressure ratios, typically less than two. For the airborne closed-cycle CO_2 EDL system, which operates at the nominal cavity pressure of 350 torr, a supersonic aerodynamic window should be selected.

Various supersonic aerodynamic windows have been reported in the literature, including TRW's axial windows, UARL's MECA, MSNW's minimum mass flow window and Northrop's multiple shock window. These may be cataloged into compression window, expansion window and shock-expansion window[14], [15], and may be evaluated accordingly. Figure 4-10 shows the mass flow required to operate an open cycle aerodynamic window as a function of the beam cross-sectional area for the pressure ratio of two across the window. H and D are the nozzle exit height and beam diameter, respectively. It is shown that the shock-expansion window requires much less mass flow than both expansion and compression windows and hence should be selected as the prime candidate for the airborne applications. The D/H ratio of 4 has been demonstrated, and it is felt that the D/H ratio of 8 should be feasible by the year 1990.

The anticipated far field optical degradation of the shock-expansion windows is found to be moderately low as shown in Figure 4-11. In Figure 4-12 the calculated weight of the gas supply and the associated tankage is plotted versus the mass flow rate for the 300 second system. For a given beam aperture, one may easily obtain the mass flow rate and gas supply system weight from Figures 4-10 and 4-12, respectively. These are tabulated in Table 4-10. The conceptual design is shown in Figure 4-13. The projected weight is sixty pounds and the volume is 0.44 cubic feet.

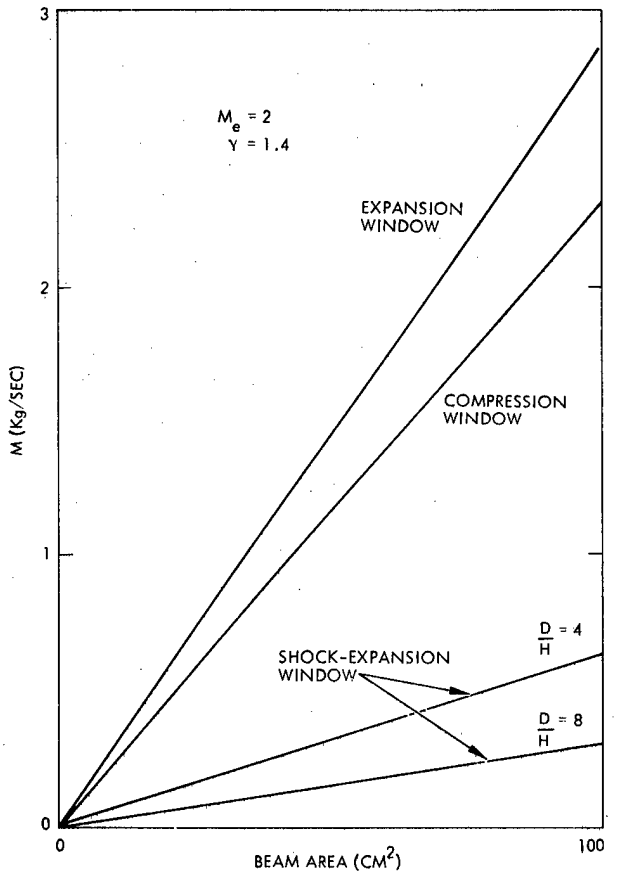

Figure 4-10. Mass flow requirement of various aerodynamic windows for 300 second run time.

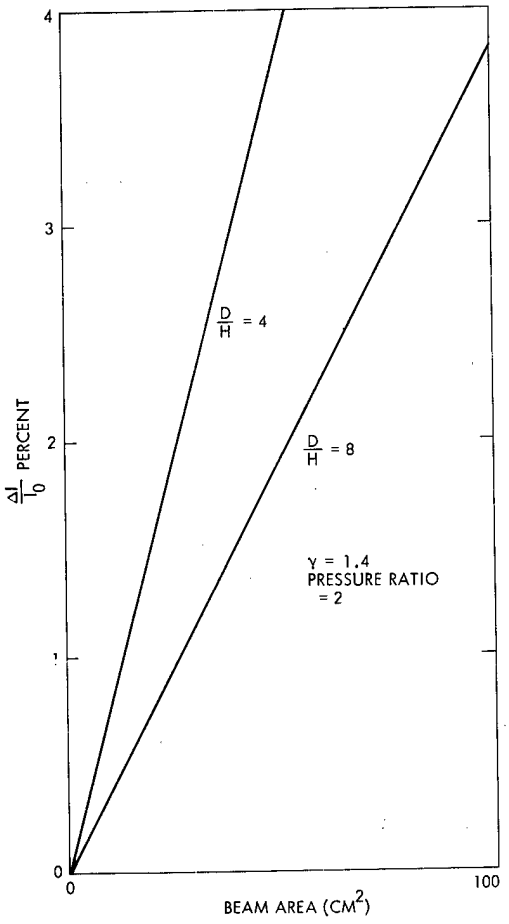

Figure 4-11. Optical degradation versus beam area.

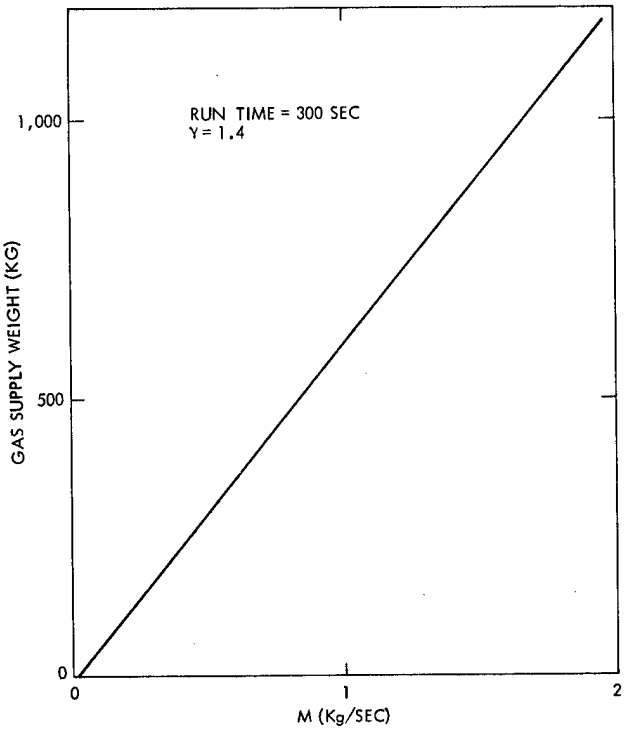

Figure 4-12. Gas supply weight versus mass flow rate.

TABLE 4-10. GAS REQUIREMENTS FOR AERODYNAMIC WINDOW FOR AIRBORNE SYSTEMS (300 SEC)

	N^2 Flow	Weight*
Present technology	0.4 kG/sec	230 kG
1990 technology	0.2 kG/sec	120 kG

*Nitrogen and tankage

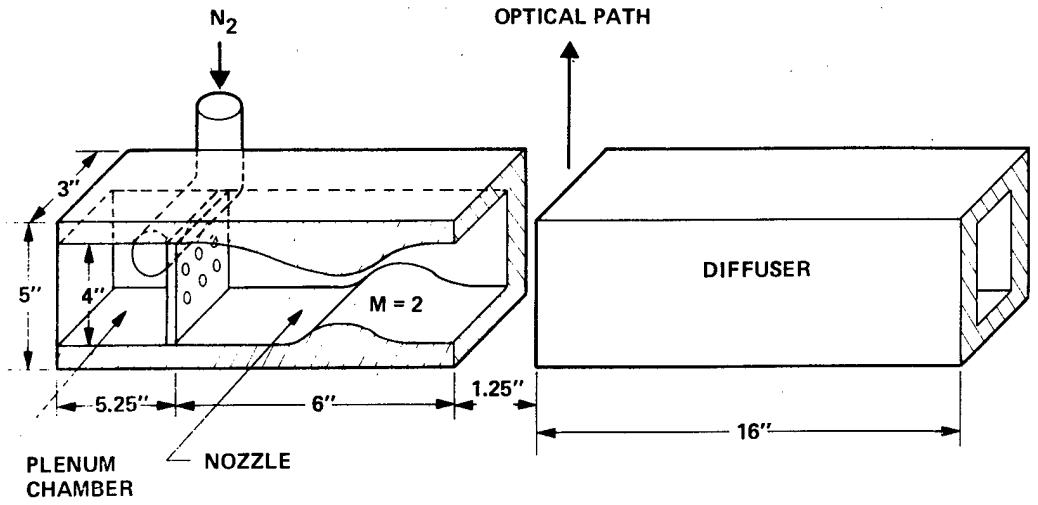

Figure 4-13. Supersonic aerowindow.

4.6 HEAT EXCHANGERS

Typically, tube bundle designs are used in high-pressure fluid applications whereas the lower cost, more compact, plate-fin designs are used for low pressure applications. Until recently plate-fin designs because of their many internal joints throughout the core have not been suitable for zero internal leakage applications, typically giving way to a welded tube bundle design. However, with recent advancements in vacuum brazing and fabrication technology the plate-fin design can be manufactured to provide essentially zero internal leakage. With this technology advancement, a plate-fin design becomes much more attractive, particularly on the basis of cost. A shell and tube design utilizing small-diameter, thin-walled tubes numbering in the thousands requires considerably more labor hours for setup and braze than that for a plate-fin core. An additional advantage of a plate-fin core is its high ratio of j, the Colburn heat transfer factor, to f, the Fanno friction factor. The plate fin j/f is typically up to two times higher than that of a tube bundle design. This results in a 30 percent reduction in frontal area for the same ΔP but a somewhat longer flow length. Based on these considerations, a plate-fin design was selected as the baseline concept for both the open-cycle airborne systems and the closed-cycle space systems. Highly compact surfaces with high j/f ratios and large core surface areas were selected. Core geometry and j/f data was based on configuration and experimental data reported by Kays and London[16].

A counterflow configuration was chosen with JP4 as the coolant for the airborne systems and Therminol 55 as the coolant for the space systems. The final design parameters are given in Table 4-11.

4.7 COMPRESSORS

The axial flow compressors have been sized as indicated in Section 3.3.2. The dimensions are summarized in Figure 4-14. The design parameters are presented in Table 4-12. For the ten megawatt systems, the parameters are based upon the use of two five megawatt systems.

4.8 SYSTEM CONCEPTUAL DESIGNS

The system packages for the 5 and 10 MW airborne EDLs have been configured to fit within the cargo envelope of the C5A aircraft. This installation provides access along both sides of the equipment. The size of the 1 MW airborne EDL package is sufficiently small to allow the use of other aircraft to be used as the host aircraft. To facilitate system logistics, ancillary equipment such as power generation and conditioning units, control units, consumables, etc., may be integrated into a module separate from the laser device. The space EDL systems have been configured for transportation in the space shuttle.

TABLE 4-11. HEAT EXCHANGERS

	Coolant Flow (GPM)	Weight (kG)	Volume (M^3)
1 MW airborne	320	200	0.5
5 MW airborne	1,280	880	2.2
10 MW airborne	2,560	1,760	4.4
1 MW space	500	240	0.6
5 MW space	2,570	1,850	4.6
10 MW space	5,140	3,700	9.2

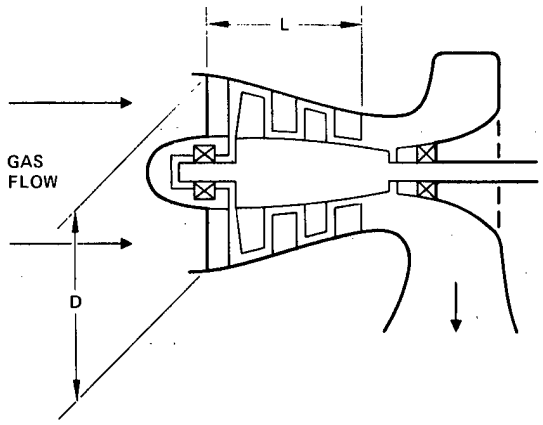

	D (CM)	L (CM)
L-A	58	69
M-A	124.7	147.4
H-A*	124.7	147.4
L-S	49	116
M-S	110	195
H-S*	110	195

*TWO REQUIRED

Figure 4-14. Axial flow compressor dimensions.

TABLE 4-12. COMPRESSORS CO_2 SYSTEMS

	Power (MW)	Mass (kG)	Volume (M^3)	No. Stages	Pres. Ratio
1 MW-air	0.62	130	0.18	2	1.64
5 MW-air	2.66	1050	1.80	2	1.54
10 MW-air	5.32	2100	3.60	2	1.54
1 MW-space	2.65	260	0.22	4	2.85
5 MW-space	7.64	1580	1.85	3	2.05
10 MW-space	15.28	3150	3.70	3	2.05

The airborne EDL system layouts are depicted in Figures 4-15 through 4-17. The airborne EDL is envisioned as being a pallet mounted, functionally modular system. The modular concept, in addition to facilitating its manufacture and subsequent maintenance, will permit greater latitude in the selection of the host aircraft. The laser device, consisting of the excitation and extraction components and the closed loop laser gas subsystem constitutes (from a size point of view) the major system module. Other EDL subsystems are: the power conditioning units, the thermal control unit, the controller, and the consumables. These ancillary subsystems will most likely be mounted to a common pallet.

The laser coolant accounts for a significant portion of the total system weight and volume. Since the coolant is not consumed by the laser, an attractive consideration is to contain the coolant, thermally conditioned JP aircraft fuel, in a modified aircraft fuel tank and, after performing its cooling function during laser operation, the coolant would be returned to the aircraft fuel storage system for aircraft consumption.

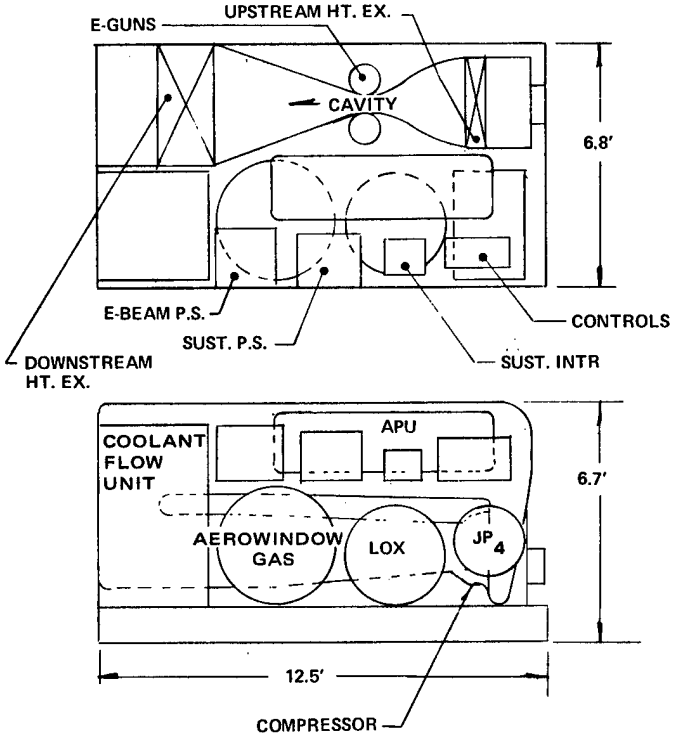

Figure 4-15. 1 MW CO_2 laser - airborne.

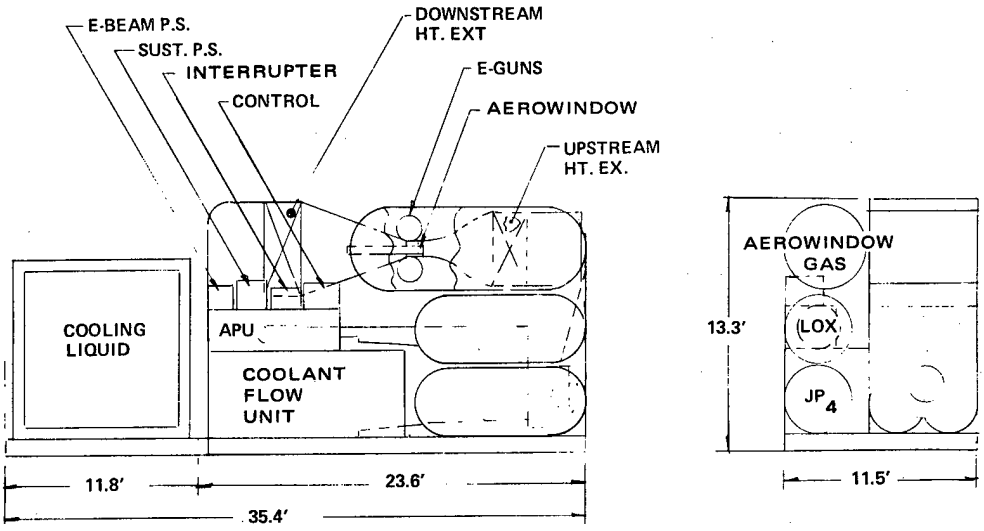

Figure 4-16. 5 MW CO_2 laser - airborne.

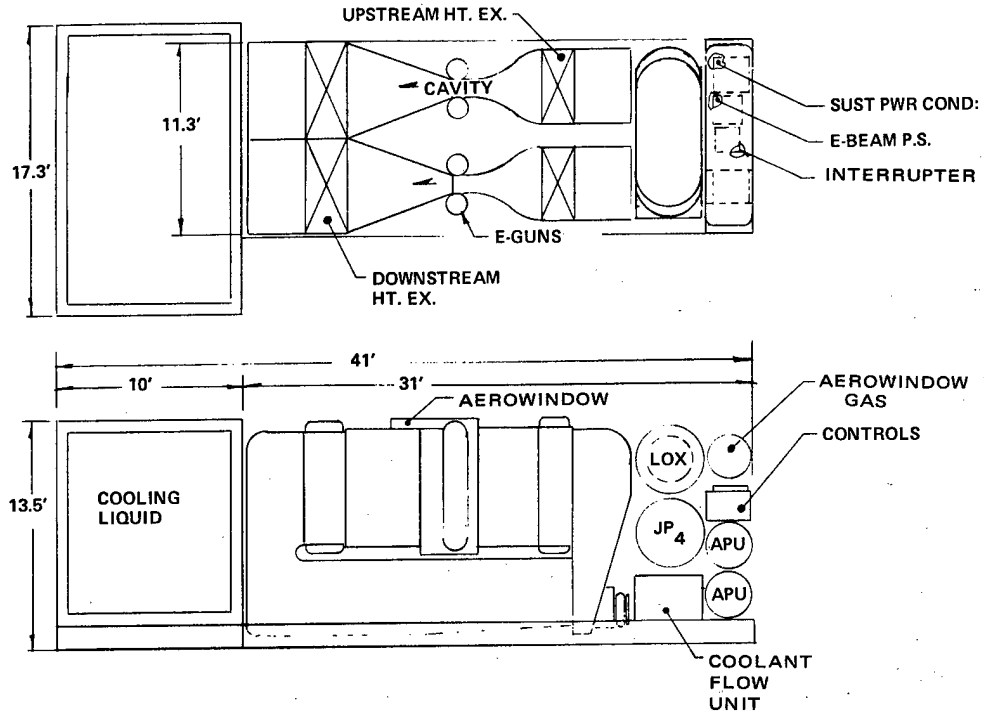

Figure 4-17. 10 MW CO_2 laser - airborne.

Figure 4-18 is a typical sectional view taken through the excitation section along the flow axis. The Inlet/Cavity/Diffuser consists of a pressure tight outer structure surrounding an aerodynamically shaped inner liner. The outer structure is fabricated totally from a graphite reinforced composite. The commercial designation for this material is GY-70/X-30 composite. The inner liner of the nozzle is fabricated from this material also. Factors favoring the selection of this material are its high stiffness to weight ratio, its dimensional insensitivity to temperature changes and gradients, and the availability of fabrication techniques to produce the desired items. Graphite composite fabrication techniques are in general common to those used in other composites, i.e., fiberglass. Conventional lay-up techniques are particularly useful for fabricating complex shapes such as are found in this device.

The inner walls of the cavity section are fabricated from Alumina, MACOR (a machineable glass ceramic), and aluminum. The choice of these materials was based on their survivability when exposed to high voltage, high x-ray and E-beam flux loadings, and high temperatures. The diffuser

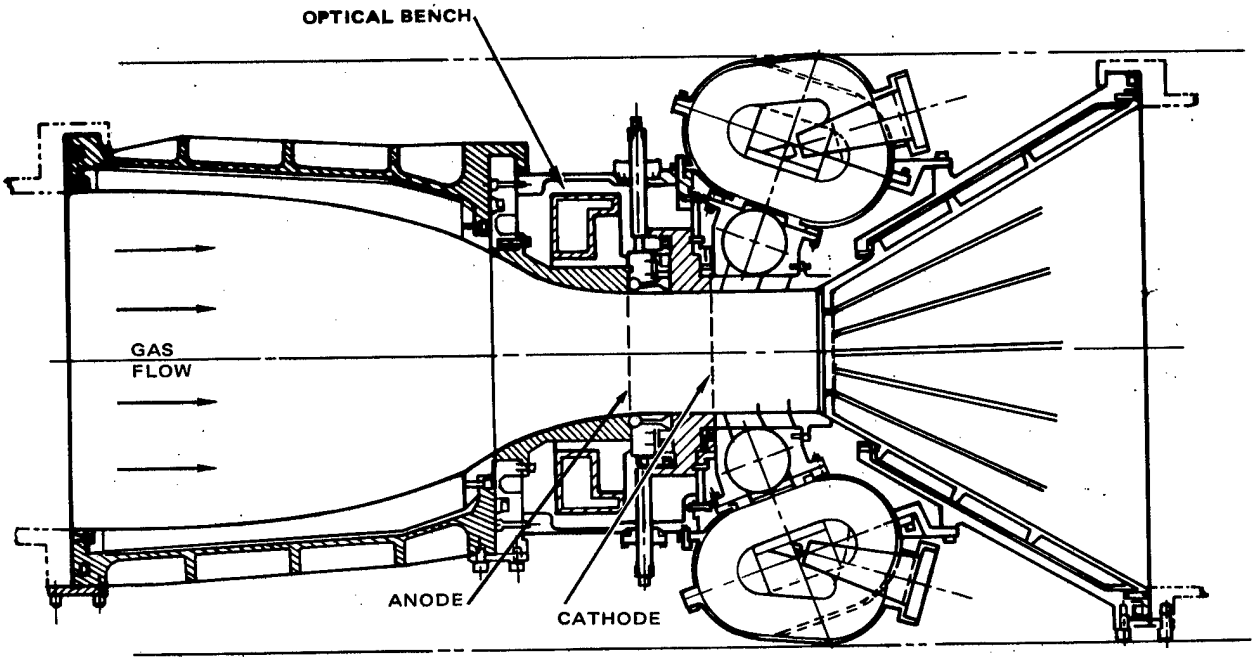

Figure 4-18. Typical section through the excitation assembly.

liner is a stainless steel weldment. The walls and vanes are permitted to thermally expand and contract independent of the graphite composite outer structure.

The E-Guns mount to the outer structure of the excitation section. The nose of the E-Gun protrudes through the outer structure and the E-Gun foil becomes part of the aerodynamic wall of the extraction region. To preserve the vacuum integrity of the system, a seal is provided around the flange which attaches the E-Gun to the structure.

As with the excitation section, the ductwork portions of the closed loop fluid supply subsystem will be fabricated of the GY-70 reinforced composite. Its selection for this application is based on its superior stiffness and strength to weight ratios. Because it has a near zero coefficient of thermal expansion some care has to be exercised where high thermally expansive components interface with this material.

The resonator optical assembly would consist of an optical bench, the resonator mirrors and their mounts, and the autoalignment subsystem. The resonator optics are situated at either end of the cavity. The optical components would be attached to auxiliary optical benches which are attached to the main optical bench as an assembly. The optical bench would be fabricated from a quasi-isotropic laminate of GY-70 graphite fibers in a high temperature epoxy matrix. The quasi-isotropic properties are achieved by selective orientation of the fibers as typically shown in Figure 4-19. The choice of this material was based primarily on its extremely low thermal growth.

As shown in Figure 4-18, the optical bench is located in the region between the excitation section outer structure and the inner aerodynamic walls of the cavity. The resonator mirrors are situated such that their optical surfaces form the cavity end walls.

The three space-based systems are shown in Figures 4-20 through 4-25. The excitation-extraction components are identical to their airborne CO_2 counterparts. The closed loop laser gas subsystem is similar in concept but the methods of heat disposal available dictate the use of a larger capacity compressor and heat exchangers, and the addition of a gas turbine to mechanically extract energy from the laser gas.

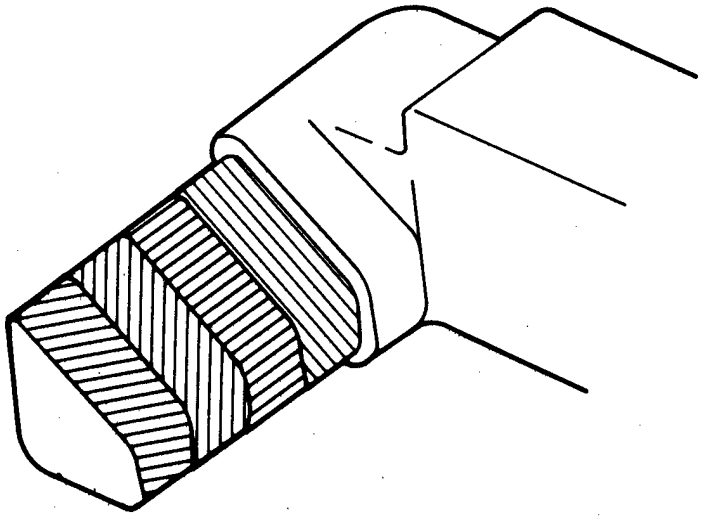

Figure 4-19. Graphite fiber orientation (optical bench corner).

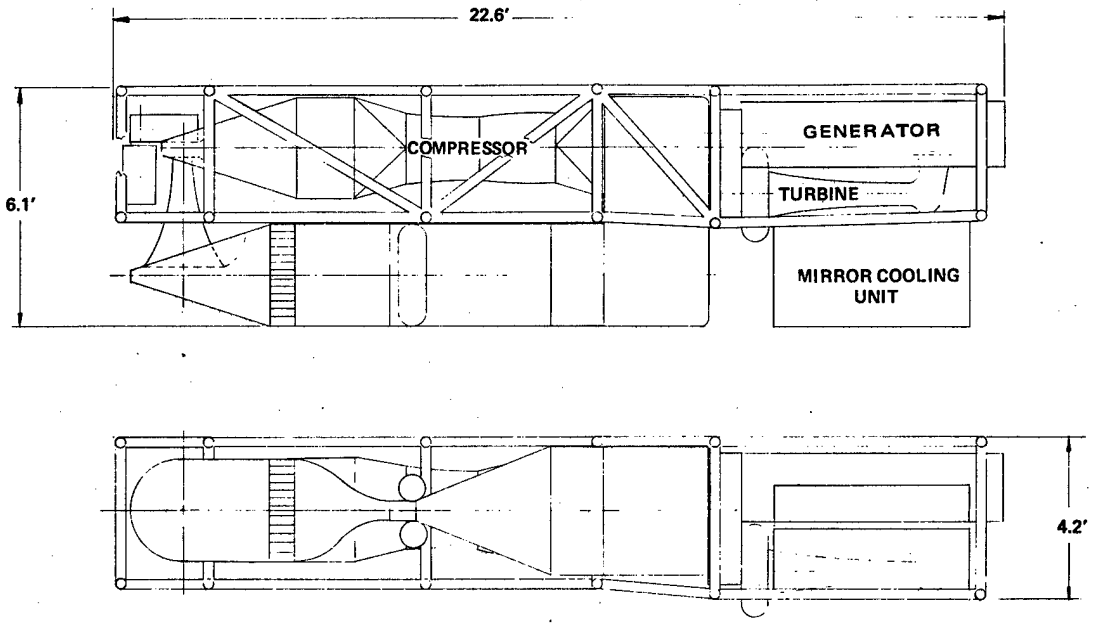

Figure 4-20. 1 Mw CO_2 laser - space.

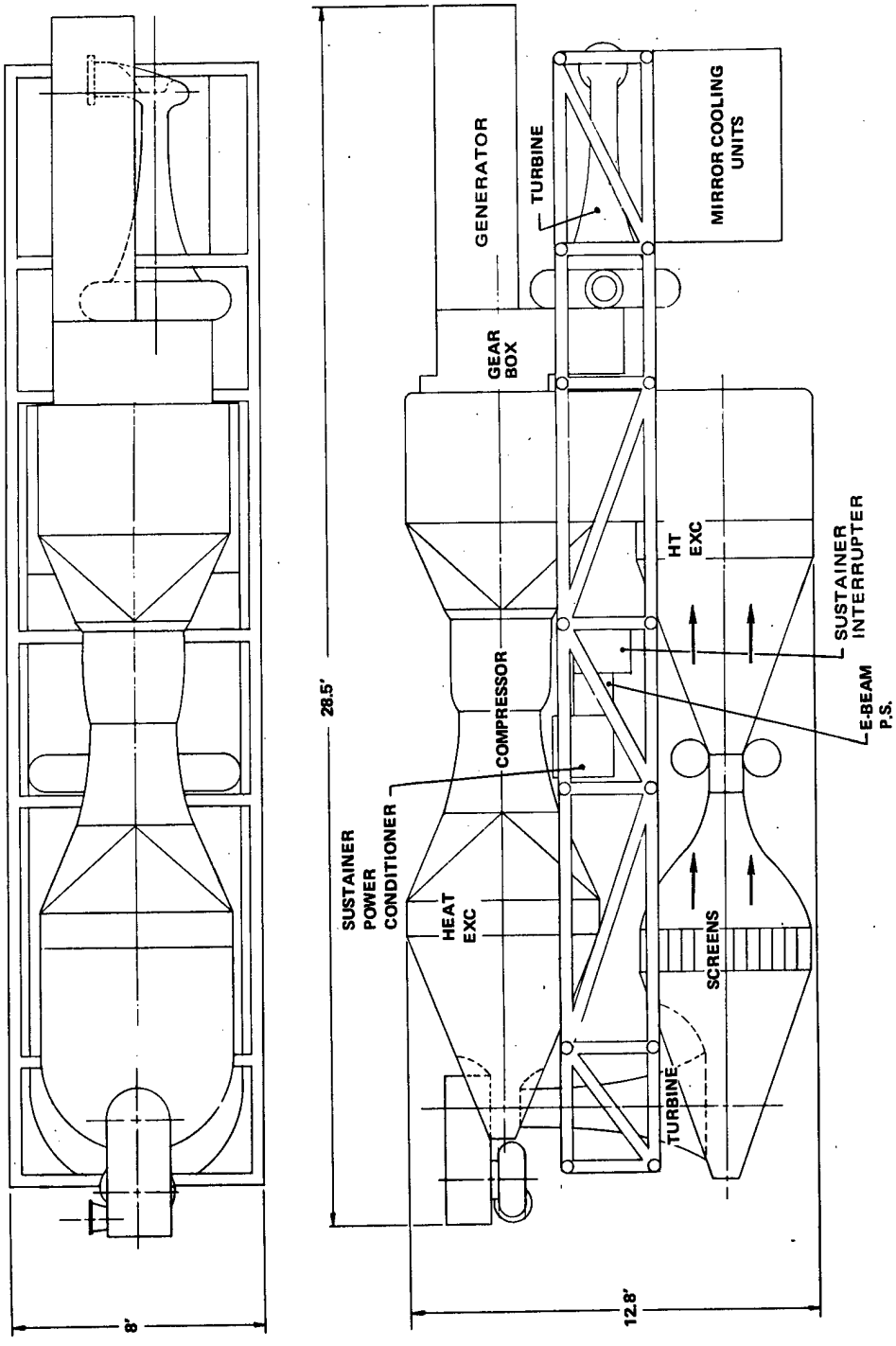

Figure 4-21. 5 Mw CO_2 laser - space.

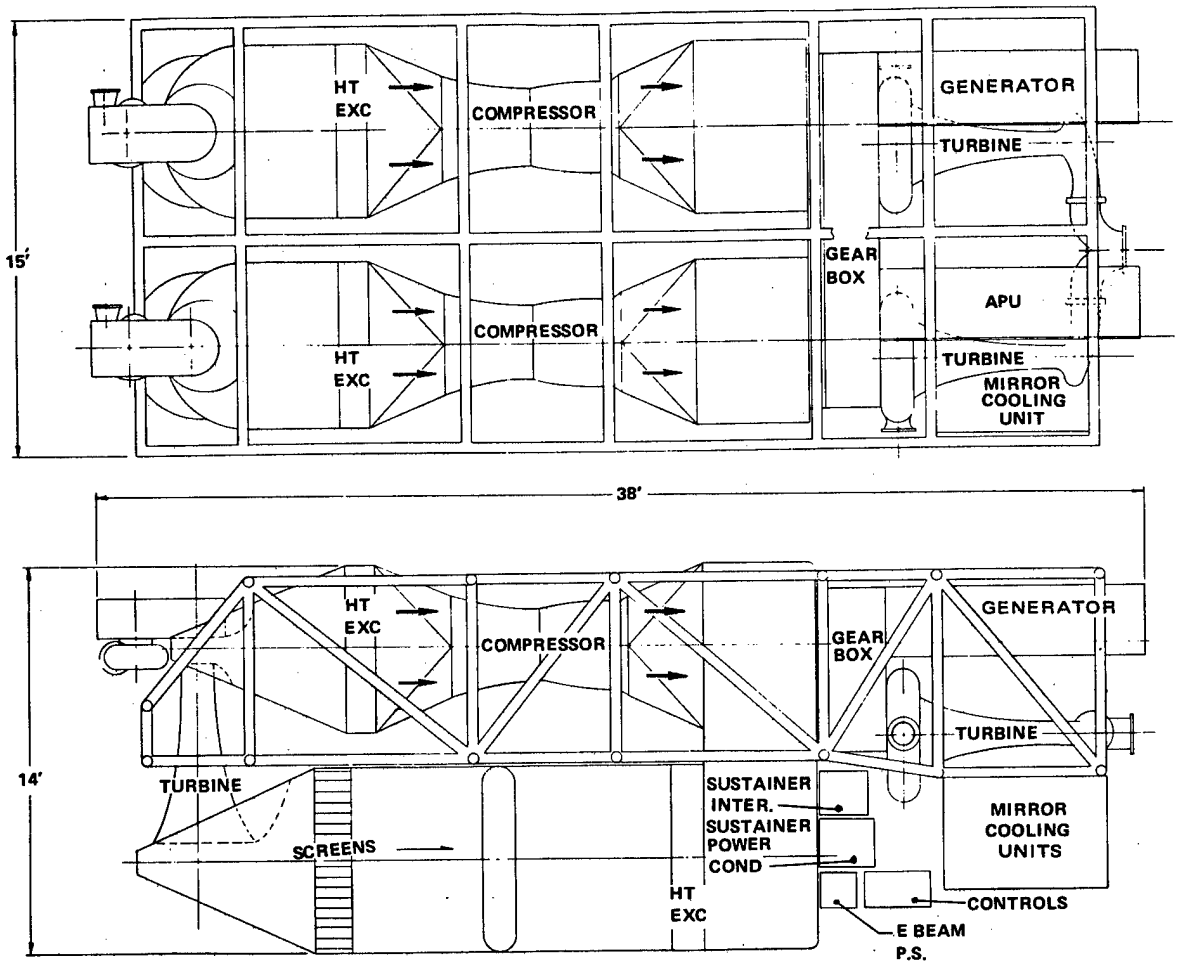

Figure 4-22. 10 Mw CO_2 laser - space.

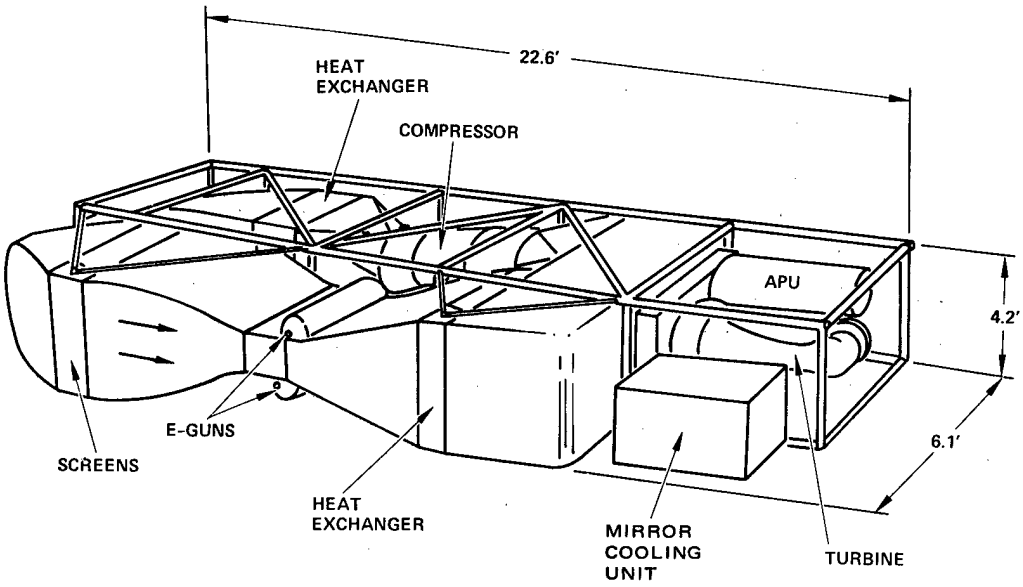

Figure 4-23. 1 Mwatt CO_2 laser - space.

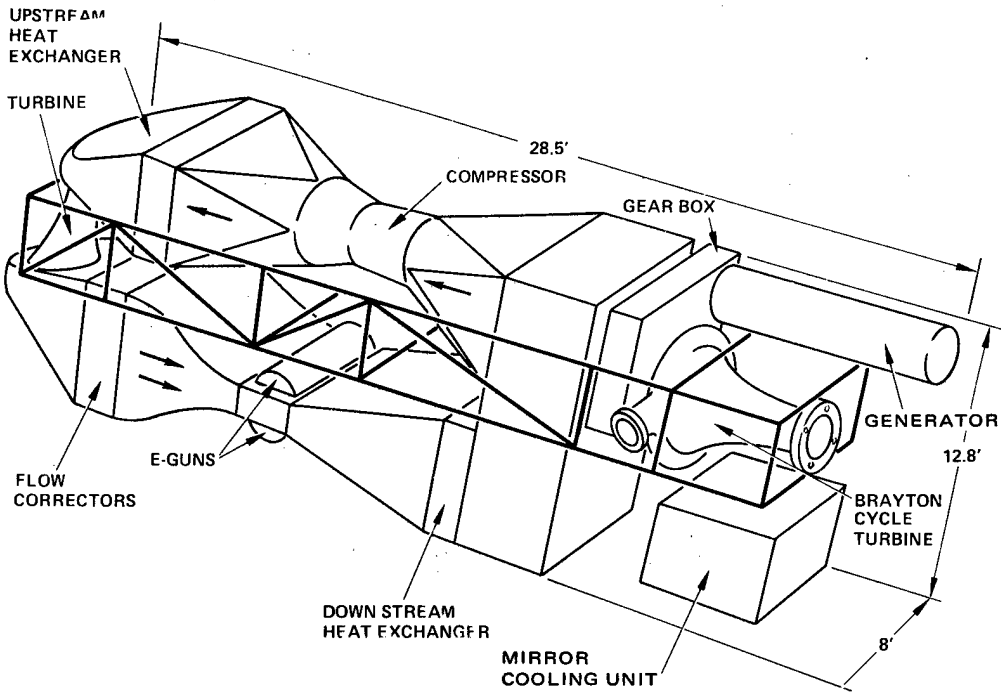

Figure 4-24. 5 Mwatt CO_2 laser - space.

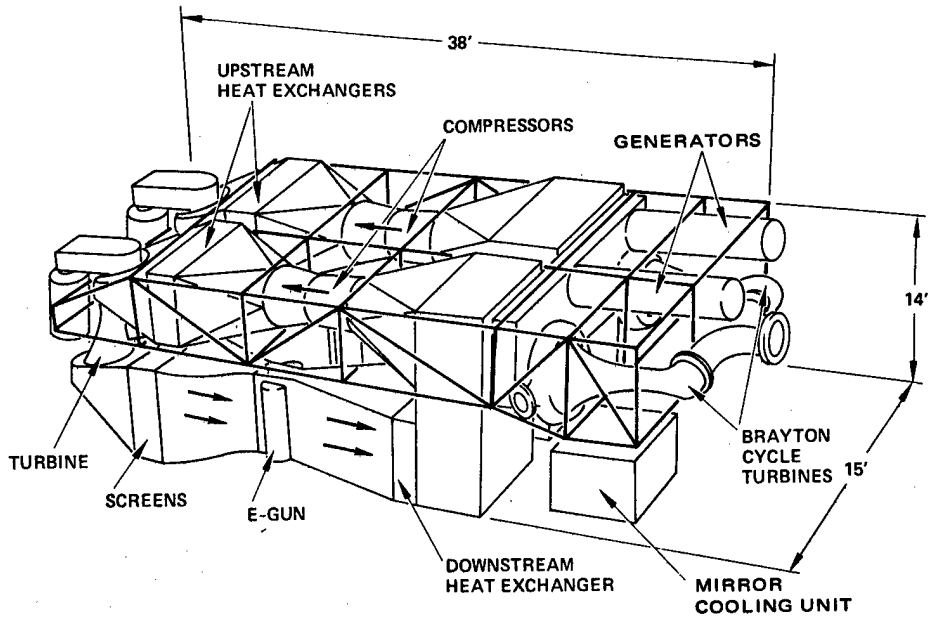

Figure 4-25. 10 Mwatt CO_2 laser - space.

Primary power for the space EDL system is obtained from solar radiation. A Brayton cycle is used to convert the absorbed thermal energy to the mechanical energy required for system operation. The Brayton cycle turbine is shown connected to the EDL gear box. It will power the fluid supply compressor, the electrical generator, the pumps in the thermal control unit and will in general provide the power requirements for EDL operation.

Waste thermal energy generated during EDL operation is convected away from the EDL by a third closed loop and ultimately radiated into space. Power to circulate the heat transfer medium in this loop is also provided by the Brayton cycle.

The system weights for this conceptual design are shown in Tables 4-13 and 4-14.

TABLE 4-13. AIRBORNE CO_2 SYSTEMS

	Weight (kG)		
	1 Mwatt	5 Mwatt	10 Mwatt
Prime power	500	1,850	3,460
Power conditioning	205	265	365
Inlet-cavity-diffuser	690	7,300	14,600
Electron guns	120	210	420
Optical assembly	41	110	320
Ductwork/structure	684	3,630	7,110
Heat exchangers	200	880	1,760
Turbo-compressor	130	1,050	2,100
Aerodynamic window	27	27	54
Tankage	392	928	1,650
Mirrow cooling unit	225	540	810
Aero-window gas	27	27	54
Consumable JP4/lox	340	1,700	3,500
Misc. (pumps, controls, etc.)	360	1,854	3,619
Totals	3941	20,371	39,822

TABLE 4-14. SPACE CO_2 SYSTEMS

	Weight (kG)		
	1 Mwatt	5 Mwatt	10 Mwatt
Power conditioning	205	265	365
Inlet-cavity-diffuser	690	7,300	14,600
Electron guns	120	210	420
Optical assembly	41	110	320
Duct work/structure	529	3,340	6,530
Heat exchangers	240	1,850	3,700
Compressor/gearbox	275	1,620	3,275
Turbine/generator	200	1,200	2,100
Exit window	42	140	236
Mirror cooling unit	240	565	850
Misc. (pumps, controls, etc.)	258	1,660	3,240
Laser system	2,840	18,260	35,636
Solar collector	8,600	31,600	63,300
Prime power	4,500	21,800	43,300
Radiator	4,500	12,050	24,100
Total	20,440	83,710	166,336

5.0 CO SYSTEM

5.1 TASK DEFINITION

Electric discharge laser development in recent years has expanded to include CO as well as CO_2 systems. In the CO molecule, laser action is produced on several vibrational transitions. The efficient vibrational excitation that can be achieved coupled with the utilization of a single molecule on several successive cascade transitions gives rise to higher theoretical electrical efficiencies in the laser cavity than in the CO_2 system. The achievement of these efficiencies however requires low (60-90°K) temperature operation. The result of an overall comparison of such a system with a CO_2 system is not obvious a priori, because of the cost of the achievement of low temperature in a closed cycle flow system. Consequently, the conceptual design of a one megawatt space-based cw CO electric discharge laser system, subject to the same guidelines and constraints as the CO_2 designs, was undertaken.

Two alternative methods for achieving low temperature were considered. A subsonic flow loop with low temperature heat exchangers is one obvious method. The alternative method consists of using supersonic expansion to decrease the gas temperature. This method results in a high pressure ratio, high energy consumption compressor. However, high gas temperature (and therefore thermal radiation temperature) are automatically achieved. Consequently this task included a comparison between these approaches. Alternative systems were scaled and the lighter one was chosen for the conceptual design.

5.2 SUBSONIC SYSTEMS

A rough preliminary analysis was performed to investigate the weight comparison between a subsonic CO electric laser and the CO_2 laser systems already described. Cavity performance for 20 kw output lasers[17] was scaled to 1 Mw by a scaling law, which states that two CO laser cavities are similar in performance if they have the same power loading per CO molecule and if the laser gas in each case has the same residence time in the cavity. Table 5-1 summarizes the parameters which characterize the basic laser. The additional elements of a closed cycle gas flow loop were then combined with the cavity, the total flow loop mass was estimated, and added to the estimated mass of the radiator and the solar-to-electric power conversion module. The parameters associated with such items as the compressor, the heat exchangers, etc., are shown in Table 5-2 as are the specific mass figures adopted for the radiator and the electrical power supply. These figures are similar to those used in preliminary sizing of the CO_2 1 Mw space system. Results for this basic system summarized in Table 5-3 suggest that this low temperature subsonic system is impractical for space because radiation of even the relatively small quantity of waste heat produced requires 25 shuttle loads of radiator due to the low temperature at which it must be radiated.

TABLE 5-1. BASIC SUBSONIC CO LASER PARAMETERS

Gas mix CO:He	= 1:9	Average molecular mass	= 6.4
Inlet M	= 0.2	Cavity dimensions (cm):	8 x 100 x 10
Inlet pressure	= 250 torr	Power loading = 0.52 eV/CO molecule	
Inlet temp.	= $80^{o}K$	Sustainer power input	= 1.82 Mw
Specific heat (Cp)	= 3.42 J kg^{-1} $^{o}K^{-1}$	Average output λ	= 5.06μ
γ (=Cp/C_V)	= 1.625	Cavity electrical efficiency (P_{OUT}/P_{SUST})	= 55%
Mass flow	= 2.12 kg sec^{-1}		

TABLE 5-2. SUBSONIC CO SYSTEM PARAMETERS

1. Electron density = 10^{12} cm^{-3}
2. Compressor efficiency = 0.86
3. Nozzle isentropic
4. Diffuser pressure recovery coefficient = 0.7
5. 5% pressure drop in each heat exchanger
6. 2-1/2% pressure drop in each duct section
7. Radiator areal mass density = 1.6 Kg M^{-2}
8. Solar to electric power conversion system mass = 2 Kg/KWe

TABLE 5-3. SUBSONIC CO SYSTEM SCALING RESULTS

Overall electrical efficiency (Output Power/ Total Input Power)	= 52.1%
Solar-to-electric power system mass	= 3840 Kg
Radiator Mass	= 6.5×10^5 Kg

The radiation temperature must be raised to reduce the total mass, and the two approaches used in the CO_2 study, raising cavity inlet temperature and employing a refrigeration step in the gas flow loop will now be investigated separately. Should they appear promising, a best combination of cavity temperature and refrigeration will be sought. In the refrigerator system the same cavity is used as in the basic system, but the gas flow loop includes a much larger compressor which raises the gas temperature to reduce radiator size. Heat is then removed. This approach has already been described for the space CO_2 systems. With a turbine efficiency of 0.85, and an effective radiating temperature of 300°K, the figures shown in Table 5-4 are obtained.

A warm CO cavity was scaled to investigate what gain in system mass minimization might be expected from higher cavity inlet temperature. Its difference from the basic system is summarized in Table 5-5. This warm cavity temperature system also gives a large reduction in weight over the basic subsonic system as Table 5-6 shows but not enough to make it a

TABLE 5-4. REFRIGERATOR SUBSONIC CO SYSTEM SCALING RESULTS

Overall electrical efficiency	= 18.7%
Solar-to-electric power system mass	= 10,700 Kg
Radiator mass	= 16,000 Kg

TABLE 5-5. WARM SUBSONIC CO SYSTEM PARAMETERS

Same as basic subsonic system except for:

- Inlet temp = $300^{\circ}K$
- Cavity efficiency = 19.2%
- Sustainer power input = 5.21 Mw
- Mass flow = 6.6 kg sec^{-1}
- Average output λ = 5.55μ
- Cavity dimensions (cm): 12 x 400 x 10

TABLE 5-6. WARM SUBSONIC CO SYSTEM SCALING RESULTS

Overall electrical efficiency	= 16.6%
Collector mass	= 5200 Kg
Radiator mass	= 18,500 Kg

competitor to the subsonic CO_2 space laser system. It does not appear that the subsonic CO laser is a logical choice to replace the CO_2 laser for a space-based 1 Mw system. Surely an optimization would yield mass figures superior to those of either the warm or the refrigerator systems, but since the radiator and power supply system totals are already 50 percent above the CO_2 total system figures, with no allowance made for the mass of the laser loop itself, and no allowance made for losses such as those due to boundary layer growth, diffraction and the aerowindow, there is not much reason to pursue investigation of the subsonic system further.

5.3 SUPERSONIC SYSTEM

Supersonic expansion of the laser gas in the nozzle and diffusion to subsonic speed after the laser cavity offer the advantages of low temperature within the resonator and higher temperature in the rest of the flow system at the cost of considerable pressure drop in the system which has to be restored by the compressor. Both the laser cavity and the diffuser entail much larger drop in gas stagnation pressure than is the case for an all subsonic flow system. A set of assumptions for the flow loop designed to make the supersonic CO closed cycle system results comparable to systems already described was adopted and is presented in Table 5-7. The rather high pressure drop assumed for the heat exchanger situated upstream of the nozzle compared to that after the diffuser follows from the high heat of compression requiring greater heat removal upstream of the nozzle (downstream of the compressor). Another difference between assumptions in this case and those used for CO_2 lies in the allowance made for losses not modeled in the kinetics code. Mirror and diffraction losses are similar in the two cases, but boundary layer growth appears likely to consume about twice as much of the cavity in

TABLE 5-7. SUPERSONIC CO SYSTEM ASSUMPTIONS

1. Compressor efficiency = 0.86
2. Nozzle isentropic
3. Normal shock pressure recovery in supersonic to subsonic diffusion
4. Subsonic diffuser pressure recovery coefficient = 0.7
5. 12% pressure drop in pre-nozzle heat exchanger
6. 4% pressure drop in post-diffuser heat exchanger
7. 2-1/2% pressure drop in each duct section
8. Radiator areal mass density = 1.6 kg M^{-2}
9. Collector areal mass density = 0.29 kg M^{-2}
10. 35% 'pad' needed to account for unmodelled losses, mainly:
    a. Boundary layers
    b. Mirrors
    c. Diffraction

supersonic flow as it does in subsonic flow. Therefore the 25 percent pad (i.e., 1.25 Mw code output = 1.00 Mw usable laser power output) of the CO_2 scaling has been increased to 35 percent for the supersonic CO EDL.

Peak pumping efficiency is again a useful guide in selection of a gas mix. As the gas traverses the laser cavity, both static temperature and static pressure rise and as a result, density variation is only of the order of 2 percent. For a constant electric field, E/N is nearly constant in the discharge region. Extensive computer code examination of various gas mixes has shown that for a molecular ratio of 1 part CO to 9 parts argon, about 99.5 percent of sustainer power is pumped into the CO vibrational levels for $E/N = 0.2 - 0.4 \times N^{-16}$ Vcm^2 [18]. For the system finally selected, replacement of this mix with CO:Ar:He = 1:6:3 increases system mass by 16 percent. The CO:Ar = 1:9 mixture has therefore been chosen. There is some recent evidence that more complex gas mixtures providing lower pumping efficiency may be needed to optimize beam quality[19] but it is assumed that by 1990, better flow control will provide good beam quality with the selected mixture.

The system was optimized by finding the set of values of inlet static pressure, static temperature, and stagnation temperature which yielded the lowest overall system mass. Scaling laws for laser loop components from Reference 3 together with the same figures used in other sections of this report for radiator area mass density (1.6 Kg/m^2) and solar-to-electric conversion specific mass (2 Kg/kwe) were used. It was assumed that, through the use of very thin beryllium foil for the e-gun exit window, an electron beam current density of 5 Ma/cm^2 will be possible by 1990. Figure 5-1 shows the effect upon total mass of varying static temperature about the optimal value, while Figures 5-2 and 5-3 present similar information about pressure and stagnation temperature. In Figure 5-2, pressure is limited on the low side since at about 60 torr, flow chokes in the diffuser.

The selected CO 1Mw space system is summarized in Table 5-8. The total mass figure is preliminary and a figure based upon detailed component sizing will be presented in the next section. It is appropriate to compare this to the minimum of Figure 3-20 since CO system masses were obtained in a similar manner to that used to obtain preliminary CO_2 mass totals.

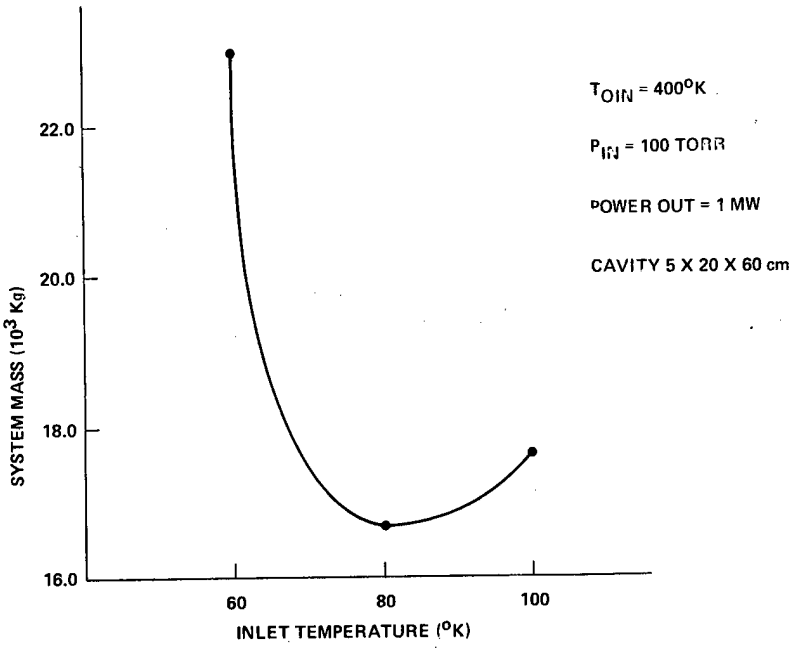

Figure 5-1. System mass vs inlet temperature.

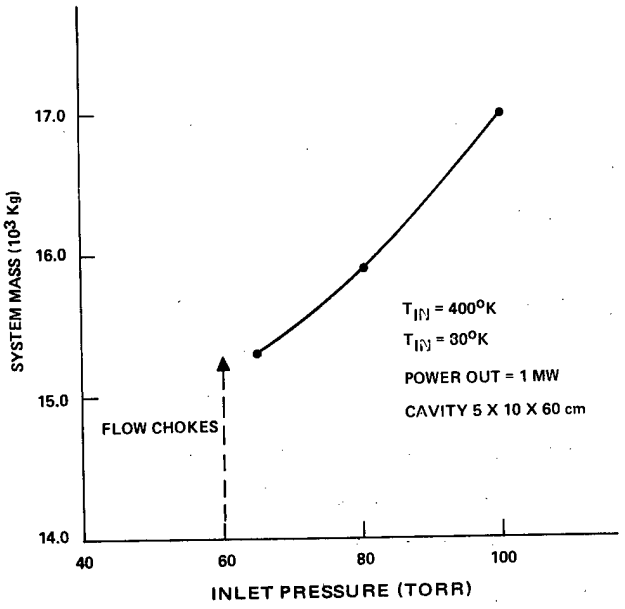

Figure 5-2. System mass vs inlet pressure.

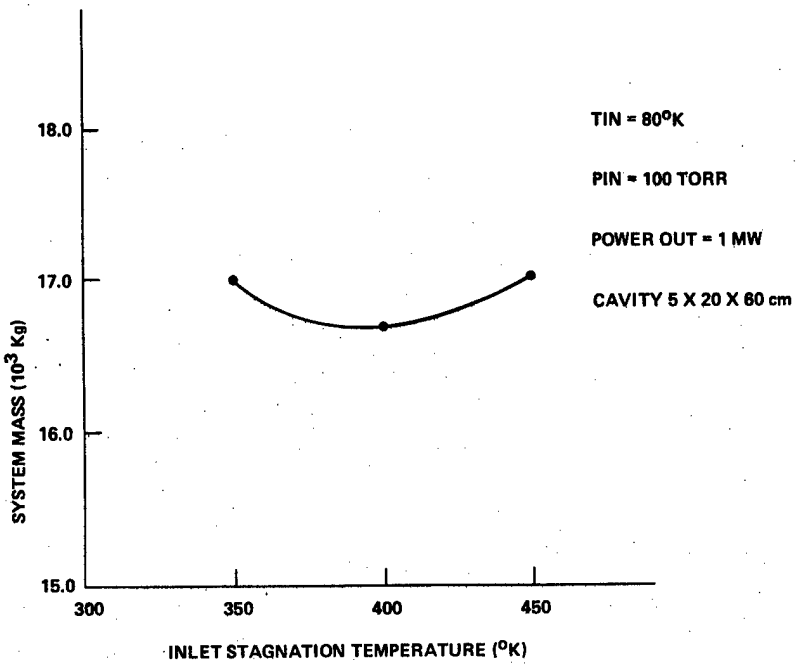

Figure 5-3. System mass vs inlet stagnation temperature

TABLE 5-8. SUPERSONIC CO SYSTEM PARAMETERS

Gas mix CO:Ar = 1:9
Inlet mach no. = 3.58
Inlet pressure = 65 torr
Inlet temperature = 80°K
Cavity dimensions 5 x 10 x 60 cm
Sustainer voltage = 1569 volts
E-beam current density = 5.0 ma/cm^2
Sustainer power = 1.835 Mw
Compressor power = 2.084 Mw
Electron beam power = 0.455 Mw
Estimated pump power = 0.025 Mw
Total electrical power = 4.399 Mw
System efficiency = 22.7%
System mass (preliminary) = 15.34 x 10^3 kg

Although an accurate comparison requires a more detailed sizing of individual components, which appears in a later section, for a 1 Mw space based closed cycle EDL, the supersonic CO system appears at this point to be lighter by about 2000 Kg than the subsonic CO_2 system.

5.4 CONCEPTUAL DESIGN

The CO electric discharge laser system is similar in concept to the CO_2 systems, but the cavity flow is supersonic, requiring a compressor with a higher compression ratio driven by more energy. There are, of course, other differences as a consequence of the supersonic flow. The supersonic nozzle is of course different from a subsonic one. A number of options including a de Laval nozzle are available. For this conceptual design we have chosen an "array nozzle" of a type successfully demonstrated at Hughes. The nozzle is an array of two-dimensional square output expansion nozzles as indicated in Figure 5-4. The other differences are also illustrated in the sketch of the laser shown in Figure 5-4. A transverse discharge is used, and a single pass unstable resonator is envisioned. To achieve a confined discharge, Busemann biplane confinement shields are inserted in the supersonic flow downstream of the laser cavity. A straight duct supersonic diffuser with vanes perpendicular to the optical axis is followed by a vaned subsonic diffuser of the same type used for the CO_2 systems. Other aspects of the CO system are similar to the CO_2 systems, although of course the performance parameters are different as shown earlier in Table 5-8. This, in turn, leads to different weights as shown in Table 5-9. Schematic layouts of the system are shown in Figures 5-5 and 5-6.

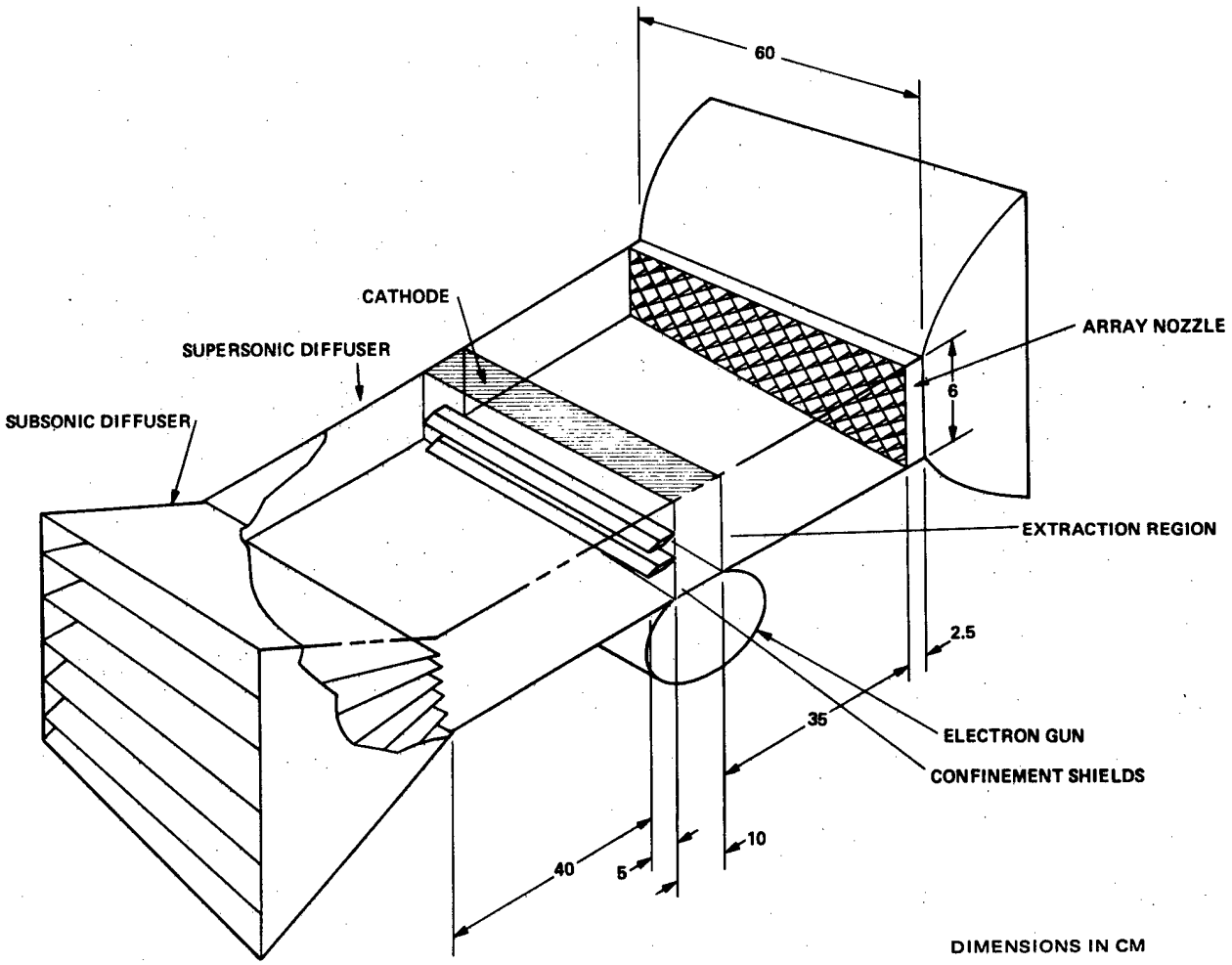

Figure 5-4. CO excitation region.

TABLE 5-9. CO SYSTEM

	Weight (Kg)
Power conditioning	260
Inlet - cavity - diffuser	490
Electron gun	120
Optical assembly	32
Ductwork/structure	690
Heat exchangers	445
Compressor/gearbox	250
Exit window	42
Mirror cooling unit	200
Misc (pumps, controls, etc.)	250
Laser system	2,780
Solar collector	5,670
Prime power	4,350
Radiator	4,163
Total	16,962

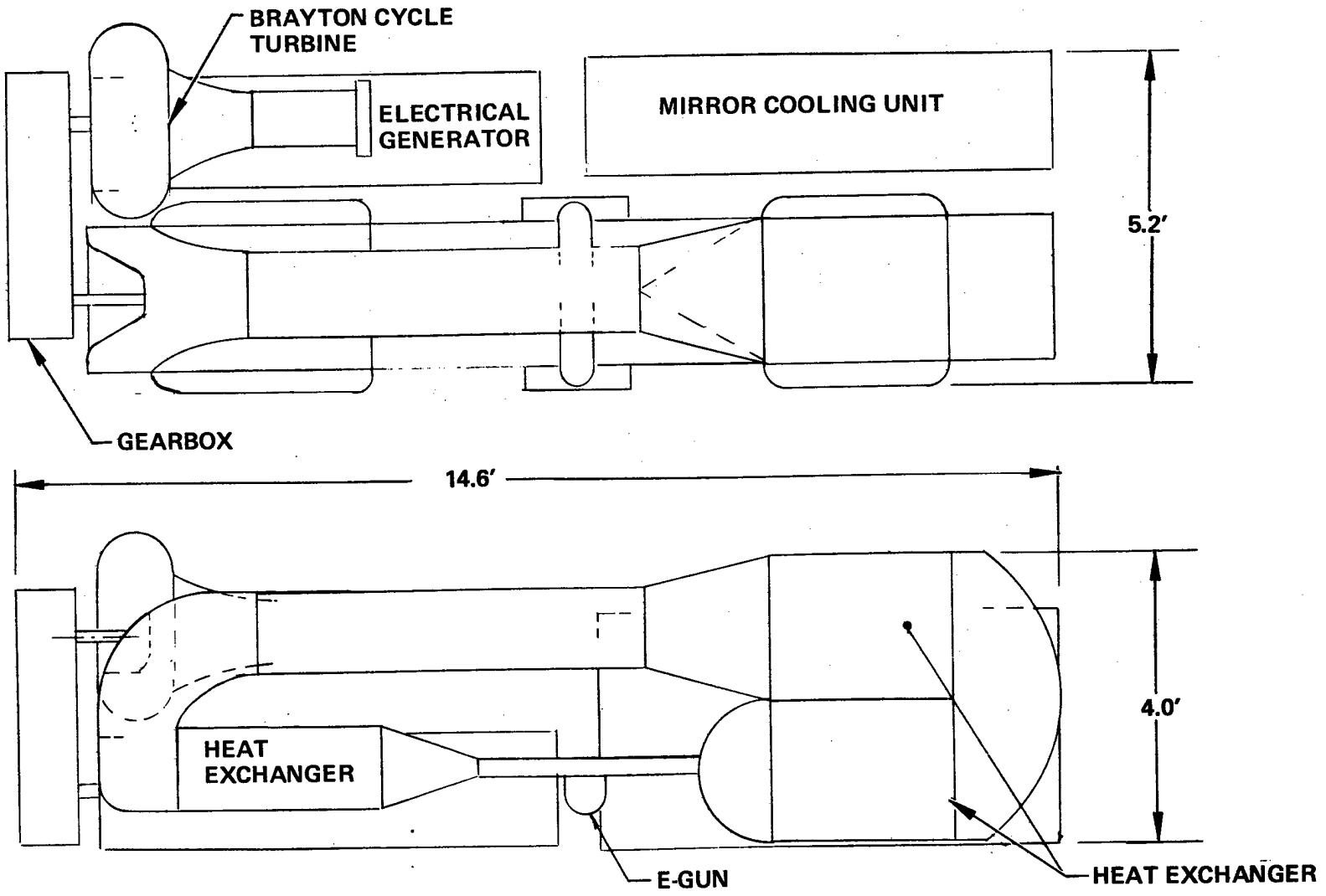

Figure 5-5. 1 Mw CO laser - space.

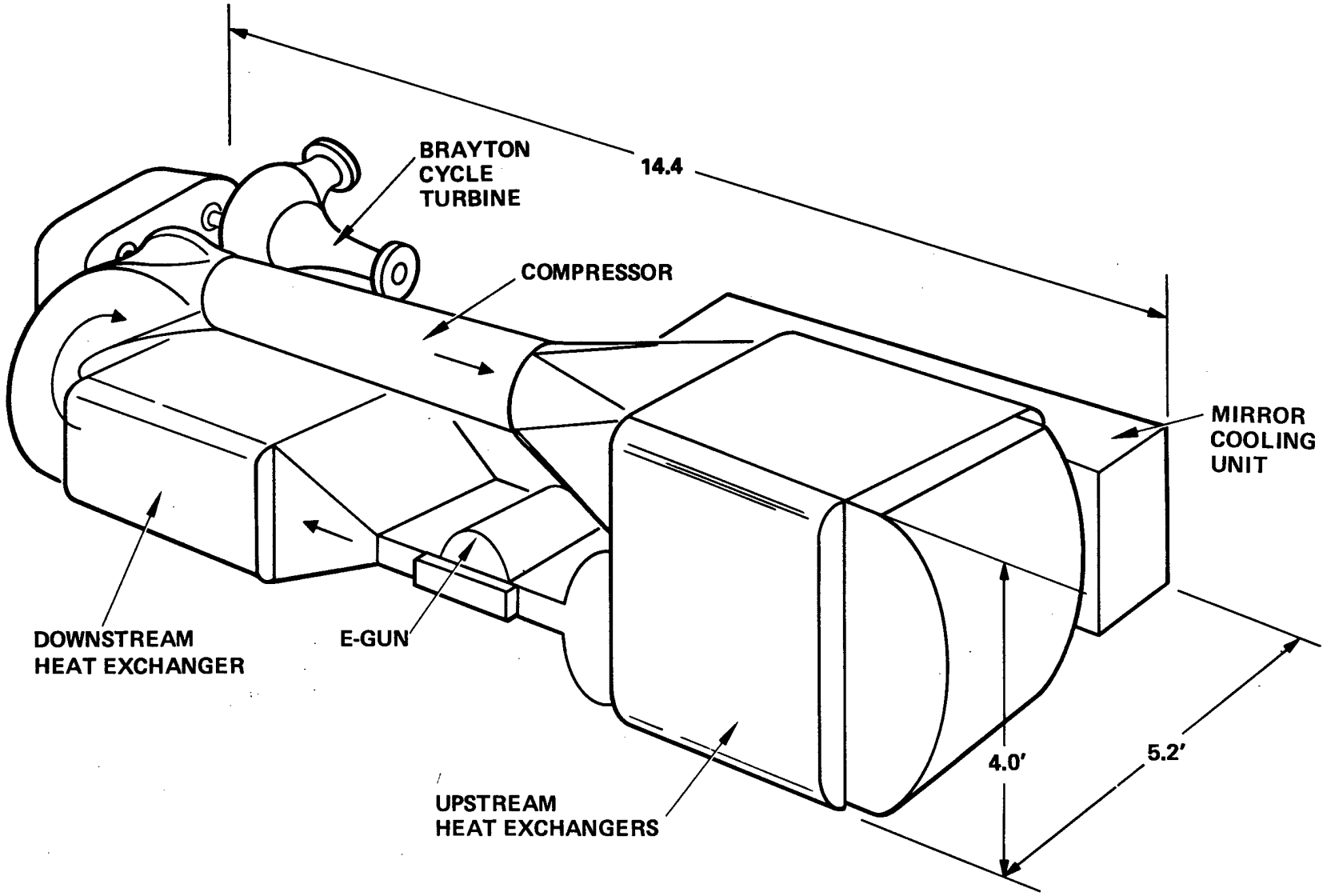

Figure 5-6. 1 Mw CO laser space.

6.0 CONCLUSIONS

It is interesting to compare the different types of laser systems which have been studied. Table 6-1 shows some of the major parameters for the 1 megawatt space-based electric discharge laser systems investigated in this study along with some data from a previous study in which a CO_2 gas dynamic laser (GDL) was investigated. The prime power source for the GDL was an unshielded nuclear reactor, while solar energy was investigated in the present study. The electric discharge laser systems are approximately an order of magnitude lighter than the gas dynamic laser system. An entire EDL system is within the weight capability of the space shuttle (approximately 27,000 Kg). In looking at the table one should also remember that the EDL systems are not designed for maximum efficiency, but rather are designed for minimum weight. In fact, a factor of 1.5 improvement in efficiency can probably be realized.

TABLE 6-1. 1 M WATT SPACE SYSTEMS

	Supersonic CO_2 GDL	Subsonic CO_2 EDL	Supersonic CO EDL
System weight (Kg)	316,154	20,440	16,963
Laser loop (Kg)	38,669	2,840	2,780
Laser loop power conversion (%)	—	15.1	22.7
Solar-laser conversion (%)	—	2.5	3.8
Collector area (M^2)	—	29,500	19,500
Radiator area (M^2)	—	2,800	2,600

While this study appears to lead to the conclusion that the CO system will be superior to the CO_2 system in terms of efficiency and weight, one must not leap to this conclusion. While every attempt was made to evaluate the two systems on an equal footing, the CO technology development is in a much earlier stage and the projected future performance entails a much greater degree of uncertainty. The CO_2 kinetics, for example, are much better understood than are those of the multi-line vibrational cascade lasing of the CO molecule. The multi-line nature of CO and the single line oscillation of CO_2 must be considered in making the choice for any particular application. The problem of chemical stability in closed cycle laser systems has not been addressed as yet and such research is essential if either system is to become a reality. While not much is known about this question, the risk of molecule changes is much greater with CO than CO_2. The CO_2 system requires further work on the problem of mode-medium interaction, although significant progress has been made recently. The CO system requires engineering development of a high current density electron window. In view of the differences in the ages of the two technologies, and the uncertainties in the two system designs, it is reasonable to view the two systems as comparable. The CO system probably should not enjoy the degree of superiority indicated by the weight figures in Table 6-1. Attainment of those parameters is more risky for the CO system.

In order to bring the systems to fruition technology development programs in a number of areas will be required. It is of interest to enumerate the most important areas indicated by our design investigation. First and foremost is the area of prime power generation. Unless a major effort is undertaken, solar power generators of this size will not be available for many years to come. Other areas where reasonable technological advancement has been postulated include high order mirror figuring (for the CO_2 system), mirror coating durability, high current electron beam window development (for the CO system), and high power laser window performance (both aerodynamic and material). In addition, the area of discharge induced chemistry which is just beginning to be investigated, should be pursued.

REFERENCES

1. Kelch, G.W. and Young, W.E., Closed-Cycle Gas Dynamic Laser Design Investigation, NASA CR-135130, January, 1977.

2. Chalfant, A.I., et al., Studies to Determine the Technical and Development Characteristics of Airborne Electrical Aerodynamic Laser Systems, March, 1971, AFAPL-TR-71-3 (Secret).

3. Davis, R.W., and Wilcox, J.D., High-Powered Gas Laser Technology Forecast, February 1975, AFWL-TP-74-346 (Secret).

4. Seikel, G.R. and Nichols, L.D., "Potential of Nuclear MHD Electric Power Systems," J. Spacecraft and Rockets 9, pp. 322-326, May 1972.

5. Space-Based Power Conversion and Power Relay Systems, Boeing Aerospace Company, NASA CR-150171, May 1976.

6. Satellite Solar Power Station, Spectrolab, Report Q-71098, November 1971.

7. Gregory, D.L., "Thermal Engine Solar Power Satellites," Intersociety Energy Conversion Engineering Conference, 12th, 1977.

8. Cox, R.L., et al., "Deployable Radiators for Waste Heat Dissipation from Shuttle Payloads," Raumfahrtforschung 5, pp. 232-237, 1976.

9. Libby, P.A. and Reiss, H.R., "The Design of Two-Dimensional Contraction Sections," Quarterly of Applied Mathematics 1X, 1951.

10. Morel, T., "Design of Two-Dimensional Wind Tunnel Contractions," ASME Paper 76-WA/FE-4, December 1976.

11. Cochran, D.L. and Kline, S.J., "Use of Short Flat Vanes for Producing Efficient Wide-Angle Two-Dimensional Subsonic Diffusers," NACA Technical Note 4309, September 1958.

12. Advanced Laser System, Laser Device Subsystem Engineering Confirmation Test Report, January, 1978, Hughes Report No. P77-288 (Confidential).

13. Private Communication, E. Locke.

14. E. M. Parmentier and R. A. Greenberg, "Supersonic Flow Aerodynamic Windows for High-Power Lasers," AIA Journal, Vol. 11, No. 7, July 1973 pp. 943-949.

15. "Development of an EDL Aerodynamic Window, "Project 107. MSNW, Inc., June 1972.

16. Kays, W. M. and London, A. L., Compact Heat Exchangers, McGraw-Hill, New York, 1964.

17. Hamilton, M. L. and Falk, T. J., CO Laser Research Program, Jan 1974, AFWL-TR-F3-158.

18. Lacina, W. B., et al, Supersonic Continuous Wave Carbon Monoxide Laser Development, Phase 1, Vol. 4, March 1976, AFWL-TR-75-144.

19. Klosterman, E. L., et al., Supersonic Continuous Wave Carbon Monoxide Electric Discharge Laser Parametric Investigation, April 1977, AFWL-TR-76-298.

DISTRIBUTION LIST FOR FINAL REPORT NAS 3-20100

1. National Aeronautics and Space Administration
Lewis Research Center
21000 Brookpark Road
Cleveland, OH 44135

Attn:	Contracting Officer, MS 500-312	1
	Technical Utilization Office, MS 3-16	1
	Technical Report Control Office, MS 5-5	
	AFSC Liaison Office, MS 501-3	2
	Library, MS 60-3	1
	Office of R & QA, MS 500-211	1
	N. T. Musial, Patent Counsel, MS 500-113	1
	Jack G. Slaby, Project Manager, MS 500-215	5
	Wolfgang E. Moeckel, MS 301-1	1

2. National Aeronautics and Space Administration
Headquarters
Washington, DC 20546

Attn:	Office of Aeronautics and Space Technology	
	Director, Research Division/RR-6	1
	J. G. Lundholm/RR-6	1
	J. P. Mullin/RP-6	1
Attn:	Office of Manned Space Flight	
	Director, Advanced Manned Mission/MT-3	1
Attn:	Office of Space Science	
	Director, Launch Vehicles and Propulsion/SV	1
Attn:	Office of Technology Utilization Division	
	Director, Technology Utilization/ET-6	1

3. National Aeronautics and Space Administration
Ames Research Center
Moffett Field, CA 94035

Attn:	Library	1
	Dr. Kenneth W. Billman	1

4. National Aeronautics and Space Administration
Flight Research Center
P. O. Box 273
Edwards, California 93523

Attn: Library 1

5. National Aeronautics and Space Administration
George C. Marshall Space Flight Center
Huntsville, Alabama 35912

Attn: Library 1

6. National Aeronautics and Space Administration
Goddard Space Flight Center
Greenbelt, Maryland 20771

Attn: Library 1

7. National Aeronautics and Space Administration
John F. Kennedy Space Center
Cocoa Beach, Florida 32931

Attn: Library 1

8. National Aeronautics and Space Administration
Lyndon B. Johnson Space Center
Houston, Texas 77058

Attn: Library 1

9. National Aeronautics and Space Administration
Langley Research Center
Hampton, Virginia 23365

Attn: Library 1
Bernie Garrett 1

10. NASA Scientific and Technical Information Facility
P. O. Box 8757
Balt/Wash International Airport
Maryland 21240

Attn: Accessioning Department 10

11. Jet Propulsion Laboratory
4800 Oak Grove Drive
Pasadena, California 91103

Attn: Library 1

12. Defense Documentation Center
Cameron Station
Building 5
5010 Duke Street
Alexandria, Virginia 22314

Attn: TISIA 1

13. Air Force Rocket Propulsion Laboratory
Edwards, Califonria 93523

Attn: Library 1

14. Defense Advanced Research Projects Agency
1400 Wilson Blvd
Arlington, Virginia 22209

Attn: Dr. Peter Clark 1

15. ODDR&G
Pentagon
Washington, DC 20301

Attn: Dr. Robert Greenberg 1

16. Commander
US Army Missile Command
Redstone Arsenal, Alabama 35809

Attn: Walter B. Jennings, Jr. 1

17. Director
Ballistic Missile Defense Advanced Technology Center
P.O. Box 1500
Huntsville, Alabama 35807

Attn: ATC-O, Mr. W.O. Davies 1

18. Director
US Army Ballistic Research Lab
Aberdeen Proving Ground, Maryland 21005

Attn: Dr. Robert Eichelberger 1

19. Office of Naval Research
495 Summer Street
Boston, Massachuetts

20. Office of Naval Research
800 N. Quincy Street
Arlington, Virigina

Attn: Dr. W.J. Condell (421) 1

21. Naval Missile Center
Point Mugu, California 93042

Attn: Gary Gibbs (Code 5352) 1

22. Superintendent
Naval Postgraduate School
Monterey, California 93940

Attn: Library (Code 2124) 1

23. Commander
Naval Weapons Center
China Lake, California 93555

Attn: Mr. E.B. Niccum, (Code 4011) 1

24. Naval Research Laboratory
Washington, DC 20375

Attn: Dr. P. Livingston (Code 5560) 1

25. Naval Ordnance Lab
White Oak
Silver Spring, Maryland 20910

Attn: Dr. Leroy Harris (Code 313) 1

26. Air Force Weapons Lab
Kirtland AFB, New Mexico 87117

Attn: Col. Donald L. Lamberson (AR) 1
Col. John C. Scholtz (PG) 1
Col. Russell K. Parsons (LR) 1
Lt. Col. John C. Rich (AL) 1

27. Headquarters SAMSO
P.O. Box 92960, Worldway Postal Center
Los Angeles, California 90009

Attn: Capt. Dorian A. DeMaio (XRTD) 1

28. AF Avionics Lab (TEO)
Wright Patterson AFB, Ohio 45433

Attn: Mr. K. Hutchinson 1

29. AF Materials Lab
Wright Patterson AFB, Ohio 45433

Attn: Major Paul Elder (LPJ) 1

30. AF Aero Propulsion Laboratory
Wright Patterson AFB, Ohio 45433

Attn: Major George Uhlig (AFAPL/NA) 1

31. RADO (OCSE/Mr. R. Urtz)
Griffiss AFB, New York 13441

Attn: OCSE/Mr. R. Urtz) 1

32. Headquarters Electronics Systems Division (ESD)
Hanscaom AFB, Main

Attn: Capt. Allen R. Tobin (XRE) 1

33. Air University
Institute for Professional Development
Maxwell AFB, Alabama 36112

Attn: ACSC/EDCS 1

34. Aerojet Liquid Rocket Company
P.O. Box 13222
Sacramento, California 95813

Attn: Dr. Sandy D. Rosenberg 1

35. Aerospace Corporation
P.O. Box 92957
Los Angeles, California 90009

Attn: Dr. Walter B. Warren, Jr. 1

36. Mr. A. Colin Stancliffe
AiResearch Manufacturing Company
2525 West 190th Street
Torrance, California 90503

Attn: Dept. 93-6 1

37. Astro Research Corporation
1330 Cacique
Box 4128
Santa Barbara, California 93103

Attn: R.F. Crawford, Dir. of Eng. 1

38. Atlantic Research Corporation
Shirley Highway at Edsall Road
Alexandria, Viriginia 22314

Attn: Mr. Robert Naismith 1

39. AVCO Everett Research Laboratory
2385 Revere Beach Parkway
Everett, MA 02149

Attn: Dr. George Sutton 1
Dr. Phillip Chapman 1

40. Battelle Columbus Laboratories
505 King Avenue
Columbus, Ohio 43201

Attn: Mr. Fred Tietzel (STOIAC) 1

41. Bell Aerospace Company
Buffalo, New York 14240

Attn: Dr. Wayne C. Solomon 1

42. Boeing Company
P.O. Box 3999
Seattle, Washington 98124

Attn: Mr. M.I. Gamble 1

43. ESI, Inc.
495 Java Drive
Sunnyvale, California 94086

Attn: Arthur Einhorn 1

44. Electro-Optical Systems
300 N. Halstead
Pasadena, California 91107

Attn: Dr. Andrew Jensen 1

45. General Electric Company
P. O. Box 8555
Philadelphia, Pennsylvania 19101

Attn: Mr. W.J. East 1

46. General Research Corporation
P. O. Box 3587
Santa Barbara, California 93105

Attn: Dr. R. Holbrook 1

47. Hercules, Inc.
P. O. Box 210
Cumberland, MD 21502

Attn: Dr. Ralph F. Preckel 1

48. Hughes Research Labs
3011 Malibu Canyon Road
Malibu, Calif 90265

Attn: Dr. Arthur N. Chester 1
Dr. Viktor Evtuhov 1

49. Hughes Aircraft Company
Centinela and Teale Streets
Culver City, Cal 90230

Attn: Dr. Eugene Peressini (Bldg. 6, MS/E-125) 1

50. Hughes Aircraft Company
P. O. Box 3310
Fullerton, Ca 90230

Attn: Dr. William Yates 1

51. Institute for Defense Analyses
400 Army Navy Drive
Ar ington, VA 22202

Attn: Dr. Alvin Schnitzler 1

52. Itek Corporation
Optical Systems Division
10 Maguire Road
Lexington, MA 02173

Attn: R.J. Wollensak 1

53. Johns Hopkins University
Applied Physics Lab
8621 Ga. Avenue
Silver Spring, MD 20910

Attn: Dr. Albert M. Stone 1

54. Lawrence Livermore Lab
P.O. Box 808
Livermore, Calif 94550

Attn: Dr. R.E. Kidder 1
Dr. E. Teller 1
Dr. John Emmett 1

55. Los Alamos Scientific Labs
P.O. Box 1663
Los Alamos, NM 87544

Attn: Dr. Keith Boyer (MS 530) 1

56. Lulejian and Associates, Inc.
Del Amo Financial Center Suite 500
21515 Hawthorne Blvd
Torrance, Ca 90503 1

57. Lockheed Palo Alto Research Lab
3251 Hanover Street
Palo Alto, Calif 94304

Attn: L.R. Lunsford 1
Orgn. 52-24, Bldg. 201

Wayne Jones
Dept. 5256, Bldg. 201 1

58. Mathematical Sciences Northwest, Inc.
P.O. Box 1887
Bellevue, Wash 98009

Attn: Mr. Abraham Hertzberg 1

59. Martin Marietta Aerospace
P.O. Box 179
Denver, CO 90201

Attn: Mr. Stewart Chapin (Mail No. 0485) 1

60. Massachusetts Institute of Technology
Lincoln Lab.
P. O. Box 73
Lexington, MA 02173

Attn: Dr. S. Edelberg 1
Dr. R.H. Rediker 1

61. McDonnell Doublas Astronautics Company
5301 Bolsa Avenue
Huntington Beach, Cal 92647

Attn: Mr. P. L. Klevatt
Dept. A3-360-B3GO, M/S 14-1 1

62. McDonnell Doublas Research Labs
Dept. 220, Box 516
St. Louis, MO 63166

Attn: Dr. D. P. Ames 1

63. MITRE Corporation
P. O. Box 208
Bedford, MA 01730

Attn: Mr. A. C. Cron 1

64. Northrop Corporation
Research and Technology Center
3401 West Broadway
Hawthorne, Cal 90250

Attn: Dr. Manny Bhaumik 1

65. Physical Sciences, Inc.
30 Commerce Way
Woburn, MA 01801

Attn: Dr. Anthony N. Pirri 1

66. Perkin Elmer Corporation
Norwalk, CT 06852

Attn: Dr. D.A. Dooley 1

67. Phaser Telepropulsion, Inc.
1888 Century Park East
Suite 1606
Los Angeles, CA 90067

Attn: Dr. M.A. Minovitch 1

68. Radio Corporation of America
Missile and Surface Radar Division
Morristown, NJ 08057

Attn: Mr. J.J. Mayman, Systems Project 1

69. RAND Corporation
1700 Main Street
Santa Monica, CA 90406

Attn: Dr. Claude R. Culp 1

70. Rasor Associates
420 Persian Drive
Sunnyvale, CA 94086

Attn: Dr. Ned S. Rasor 1

71. Raytheon Company
28 Seyon Street
Waltham, MA 02154

Attn: Dr. Frank A. Horrigan (Res. Div.) 1

72. Raytheon Company
Bedford Laboratories
Missile Systems Div.
Bedford, MA 01730

Attn: Dr. H.A. Mehlhorn 1
Optical Systems Department
M/S S4-55

73. Riverside Research Institute
80 West End Street
New York, NY 10023

Attn: Dr. L.H. O'Neill 1

74. R&D Associates, Inc.
P.O. Box 3580
Santa Monica, CA 90431

Attn: Dr. R.E. LeLevier 1

75. Rockwell International Corporation
3370 Miraloma Avenue
Anaheim, CA 92803

Attn: Dr. J. Winocur (D/528. HA14) 1

76. Rockwell International Corporation
Rocketdyne Division
6633 Canoga Avenue
Canoga Park, Calif 91304

Attn: Mr. Marc T. Constantine 1
Dr. Stan V. Gunn 1

77. SANDIA Labs
P.O. Box 5800
Albuquerque, NM 87115

Attn: Dr. E.H. Beckner - Org. 5200 1

78. W.J. Schafer Associates, Inc.
Lakeside Office Park
607 N. Avenue, Door 14
Wakefield, MA 01880

Attn: Francis W. French 1
Robert Ricles 1

79. Stanford Research Institute
Menlo Park, CA 94025

Attn: Dr. R.A. Armistead 1

80. Science Applications, Inc.
P.O. Box 2351
La Jolla, Ca 92037

Attn: Dr. John Asmus 1

81. Mr. Lawrence Peckham
Science Applications, Inc.
1911 N. Ft. Myer Drive, Suite 1200
Arlington, VA 22209 1

82. Science Applications, Inc.
P.O. Box 328
Ann Arbor, MI 48103

Attn: Dr. R.E. Meredith 1

83. Dr. Michael M. Monsler
Science Applications, Inc.
6 Preston Court
Bedford, MA 01730

84. Systems Consultants, Inc.
1050 31st Street, NW
Washington, DC 20007

Attn: Dr. Robert B. Keller 1

85. Systems, Science and Software
P. O. Box 1620
La Jolla, Caif 92037

Attn: Mr. Alan F. Klein 1

86. Thiokol Chemical Company
WASATCH Division
P. O. Box 524
Brigham City, UT 84302

Attn: Mr. James E. Hansen 1

87. TRW Systems Group
One Space Park
Bldg. 01, Room 1050
Redondo Beach, Ca 90278

Attn: Mr. Norman F. Campbell 1

88. United Aircraft Research Lab
400 Main Street
East Hartford, CT 06108

Attn: Mr. G.H. McLafferty 1

89. United Aircraft Corporation
Pratt and Whitney Division
Florida R&D Center
West Palm Beach, FL 33402

Attn: Dr. R.A. Schmidtke 1

90. VARIAN Associates
EIMAC Division
301 Indistrial Way
San Carlos, Ca 94070

Attn: Mr. Jack Quinn 1

91. Vought Systems Division
LTV Aerospace Corporation
P. O. Box 5907
Dallas, TX 75222

Attn: Mr. F.G. Simpson
Mail Station 2-54142 1

92. Westinghouse Electric Corporation
Defense and Space Center
Friendship International Airport - Box 746
Baltimore, MD 21203

Attn: Mr. W.F. List 1

93. Westinghouse Research Lab
Beulah Road, Churchill Boro.
Pittsburg, PA 15235

Attn: Mr. R.L. Hundstad 1